Prog. Energy Combust. Sci. 1989. Vol. 15. pp. 287–338
Printed in Great Britain. All rights reserved.

0360-1285/89 $0.00 + .50
© 1989 Pergamon Press plc

MECHANISM AND MODELING OF NITROGEN CHEMISTRY IN COMBUSTION

JAMES A. MILLER*‡ and CRAIG T. BOWMAN†§

*Combustion Research Facility, Sandia National Laboratories, Livermore, CA 94551, U.S.A.
†Department of Mechanical Engineering, Stanford University, Stanford, CA 94305, U.S.A.

Received 16 June 1989

Abstract—Our current understanding of the mechanisms and rate parameters for the gas-phase reactions of nitrogen compounds that are applicable to combustion-generated air pollution is discussed and illustrated by comparison of results from detailed kinetics calculations with experimental data. In particular, the mechanisms and rate parameters for thermal and prompt NO formation, for fuel nitrogen conversion, for the Thermal De-NO_x and RAPRENO$_x$ processes, and for NO_2 and N_2O formation and removal processes are considered. Sensitivity and rate-of-production analyses are applied in the calculations to determine which elementary reactions are of greatest importance in the nitrogen conversion process. Available information on the rate parameters for these important elementary reactions has been surveyed, and recommendations for the rate coefficients for these reactions are provided. The principal areas of uncertainty in nitrogen reaction mechanisms and rate parameters are outlined.

CONTENTS

1. INTRODUCTION

The chemical reactions of nitrogen compounds that occur in combustion processes have been the subject of intensive study for more than fifty years. Much of this research has been motivated by the impact of the nitrogen compounds emitted from combustion sources on the environment and by the role that these species play in combustion of energetic materials. At the present time, many of the complex reaction paths for formation and destruction of nitrogen species in combustion have been established and rate parameters for many of the elementary reactions have been determined.

In the present paper, our current understanding of the mechanisms and rate parameters for the gas-phase reactions of nitrogen compounds that are relevant to combustion-generated air pollution is illustrated by comparison of results from detailed kinetics calculations with experimental data. Sensitivity and rate-of-production analyses are applied in these calculations to determine which elementary reactions are of greatest importance in the nitrogen conversion process. Available information on the rate parameters for these important elementary reactions has been

‡Work sponsored by the U.S. Department of Energy, Office of Basic Energy Sciences, Division of Chemical Sciences.
§Work sponsored by the U.S. Department of Energy, Office of Basic Energy Sciences, Division of Chemical Sciences, by the Physical Sciences Department of the Gas Research Institute, and by the U.S. Environmental Protection Agency.

surveyed, and recommendations for the rate coefficients for these reactions are provided. Finally, the principal areas of uncertainty in nitrogen reaction mechanisms and rate parameters are outlined.

In the following sections, the gas-phase reaction mechanisms and rate parameters for thermal and prompt NO formation, for fuel nitrogen conversion, for the Thermal De-NO_x and RAPRENO$_x$ processes, and for NO_2 and N_2O formation and removal processes are discussed separately; however, as will be seen, there are instances where particular reactions are important in several of the reaction mechanisms. For example, there are many common features in the reaction mechanisms for prompt NO formation and fuel nitrogen conversion.

In preparing this paper, we were fortunate to be able to draw upon a large body of published work, including several extensive compilations of elementary rate coefficients.[1,2,160,169,170] As appropriate, we direct the reader to these sources.

2. COMPUTATIONAL METHODS AND REACTION MECHANISMS

Three different types of kinetics calculations are reported in this paper: (i) the structure of a one-dimensional, premixed, laminar flame, (ii) the output of a perfectly stirred reactor (PSR), and (iii) the time history of a homogeneous reaction (mathematically equivalent to a diffusion-free plug-flow reactor). All calculations utilize Chemkin[3] and the Chemkin thermodynamic data base.[4] The flame calculations use the Sandia transport package and data base.[5] The three different types of calculations are performed, respectively, with the Sandia flame code,[6] PSR,[7] and Senkin.[8] Table 1 lists the standard heats of formation of some of the more important species considered in the calculations.

Sensitivity and rate-of-production analyses play a central role in the discussions that follow. The methods used in performing the sensitivity analyses have been described in detail in previous articles.[9-12] In the flame and homogeneous reaction calculations, the sensitivity coefficients are displayed as

$$\beta_{ik}(x) = \frac{A_i}{X_k^{(\max)}} \frac{\partial X_k}{\partial A_i}(x),$$

where $\beta_{ik}(x)$ is the sensitivity coefficient for change in the mole fraction of the k^{th} species, X_k, due to a small change in the temperature-independent factor of the i^{th} reaction rate coefficient, A_i. The superscript on $X_k^{(\max)}$ indicates the maximum value of X_k that occurred in the calculation; x is position above the burner surface (for a homogeneous reaction x is replaced by time, t). For a PSR calculation, there is no spatial or time dependence, and $X_k = X_k^{(\max)}$. Otherwise, β_{ik} is specified in the same way as in the flame and homogeneous reaction calculations. Contribution factors obtained from rate-of-production (or reaction path) analysis are displayed as

$$R_{ik}(x) = r_{ik\ \text{forward}}(x) - r_{ik\ \text{reverse}}(x)$$

where r_{ik} is the rate of the forward or reverse reaction i involving the k^{th} species.

The reaction mechanism used in our calculations is given in Appendices A and B. Appendix A contains reactions that describe the oxidation of the C_1 and C_2 hydrocarbons under most conditions (not too fuel-rich), as well as all reactions that we know to be important in prompt NO formation and fuel-nitrogen conversion. Appendix B is essentially an ammonia oxidation mechanism (N/H/O reactions only). Most of the reactions in Appendix B are also included in Appendix A with the same rate coefficients. However, a few of the reactions in Appendix B are not in Appendix A; viz. reactions of the type $NH_i + NH_j \rightleftharpoons$ products ($i, j = 0, 1, 2$) and subsequent reactions of the products. These reactions do not play an important role in situations where the fixed nitrogen (nitrogen in a form other than N_2) is present in small quantities, as is often the case. Consequently, they are included in Appendix B only for the purpose of modeling situations in which ammonia is a principal constituent. In constructing Appendices A and B, we have attempted to be complete, rather than exhaustive. All reactions that we believe to be important under most combustion conditions are included. However, unusual conditions may involve reactions not included here.

The reaction mechanism of Appendices A and B is largely drawn from and discussed in a series of papers by Miller and coworkers.[10-15] However, a number of significant improvements to the reaction mechanisms discussed in these earlier papers have been made. We shall defer discussion of individual reactions until they arise in the text. However, two improvements are noted here. First, we have introduced a number of reactions of $^1CH_2$, distinguishing $^1CH_2$ and $^3CH_2$ as separate species. Indeed, reactions of $^1CH_2$ are not

TABLE 1. Standard heats of formation of selected species in the reaction mechanism (reference temperature = 298 K)

Species	ΔH_f^0 (kcal/mol)
$^1CH_2$	101.46
$^3CH_2$	92.45
C_2H	134.0
C_2H_3	68.4
C_2H_5	28.0
CH_3O	3.9
HCCO	42.4
NH	85.2
NH_2	45.5
NCO	38.1
NNH	58.5
HOCN	−2.28
HNCO	−24.9
HCNO	38.4
H_2CN	59.08
N_2H_2	50.9

negligible, the most important one being

$$^1CH_2 + H_2 \rightleftharpoons CH_3 + H. \quad (A110)$$

In the following sections the triplet state is written CH_2 and the singlet state is written $^1CH_2$. In addition, we have introduced more accurate formulations of the pressure dependence of the reactions

$$CH_3 + H(+M) \rightleftharpoons CH_4(+M) \quad (A2)$$

and

$$CH_3 + CH_3(+M) \rightleftharpoons C_2H_6(+M). \quad (A1)$$

For reaction (A1) we have adopted the expression given by Wagner and Wardlaw,[16] and for reaction (A2) our rate coefficient is essentially the same as that of Stewart, Smith, and Golden.[17] For the other important pressure-dependent dissociation/recombination reactions,

$$H + C_2H_4(+M) \rightleftharpoons C_2H_5(+M) \quad (A73)$$

and

$$H + C_2H_2(+M) \rightleftharpoons C_2H_3(+M), \quad (A79)$$

we continue to describe the pressure dependence in terms of the Lindemann form.[14,17] Such a description appears to be adequate for the present purposes.

3. THERMAL NO MECHANISM

Nitric oxide (NO) is an important nitrogen oxide emitted from combustion sources. In the combustion of clean fuels (fuels not containing nitrogen compounds), oxidation of atmospheric nitrogen (N_2) by the 'thermal' mechanism is a major source of NO_x emissions. The three principal reactions that comprise the thermal NO formation mechanism are

$$O + N_2 \rightleftharpoons NO + N, \quad (-A232)$$

$$N + O_2 \rightleftharpoons NO + O, \quad (A233)$$

and

$$N + OH \rightleftharpoons NO + H. \quad (A234)$$

There have been indirect and direct measurements of the rate coefficients of these three reactions, and these data have been critically evaluated by Baulch *et al.*[1] and Hanson and Salimian.[2] The expressions for the rate coefficients for reactions (A232)–(A234) used in the present calculations are given in Appendix A, and are the same as those given and discussed by Miller *et al.*[10] The expression for k_{A232} is given for the reaction, $N + NO \rightarrow O + N_2$, and was derived from the high-temperature data of Ref. 18 for the reverse reaction (using the equilibrium constant) and the low-temperature recommendation of Baulch *et al.* for the forward reaction. The expression for k_{A233} is the same as that recommended in Ref. 1. The expression for k_{A234} is given for the reaction, $N + OH \rightarrow NO + H$, as discussed by Miller *et al.*[10]

Reactions (A232)–(A234) involve the O and OH radicals, which also play an important role in the fuel oxidation mechanism. Hence, in general, it is necessary to couple the thermal NO reactions to the reaction sequence describing oxidation of the fuel. Since the overall rate of NO formation by the thermal mechanism generally is slow compared to the fuel oxidation reactions, it often is assumed, following the suggestion of Zeldovich,[19] that the thermal NO formation reactions can be decoupled from the fuel oxidation process. In this situation, NO formation rates are calculated assuming equilibrium values of temperature and concentrations of O_2, N_2, O, and OH (the N-atom concentration is calculated from a steady-state approximation applied to reactions (A232)–(A234)).

The errors that may be introduced by this approximation are illustrated in Fig. 1. Here, the maximum (initial) NO formation rates calculated from the Zeldovich model are compared with the maximum NO formation rates calculated from a detailed kinetics model for oxidation of methane–air for a fuel-rich mixture (see Appendix A for a complete tabulation of the reactions and rate parameters used in the detailed calculation). In this comparison, an isothermal reaction was assumed (to allow independent variation of temperature) and the prompt NO initiation reactions, discussed in Section 4, were deleted from the mechanism so that the observed differences in NO formation rates are due entirely to

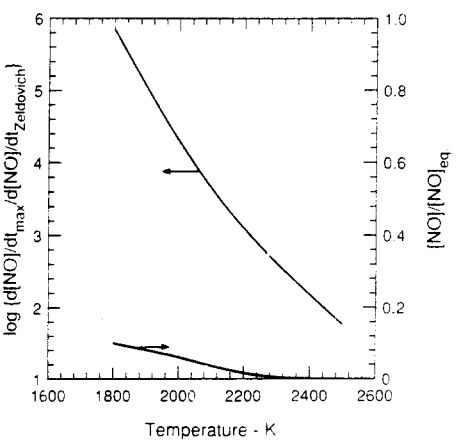

FIG. 1. The effect of superequilibrium radical concentrations on NO formation rates in the isothermal reaction of 13% methane in air (ϕ = 1.37). The upper curve is the ratio of the maximum NO formation rate calculated using the reaction mechanism of Appendix A (with prompt NO initiation reactions deleted) to the initial NO formation rate calculated using the Zeldovich model. The lower curve is the ratio of the NO concentration at the time of the maximum NO formation rate calculated using the detailed reaction mechanism to the equilibrium NO concentration.

nonequilibrium radical concentrations during the oxidation process. There is a noticeable acceleration of the maximum NO formation rate above that calculated using the Zeldovich model during the initial stages of reaction due to nonequilibrium effects, with the departures from the Zeldovich model results decreasing with increasing temperature. While nonequilibrium effects on the NO formation rate are evident over a wide temperature range, the accelerated rates are sufficiently low so that very little NO is formed by the accelerated reaction. This result is illustrated by the lower curve in Fig. 1, where the NO concentration at the time of maximum rate of formation calculated from the detailed kinetics model is compared with the equilibrium NO concentration.

4. PROMPT NO MECHANISM

Nitric oxide formation rates in combustion of hydrocarbon fuels can exceed those attributable to direct oxidation of molecular nitrogen by the thermal mechanism discussed above, especially for fuel-rich conditions. This rapidly formed NO was termed 'prompt NO' by Fenimore[20] since the rapid NO formation was confined to regions near the flame zone. Typical levels of prompt NO range from a few parts per million by volume to more than 100 ppmv. Available data indicate that some prompt NO formation occurs due to superequilibrium concentrations of O and OH, which accelerate the rates of reactions (A232)–(A234). However, numerous studies have shown that prompt NO in hydrocarbon flames is formed primarily by a reaction sequence that is initiated by the rapid reaction of hydrocarbon radicals with molecular nitrogen, leading to formation of amines or cyano compounds that subsequently react to form NO.[20–29]

What hydrocarbon radical is responsible for the prompt NO in hydrocarbon flames? A number of species have been suggested, e.g. CH, CH_2, C_2, C_2H, and C,[20–29] although the experiments of Blauwens *et al.*[26] suggest that CH and CH_2 are the major contributors. The mechanism used here explicitly considers the following reactions:

$$CH + N_2 \rightleftharpoons HCN + N \qquad (A151)$$

$$CH_2 + N_2 \rightleftharpoons HCN + NH \qquad (A153)$$

$$CH_2 + N_2 \rightleftharpoons H_2CN + N \qquad (-A154)$$

and

$$C + N_2 \rightleftharpoons CN + N. \qquad (-A152)$$

Figure 2 is a reaction coordinate diagram on which estimates of the two $CH_2 + N_2$ rate coefficients can be based. Consider first the HCN + NH channel, reaction (A153). In the following discussion, it is convenient to consider the reaction in reverse. By comparing reaction (A153) with BAC-MP4 (bond additivity corrected Möller Plesset fourth-order perturbation theory) calculations for the isoelectronic reaction O + HCN,[30,31] we conclude that the addition complex for adding NH to the *nitrogen* end of HCN lies about 20 kcal/mol above NH + HCN. To form $CH_2 + N_2$ this complex must undergo a 1,3 hydrogen shift from the nitrogen to the carbon atom, as shown in the diagram. Such hydrogen transfers in open-shell systems, where the hydrogen atom is accepted at a free valence site, normally have intrinsic energy barriers (in the exothermic direction) of approximately 40 kcal/mol. This information and the endothermicity of the reaction suggest an activation energy for reaction (A153) of approximately 85 kcal/mol, a very high value. In addition, the transition state for the reaction corresponds to that for the 1,3 hydrogen transfer. Such transition states normally are very tight and lead to low A-factors, probably about 10^{12} cm^3/mol-sec at high temperature. The rate coefficient expression used in the present calculations, $k_{A153} = 10^{13}\exp(-74000/RT)$ cm^3/mol-sec, is taken from Glarborg *et al.*[11] and represents a reasonable upper limit for the rate coefficient; a value of $k_{A153} = 10^{12}\exp(-85000/RT)$ cm^3/mol-sec appears more likely. These values of k_{A153} appear to be consistent with Benson's[32] estimate, using current thermochemistry, of an activation energy exceeding 70 kcal/mol and a low A-factor.

The present estimate of k_{A153} differs markedly from the similar analysis of Sanders *et al.*[33] The source of the discrepancy is the incorrect assumption in the latter paper that the four-centered transition state, discussed above, is analogous to the transition state for an oxygen atom adding to the *carbon* atom in HCN. This assumption leads to an estimate of the activation energy that is too low. With the rate coefficient given in Ref. 33, reaction (A153) could be an important contributor to prompt NO. However, even with a rate coefficient much faster than used here,

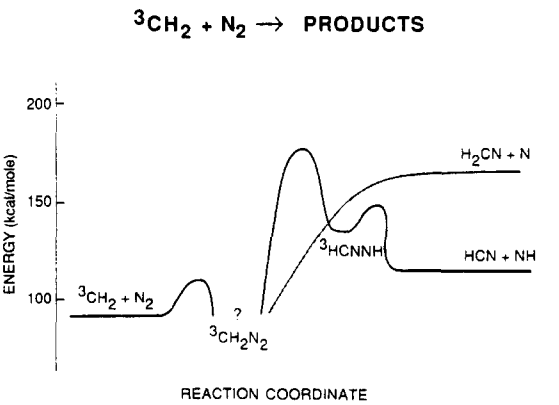

FIG. 2. Reaction coordinate diagram for the reaction $CH_2 + N_2 \rightarrow$ products.

reaction (A153) is an insignificant contributor to prompt NO in the present calculations.

The other reaction channel involving methylene and molecular nitrogen,

$$CH_2 + N_2 \rightleftharpoons H_2CN + N \quad (-A154)$$

is endothermic by 79 kcal/mol and is isoelectronic with the thermal-NO reaction, $O + N_2 \rightleftharpoons NO + N$ ($-$A232). On this basis we have estimated k_{A154} to be essentially the same as k_{A232}. This reaction also is an insignificant contributor to prompt NO in our calculations.

A reaction that does lead to prompt NO is (A151),

$$CH + N_2 \rightleftharpoons HCN + N, \quad (A151)$$

originally suggested by Fenimore.[20] A reaction coordinate diagram for reaction (A151) is shown in Fig. 3. The first step in the process is the formation of metastable HCN_2^*. According to the *ab initio* electronic structure calculations of Bair,[34] this addition process has no energy barrier and results in a bond of 18.3 kcal/mol. Berman and Lin[35] have measured the rate coefficient for the pressure-dependent reaction,

$$CH + N_2(+M) \rightleftharpoons HCN_2(+M),$$

in the temperature range 297–675 K. As expected for such reactions, the rate coefficient for this reaction at any given pressure decreases rapidly with increasing temperature, and under most combustion conditions the pressure-independent channel,

$$CH + N_2 \rightleftharpoons HCN + N, \quad (A151)$$

is dominant.

There have been several indirect inferences of k_{A151} from flame, shock tube and stirred reactor data and one direct shock tube measurement. Available rate data for reaction (A151) are summarized in Fig. 4. The most direct determination of k_{A151} is the shock tube study of Dean *et al.*[171] in the temperature range 2700–3700 K. As can be seen in Fig. 4, there are significant differences among the various determinations of k_{A151}, especially in the temperature range of interest in combustion. However, most of the determinations should be assigned relatively large uncertainties.

Theoretical estimates of k_{A151} are complicated by the failure of the reaction to conserve electron spin. Figure 3 shows that the intersystem crossing occurs at the high point along the reaction path and thus plays the deciding role in determining k_{A151}. In order to obtain rate parameters for the reaction, we fixed the activation energy at a value of 13.6 kcal/mol, as inferred from the flame data of Matsui and Nomaguchi,[28] and adjusted the A-factor to fit the well-stirred reactor data of Bartok *et al.*[36] discussed below. The reaction coordinate diagram of Fig. 3 has been constructed accordingly.

The A-factor deduced for reaction (A151), 3×10^{11} cm^3/mol-sec, is very small, approximately a factor of 100 smaller than one might anticipate for a similar reaction that conserved electron spin. This result implies that the intersystem crossing actually occurs only 1% of the time that the critical configuration is obtained. It should be noted, however, that the present determination of k_{A151} is not very sensitive to the activation energy and A-factor independently, but only to the value of k_{A151} in a narrow temperature range centered at about 2000 K. The k_{A151} which we have inferred is shown in Fig. 4 and in Table 2. Our k_{A151}, which is a factor of 1.5 larger than Glarborg *et al.*,[11] is smaller than most of the other determinations at 2000 K. However, our k_{A151} value at 2000 K is consistent with the high-temperature data of Dean *et al.*[171] if an activation energy of 26 kcal/mol is assumed for the reaction. The present value of k_{A151} accurately predicts the NO produced in the stirred-reactor experiments of Duterque *et al.*,[179] as well as the HCN

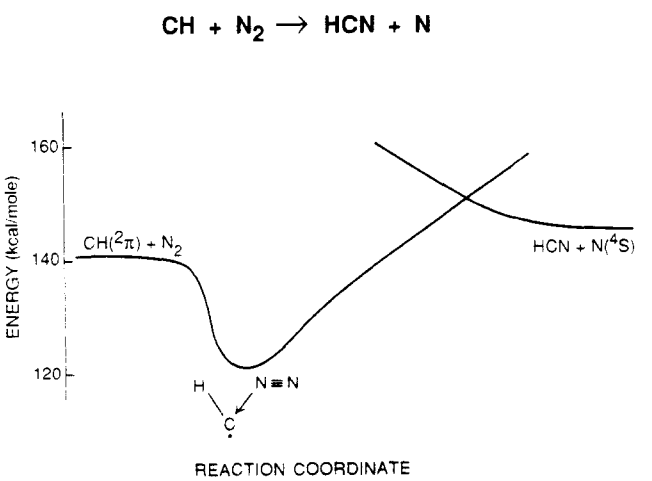

FIG. 3. Reaction coordinate diagram for the reaction CH + N_2 → HCN + N.

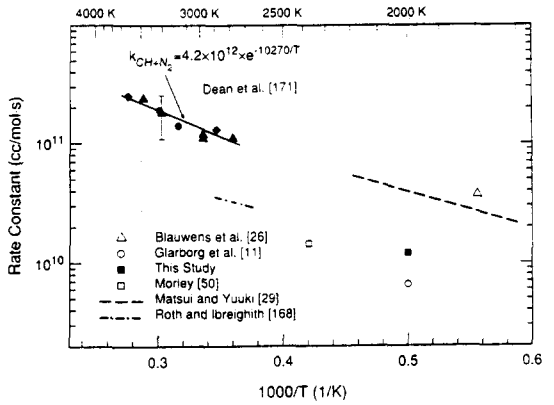

FIG. 4. Compilation of rate coefficients for $CH + N_2 \rightarrow HCN + N$.[171]

produced in the ethylene-fueled stirred reactor experiments of Sun *et al.*[87] In this latter experiment, 30 ppmv of HCN was measured at $\phi = 1.9$, $T = 1750$ K, conditions for which the model predicts 31 ppmv. Using the higher value of k_{A151} deduced in Refs 26 and 29 results in a calculated HCN mole fraction of approximately 150 ppm.

One possible explanation of the difference between the present value of the rate coefficient for reaction (A151), $CH + N_2 \rightleftharpoons HCN + N$, and that inferred from low-pressure flame experiments by Blauwens *et al.*[26] and by Matsui and Yuuki[29] is that our reaction mechanism does not predict the CH concentration accurately, thereby leading to an error in our inference of k_{A151} from the stirred reactor experiments of Bartok *et al.*[36] It is of interest, therefore, to compare CH concentrations calculated using our reaction mechanism with available experimental data. Only a few measurements of CH in combustion processes have been reported. Some measurements of CH are reported in Ref. 26, where molecular beam mass spectrometry was used to measure not only CH but also CH_2 and C-atom profiles in the flame. Figures 5 and 6 show comparisons of temperature and species concentration profiles calculated using the present kinetics model with the 'flame I' data from Ref. 26.

Figure 5 shows a comparison of calculated and measured profiles of temperature, O-atom and NO. Also shown in Fig. 5 is the calculated profile of H_2CO, a species that might interfere with a mass spectrometric measurement of NO. In the calculation, the temperature was specified to be the value reported in Ref. 26 for distances above the burner surface greater than 1 cm (where temperature data were reported) and was extrapolated to the burner surface in such a way as to replicate the measured O-atom profile as closely as possible. The calculated species profiles were found to be relatively insensitive to the extrapolated temperature profile. Two calculated NO profiles are shown in Fig. 5, one obtained using the present expression for k_{A151} and one using the expression for k_{A151} reported in Ref. 26. Figure 6 shows a comparison of calculated and measured profiles of CH_2, CH and C-atom.

The calculated profiles of CH_2, CH and C-atom agree with the experimental profiles to better than the factor-of-two uncertainty quoted in Ref. 26. However, as can be seen from Fig. 5, the experimental NO profile is not predicted using either the present value of k_{A151} or the higher value deduced in Ref. 26. Several aspects of the disagreement between measured and calculated NO profiles are noteworthy and require further discussion. At distances greater than 1 cm above the burner (where NO formation occurs solely by the thermal mechanism), the measured NO profile is not consistent with presently-accepted values of the rate coefficients of reactions (A232)–(A234), which comprise the thermal NO mechanism, or with the measured O-atom and temperature profiles. Blauwens *et al.* suggest that the NO formation rate measured in the post-flame zone is reduced due to heat losses to the surroundings. However, such heat losses are not evidenced in the measured temperature profile except for distances greater than 2 cm above the burner surface. Hence, heat losses cannot account for the discrepancy between measured and calculated NO profiles between 1 and 2 cm. Although the calculated CH profile agrees with the measured profile, the NO profile in the early region of the flame (< 1 cm), calculated using the present expression for k_{A151}, lies below the reported NO profile. When using the expression for k_{A151} reported in Ref. 26, the agreement between the calculated and measured NO profiles for distances less than 1 cm above the burner surface is improved; but, as noted above, the measured NO profile for distances greater than 1 cm does not agree with the calculation. One possible

TABLE 2. Rate coefficient expression for the reaction $CH + N_2 \rightarrow HCN + N$

Rate coefficient (cm^3/mol-sec) $k(T)$	k (2000 K)	Ref.
$8.0 \times 10^{11} \exp(-11000/RT)$	5×10^{10}	Blauwens *et al.*[26]
$4.0 \times 10^{11} \exp(-13600/RT)$	1.3×10^{10}	Matsui and Nomaguchi[28]
$1.2 \times 10^{12} \exp(-13600/RT)$	3.9×10^{10}	Matsui and Yuuki[29]
1.44×10^{10}*	1.44×10^{10}	Morley[50]
$1.0 \times 10^{12} \exp(-19200/RT)$	8.0×10^{9}	Roth and Ibreighith[168]
$4.2 \times 10^{12} \exp(-20400/RT)$	2.5×10^{10}	Dean *et al.*[171]
$3.0 \times 10^{11} \exp(-13600/RT)$	9.8×10^{9}	Present model

* Temperature range 2000 K $< T <$ 2560 K.

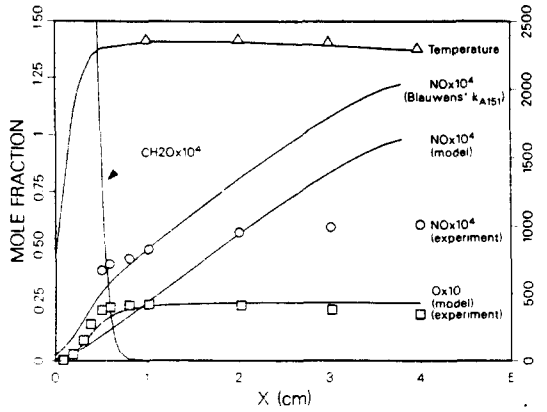

FIG. 5. Comparison of model predictions using the mechanism of Appendix A with the 'flame I' data of Blauwens *et al.*[26] for O and NO. The assumed temperature profile and experimental data are also shown. The two different NO predictions correspond to two different values of k_{A151} ((A151)—$CH + N_2 \rightleftharpoons HCN + N$), that of the present kinetic model and that deduced by Blauwens *et al.*

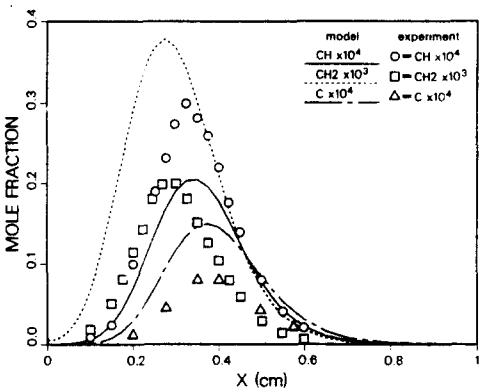

FIG. 6. Comparison of model predictions using the mechanism of Appendix A with the 'flame I' data of Blauwens *et al.*[26] for CH_2, CH, and C.

explanation for the discrepancies between calculated and measured NO profiles for distances less than 1 cm is the presence of formaldehyde, which could contribute to the $m/e = 30$ peak in the mass spectrometer. The calculations, Fig. 5, indicate the presence of formaldehyde at distances up to 0.7 cm above the burner surface, although Blauwens *et al.* imply that interference due to formaldehyde was negligible downstream of the visible reaction zone (> 0.5 cm).

In summary, the present kinetics model is able to match all of the reported species profiles, including CH, for 'flame I' of Ref. 26 except for NO. It was not possible to match the entire NO profile in this flame using either the present value of k_{A151} or the value reported in Ref. 26. Hence, we assign a relatively high uncertainty to the k_{A151} determination of Ref. 26. Clearly, further progress in modeling prompt NO in flames requires a direct and unambiguous determination of k_{A151} at flame temperatures.

The last prompt-NO reaction considered explicitly in the mechanism is

$$C + N_2 \rightleftharpoons CN + N. \qquad (-A152)$$

Experiments indicate that the reverse of this reaction,

$$CN + N \longrightarrow N_2 + C$$

is very fast both at room temperature[37] and under shock tube conditions.[38,39] Dean *et al.*[173] have reported shock tube measurements of k_{-A152} at elevated temperatures. With these rate data, reaction (A152) is a minor, but nonnegligible, contributor to prompt NO under most conditions. Because of the large endothermicity of the reaction $C + N_2 \rightarrow CN + N$, its importance with respect to reaction (A151) increases with increasing temperature.

Figure 7 shows a comparison of the present model predictions with the well-stirred reactor experiments of Bartok *et al.*[36] Following Glarborg,[40] we have made the comparison for the 3 msec residence time data. This is the only residence time for which temperatures were measured at equivalence ratios richer than stoichiometric. Use of the experimental temperatures in the calculation eliminates an important uncertainty in the calculation.

Several important results are readily apparent from Fig. 7. First, thermal NO, computed by deleting from the complete mechanism the prompt-NO initiation reactions discussed above, is insufficient to account for the experimentally observed NO above an equivalence ratio of approximately $\phi = 0.9$. At an equivalence ratio of $\phi = 1.2$, hydrogen cyanide begins to make a significant contribution to the total fixed nitrogen (TFN = NO + HCN + NH_3) in the reactor. The HCN concentration peaks at (or near) $\phi = 1.4$ and drops off quickly beyond that. The calculations predict the experimentally observed NO up to $\phi = 1.4$, but at higher equivalence ratios the model predicts smaller NO concentrations than are observed experimentally.

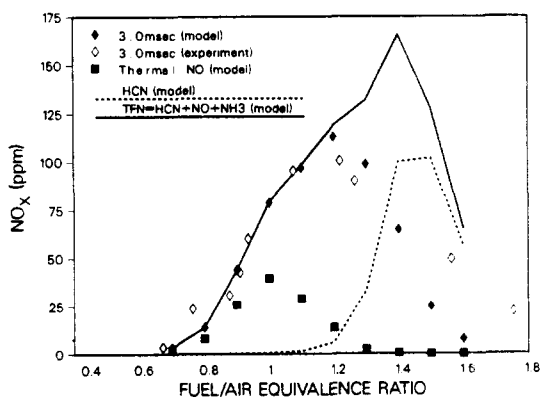

FIG. 7. Comparison of model predictions of NO concentrations with the well-stirred reactor data of Bartok *et al.*[36]

Interpretation of the computational results is facilitated by the use of sensitivity analysis and rate-of-production (or reaction path) analyses. Sensitivity coefficients for NO, HCN, and TFN, corresponding to Fig. 7 are shown in Figs 8–10. The most important reaction paths in prompt-NO formation and fuel nitrogen conversion, which have many common features, are shown diagramatically in Fig. 11.

Prompt-NO formation involves three separate kinetic issues:

(1) the CH concentration and how it is established;
(2) the rate of molecular nitrogen fixation: i.e. value of k_{A151};
(3) the rates of interconversion among fixed nitrogen fragments.

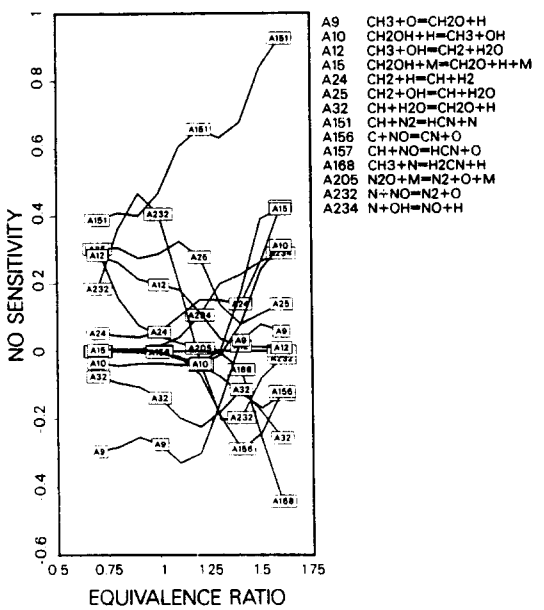

FIG. 8. Sensitivity plot of selected reactions for NO for the conditions of Fig. 7.

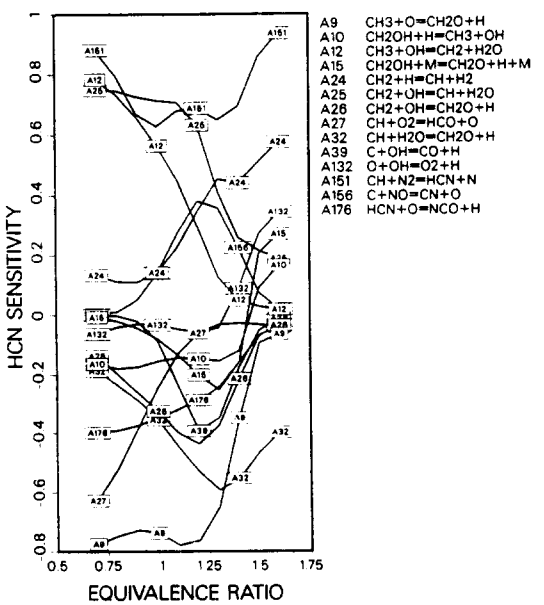

FIG. 9. Sensitivity plot of selected reactions for HCN for the conditions of Fig. 7.

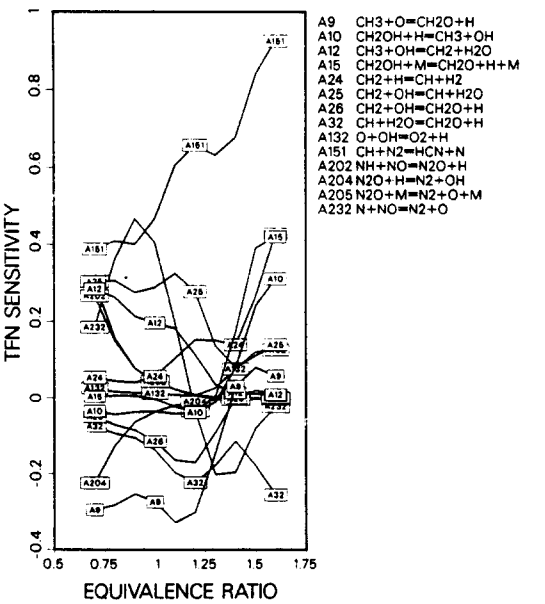

FIG. 10. Sensitivity plot of selected reactions for TFN for the conditions of Fig. 7.

As can be seen from the sensitivity analysis, reaction (A151) is an important rate-limiting step for NO, HCN, and TFN production under all conditions investigated; the reaction has sensitivity coefficients for these species approaching unity in rich mixtures, and even under lean conditions ($\phi < 0.8$) it plays a major role in NO formation. The thermal-NO mechanism is the dominant source of NO only in the equivalence-ratio range $\phi = 0.8$–1.0. For $\phi < 0.8$, the temperature in the reactor is sufficiently low that the sequence,

$$O + N_2 + M \rightleftharpoons N_2O + M \quad (-A205)$$

$$H + N_2O \rightleftharpoons NO + NH \quad (-A202)$$

$$O + N_2O \rightleftharpoons NO + NO, \quad (A207)$$

becomes an important source of NO.[11,41,42]

The mechanism of CH formation depends somewhat on the fuel. In all cases CH comes from methylene by reaction with OH and H,

$$H + CH_2 \rightleftharpoons CH + H_2 \quad (A24)$$

and

$$OH + CH_2 \rightleftharpoons CH + H_2O. \quad (A25)$$

The CH_2 can be formed either from methyl or from acetylene. As discussed by Glarborg *et al.*, in the methane experiments of Bartok *et al.*, for $\phi < 1.5$, the CH_3 source is dominant.

$$CH_3 + OH \rightleftharpoons CH_2 + H_2O \quad (A12)$$

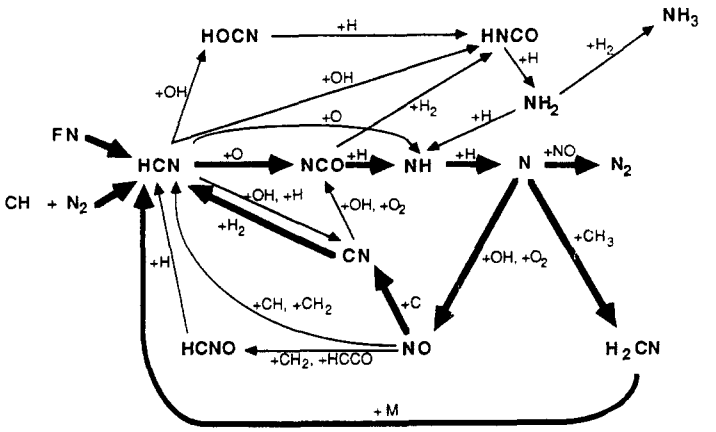

FIG. 11. Reaction path diagram illustrating the major steps in prompt NO formation and conversion of fuel nitrogen (FN) to NO. The bold lines represent the most important reaction paths.

$$CH_3 + H \rightleftharpoons CH_2 + H_2. \qquad (A13)$$

In the present calculations there is the additional CH_2 source involving the singlet species,

$$CH_3 + H \rightleftharpoons {}^1CH_2 + H_2 \qquad (-A110)$$

$${}^1CH_2 + M \rightleftharpoons CH_2 + M, \qquad (A106)$$

which is more important in the calculations than the direct abstraction (A13). Only for $\phi \geq 1.5$ does the indirect route to CH_2 through the C_2 hydrocarbons come into play.

The most important CH-consuming steps in the calculations are the reactions

$$CH + H \rightleftharpoons C + H_2, \qquad (A31)$$

$$CH + H_2O \rightleftharpoons CH_2O + H, \qquad (A32)$$

and

$$CH + CO_2 \rightleftharpoons HCO + CO. \qquad (A30)$$

Reaction (A32) was not included in the previous calculations of Glarborg *et al.*[11] The present rate coefficient expression for k_{A32} is based on the experiments of Zabarnick *et al.*[43] in the temperature range $297\,K < T < 670\,K$. However, a T^n function was used to extrapolate their results to high temperature, rather than the Arrhenius expression given in Ref. 43.

Up to an equivalence ratio of approximately $\phi = 1.2$ the HCN and N produced by reaction (A151) are converted rapidly to NO, principally by the mechanism discussed by Miller *et al.*,[10]

$$HCN + O \rightleftharpoons NCO + H \qquad (A176)$$

$$NCO + H \rightleftharpoons NH + CO \qquad (A192)$$

$$NH + H \rightleftharpoons N + H_2 \qquad (A211)$$

$$N + OH \rightleftharpoons NO + H. \qquad (A234)$$

Beyond $\phi = 1.2$, several factors combine to cause the NO concentration to decrease relative to HCN:

(a) the conversion of HCN to NO by the above mechanism is no longer rapid;
(b) the 'recycle' of NO to HCN by the mechanism discussed below begins to inhibit NO production;
(c) the reaction (A232), $N + NO \rightleftharpoons N_2 + O$, shifts directions from reverse to forward.

A decrease in the O-atom concentration contributes to all three of these occurrences. But, in particular, under rich conditions, reactions that convert CH_3 to CH_2 are better able to compete with reaction (A9), $CH_3 + O \rightleftharpoons CH_2O + H$, and allow the recycle reactions,

$$C + NO \rightleftharpoons CN + O \qquad (A156)$$

$$CH + NO \rightleftharpoons HCN + O \qquad (A157)$$

$$CH_2 + NO \rightleftharpoons HCNO + H \qquad (A158)$$

to become more effective.

At $\phi = 1.4$ the peaks in the CH and TFN concentrations occur simultaneously. Beyond $\phi = 1.4$ one enters a regime in which the fixed nitrogen concentration is limited by the availability of the chain carriers (H and OH) required for producing CH from methane, as evidenced by the increased sensitivity of the TFN to chain branching processes, i.e.

$$H + O_2 \rightleftharpoons OH + O \qquad (-A132)$$

$$OH + CH_3 \rightleftharpoons CH_2OH + H \qquad (-A10)$$

$$CH_2OH + M \rightleftharpoons CH_2O + H. \qquad (A15)$$

This regime is also characterized by the appearance of reaction (A168),

$$CH_3 + N \rightleftharpoons H_2CN + H, \qquad (A168)$$

as a competitor for nitrogen atoms, competing favorably with reaction (A234),

$$N + OH \rightleftharpoons NO + H. \qquad (A234)$$

The dissociation of H_2CN following reaction (A168) results in the formation of hydrogen cyanide, rather than nitric oxide, from the N atom.

Since the measured NO levels for $\phi > 1.6$ exceed the predicted TFN concentrations, it seems unlikely that the discrepancy between the measured and predicted NO concentrations under very rich conditions is due to failure of the parts of the mechanism that result in interconversion of HCN and NO. More likely, the discrepancy is due either to experimental error, to an additional source of CH or an additional nitrogen fixing reaction for $\phi > 1.4$, or to an inadequate description of chain-branching/chain-terminating processes in this regime.

To illustrate the relative contributions of the thermal and hydrocarbon–nitrogen mechanisms to NO formation, we have performed a series of calculations for an isothermal flow reactor and for a premixed laminar flame. The isothermal calculations are for a rich (13% methane in air) mixture ($\phi = 1.37$) at various temperatures. The flame calculations are for adiabatic conditions at various equivalence ratios.

The results of the flow reactor calculations are shown in Figs 12 and 13. In Fig. 12, the NO formation rates calculated with the complete reaction mechanism are compared with the previously discussed calculations in which the prompt-NO initiation reactions were deleted from the mechanism.

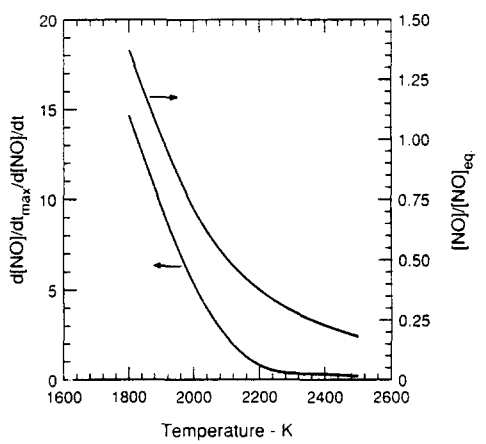

FIG. 12. The contribution of prompt NO reactions to NO formation in the isothermal reaction of 13% methane in air ($\phi = 1.37$). The lower curve is the ratio of the maximum NO formation rate calculated using the complete reaction mechanism of Appendix A to the rate calculated with the prompt NO initiation reactions deleted. The upper curve is the ratio of the NO concentration at the time of the maximum NO formation rate calculated using the complete mechanism to the equilibrium NO concentration.

In Fig. 13, sensitivity coefficients for NO are shown for 1800 K and 2500 K. At low temperatures ($T < 2000$ K), the rate of NO formation is dominated by the hydrocarbon–nitrogen prompt-NO channel. As the temperature increases, the relative importance of the hydrocarbon–nitrogen prompt-NO channel decreases, so that for temperatures above 2500 K, NO formation is controlled mainly by the thermal mechanism. The contribution of the hydrocarbon–nitrogen channel to NO formation may be quantified by comparing the calculated NO concentration at the

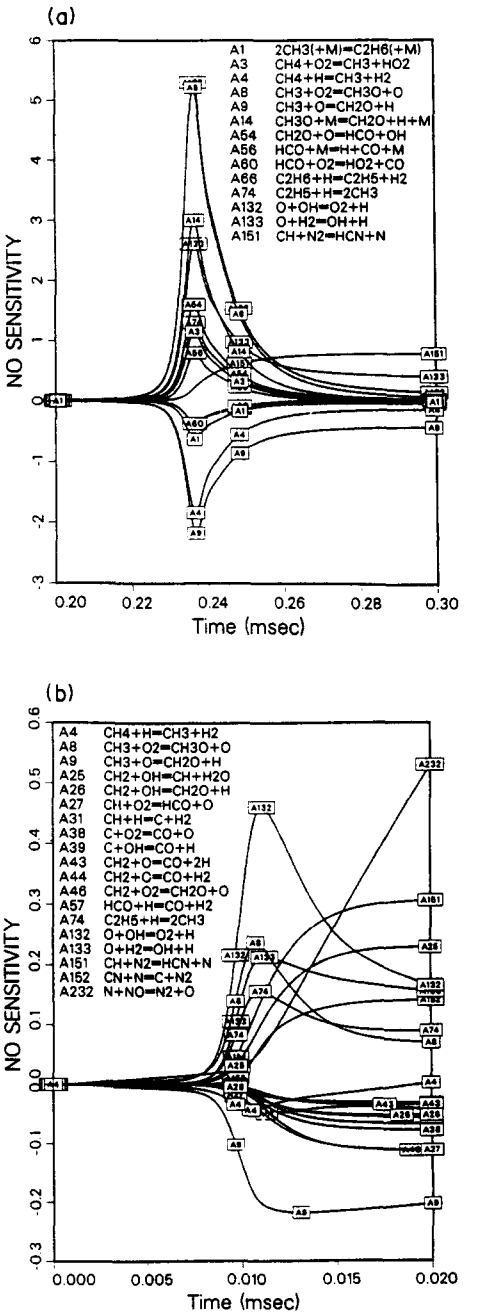

FIG. 13. Sensitivity plot of selected reactions for NO for the isothermal reaction of 13% methane in air ($\phi = 1.37$): (a) $T = 1800$ K; (b) $T = 2500$ K.

time of maximum NO formation rate with equilibrium NO concentrations (Fig. 12). At low temperatures, this channel produces NO levels in excess of equilibrium levels, while, at temperatures above 2500 K, this channel contributes only slightly to overall NO formation.

The temperature, O-atom, NO, and HCN flame profiles calculated for the same methane/air mixture as in the flow-reactor calculations, are shown in Fig. 14. Under these conditions, all the NO formed is from the hydrocarbon–nitrogen mechanism. Even though the O-atom concentration exceeds the final equilibrium value by a factor of 700, the temperatures in the flame where the superequilibrium O-atoms are achieved are so low that the thermal mechanism is ineffective in producing prompt NO. This appears to be a general observation for flames—superequilibrium O-atom concentrations are not a very important source of prompt NO *in flames* because of the low temperatures at which they occur.

In Fig. 14 the peak HCN mole fraction in the flame is more than half of the value of the final NO mole fraction farther downstream (approximately 15 ppm HCN compared to 27 ppm NO). This occurs because HCN is produced both directly by reaction (A151), $CH + N_2 \rightarrow HCN + N$, and indirectly by reaction of nitrogen atoms with methyl radicals,

$$N + CH_3 \rightleftharpoons H_2CN + H \qquad (A168)$$

$$H_2CN + M \rightleftharpoons HCN + H + M. \qquad (A155)$$

Only when the methyl concentration drops off sufficiently is the nitrogen atom oxidized directly to NO. Consequently, most of the NO formed comes from an HCN intermediate. Under relatively rich conditions, the HCN → NO conversion is not very rapid and the resulting NO is not very 'prompt,' even though the hydrocarbon–nitrogen mechanism is the dominant source of NO. It is also worth noting that the relatively constant downstream value of the NO mole fraction is about a factor of 3.4 higher than the adiabatic equilibrium value.

The mechanism of CH formation in the flame calculations is very similar to that in the well-stirred reactor calculations. The principal difference is that, for any equivalence ratio, a somewhat greater portion of the CH comes from CH_2 that has been formed via the C_2 hydrocarbon route in the flame than in the well-stirred reactor. Figure 15 shows the NO sensitivity coefficients for the flame of Fig. 14. Large positive sensitivities occur for reaction (A151), $CH + N_2 \rightarrow HCN + N$, and for reactions that produce CH from CH_2. Large negative sensitivities arise for reactions that channel methyl through non-CH-producing sequences and from the reaction of CH with water,

$$CH + H_2O \rightleftharpoons CH_2O + H, \qquad (A32)$$

which is an important sink for CH in the flame.

To illustrate the transition from the prompt (hydrocarbon–nitrogen) NO mechanism to the thermal mechanism in premixed flames as conditions become leaner, NO profiles are plotted in Fig. 16 for a series of methane/air flames. The conditions shown range from 13% methane (ϕ = 1.37) to 10% methane (ϕ = 1.06). Over this range of equivalence ratios, the NO formation mechanism changes from completely hydrocarbon–nitrogen to predominantly thermal. The origin of the term 'prompt NO' is most obvious in the 11% methane case, where there clearly are two time (or length) scales for NO formation. Approximately 10 ppm are formed very quickly in the reaction zone; the remainder is formed much more slowly downstream. An examination of the NO sensitivity plot for this flame in Fig. 17 shows that the prompt NO formation arises from the $CH + N_2 \rightarrow HCN + N$ reaction, whereas the slower increase in NO later in

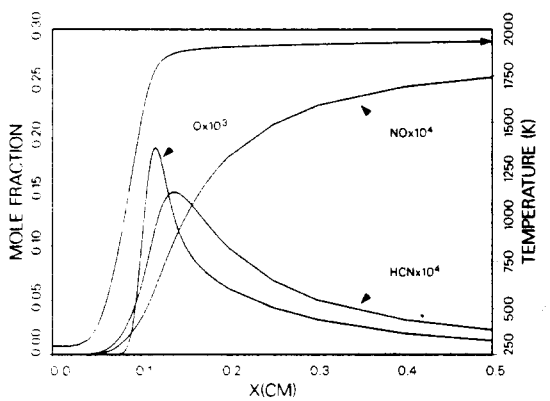

FIG. 14. Calculated temperature, O-atom, NO and HCN profiles for an atmospheric-pressure flame of 13% methane in air (ϕ = 1.37).

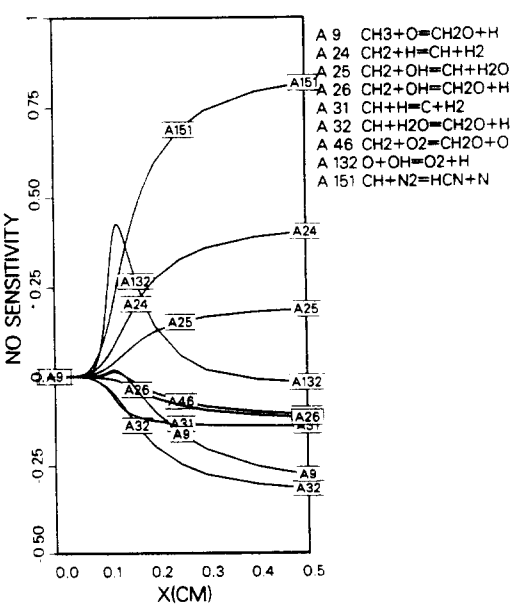

FIG. 15. Sensitivity plot for NO for the flame of Fig. 14.

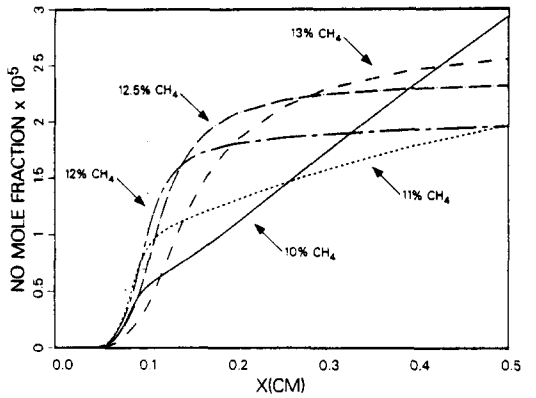

FIG. 16. Nitric oxide mole fraction profiles as a function of equivalence ratio for atmospheric pressure flames of methane in air.

the flame is controlled by the O + N_2 → NO + N reaction.

Figures 12 and 13 suggest that, for flow reactor or shock tube conditions, the contribution of the thermal-NO mechanism to NO formation in rich hydrocarbon–air mixtures is relatively small at low temperatures, and most of the NO is formed by the hydrocarbon–nitrogen prompt NO channel. At high temperatures, the importance of the hydrocarbon–nitrogen prompt NO channel decreases, and for temperatures above 2500 K most of the NO is formed by the thermal mechanism, which is accelerated by superequilibrium concentrations of O and OH. This behavior is to be contrasted with that observed in the flame calculations, where superequilibrium concentrations of O and OH in the flame zone do not significantly accelerate NO formation by the thermal mechanism because of the relatively low temperatures that occur in the flame zone, and where most of the in-flame NO is produced by the hydrocarbon–nitrogen mechanism.

5. NO PRODUCTION FROM FUEL NITROGEN

A principal source of nitrogen oxide emissions in the combustion of fossil fuels is the nitrogen chemically bound in the fuel. This 'fuel nitrogen' is a particularly important source of nitrogen oxide emissions for coal and coal-derived fuels, which typically contain 0.5–2.0% nitrogen by weight. Measurements on laboratory-scale burners with a variety of model fuel–nitrogen compounds, such as methacrylonitrile, methylamine, pyridine, and quinoline, indicate that the extent of conversion of fuel nitrogen to NO is nearly independent of the identity of the model compound, but is strongly dependent on the local combustion environment (temperature and stoichiometry) and on the initial level of nitrogen compound in the fuel–air mixture.[44] Available data also suggest that the gas-phase fuel–nitrogen reaction sequence is initiated by a rapid and nearly quantitative conversion of the parent fuel nitrogen compounds to hydrogen cyanide and ammonia.[45–51]

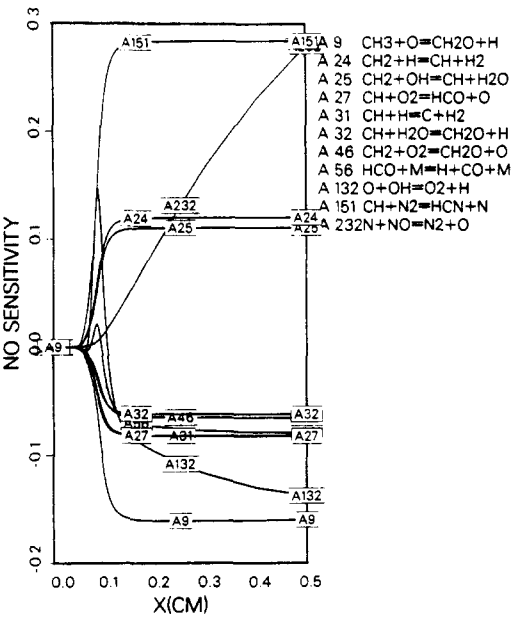

FIG. 17. Sensitivity plot for NO for an atmospheric pressure, 11% methane in air flame (ϕ = 1.16).

Hydrogen cyanide appears to be the principal product when the fuel nitrogen is bound in an aromatic ring, ammonia when the fuel nitrogen is in the form of amines. Hence, a reaction mechanism for NO production from fuel nitrogen involves reactions important in the oxidation of HCN and NH_3. As in the case of prompt NO, the reaction mechanism is shown in Fig. 11.

5.1. *The Oxidation of Hydrogen Cyanide*

An important aspect of both prompt-NO and NO formation from fuel nitrogen is the conversion of hydrogen cyanide to NO. In order to observe this process in relative isolation, Miller *et al.*[10] studied three $H_2/O_2/Ar$ flames (ϕ = 0.5, 1.0, 1.5) at low pressure to which were added 1 or 2% hydrogen cyanide. Under such conditions, in which the only source of elemental carbon is HCN, even the profiles of CO and CO_2 contain information about the nitrogen chemistry. A comparison of the predictions of the present model, which is essentially the same as that of Miller *et al.*, with these experimental results for all the stable nitrogen- and carbon-containing species is shown in Figs 18–20. The agreement between model and experiment is remarkably good.

Analysis of the computed results indicates that the reaction sequence indicated by the bold arrows in Fig. 21 is the dominant mechanism for converting HCN to NO and N_2 in all three flames. Sensitivity profiles for HCN and NO are shown in Figs 22 and 23 for the rich flame. The HCN removal is controlled by the reaction of HCN with oxygen atoms,

$$\text{HCN} + \text{O} \rightleftharpoons \text{NCO} + \text{H} \qquad \text{(A176)}$$

$$\text{HCN} + \text{O} \rightleftharpoons \text{NH} + \text{CO}, \qquad \text{(A177)}$$

even in the rich flame. Subsequent reactions of NCO

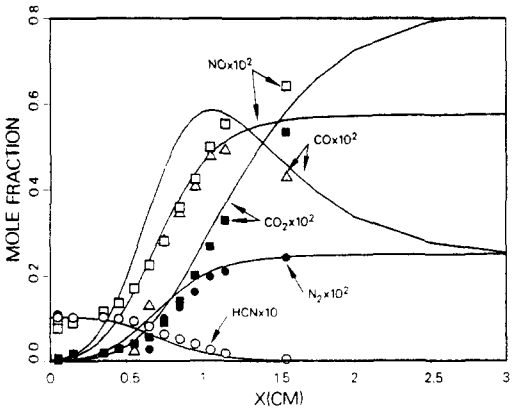

FIG. 18. Comparison of model predictions with the experimental data of Miller *et al.*[10] for a lean (ϕ = 0.5) H_2/O_2/Ar flame (P = 25 torr) to which 1% HCN was added.

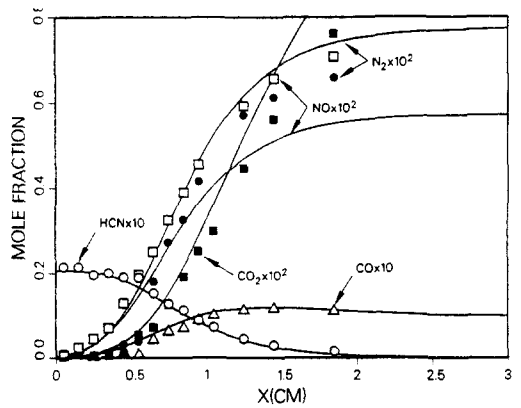

FIG. 19. Comparison of model predictions with the experimental data of Miller *et al.*[10] for a stoichiometric H_2/O_2/Ar flame (P = 25 torr) to which 2% HCN was added.

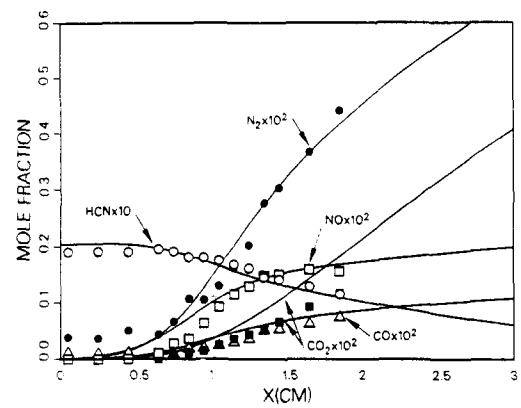

FIG. 20. Comparison of model predictions with the experimental data of Miller *et al.*[10] for a rich (ϕ = 1.5) H_2/O_2/Ar flame (P = 25 torr) to which 2% HCN was added.

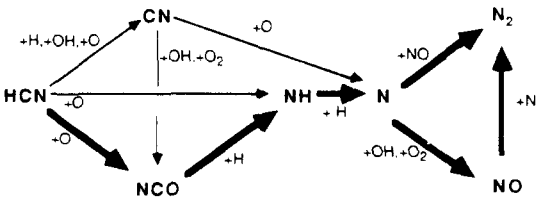

FIG. 21. Reaction path diagram illustrating the reaction mechanism by which HCN is converted to NO and N_2 in the low-pressure flames of Miller *et al.*[10] The bold lines indicate the most important reaction paths.

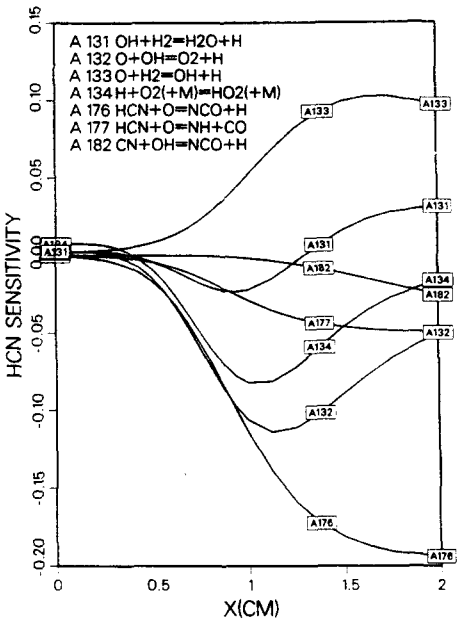

FIG. 22. Sensitivity plot for HCN in the rich flame of Fig. 20.

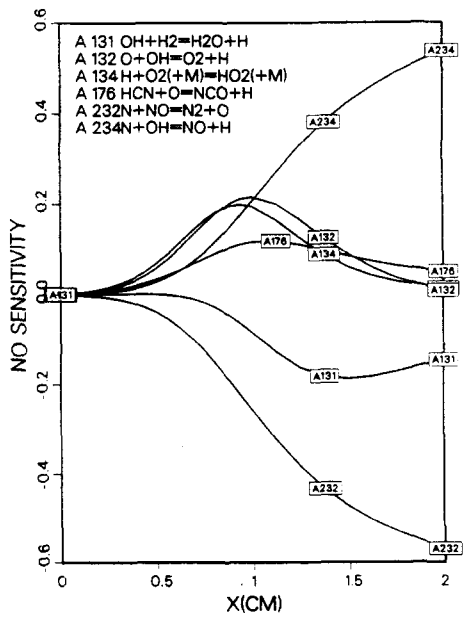

FIG. 23. Sensitivity plot for NO in the rich flame of Fig. 20.

and NH with hydrogen atoms, producing N, are relatively fast and have little influence on the observed species profiles. The distribution of NO and N_2 in the flame is governed by the N-atom reactions,

$$N + OH \rightleftharpoons NO + H \quad (A234)$$

$$N + NO \rightleftharpoons N_2 + O. \quad (A232)$$

In studying hydrogen cyanide decay in the postflame gases of very rich atmospheric-pressure flames, Haynes,[49] Morley[50,51] and Fenimore[52] concluded that HCN is removed primarily by reaction with OH. Two channels were suggested by these investigators, one that is first order in OH,

$$OH + HCN \rightleftharpoons HOCN + H, \quad (A172)$$

and one that is second order,

$$OH + HCN \rightleftharpoons CN + H_2O \quad (A171)$$

$$CN + OH \rightleftharpoons NCO + H, \quad (A182)$$

under the partially equilibrated conditions prevalent in the postflame gases of atmospheric-pressure flames. Because of the equilibration of the HCN → CN conversion, the rate of the second-order process is governed by reaction (A182). Haynes concluded that the first of these channels was dominant below 2300 K, the latter above 2300 K. It is of interest to note that the O + HCN reactions, (A176) and (A177), are also second order in the OH concentration under these conditions because of the relationship between O and OH in partial equilibrium.

Several theoretical and experimental investigations[30,31,53,55–58] have helped to reconcile the seemingly disparate conclusions of Miller *et al.* and those of Haynes, Morley, and Fenimore. The reactions of interest, the first-order O + HCN and the OH + HCN reactions, are complicated processes involving multiple potential wells and multiple product channels. Reaction coordinate diagrams based on BAC-MP4 calculations for the two processes are shown in Figs 24 and 25. Miller *et al.*[31] and Miller and Melius[53] have used the BAC-MP4 results and statistical-theoretical methods, modeling the intramolecular dynamics as stochastic processes, to predict rate coefficients for the various elementary steps of interest. For O + HCN the steps are reactions (A176) and (A177); for OH + HCN three channels are possible,

$$OH + HCN \rightleftharpoons HOCN + H \quad (A172)$$

$$OH + HCN \rightleftharpoons HNCO + H \quad (A173)$$

and

$$OH + HCN \rightleftharpoons NH_2 + CO. \quad (A174)$$

For O + HCN a comparison of the total rate coefficient predicted by the theory with the experimental results of Davies and Thrush,[54] Perry and Melius,[30] and Roth *et al.*[55] is shown in Fig. 26. The agreement is excellent, particularly when a minor modification is made to the barrier height for adding

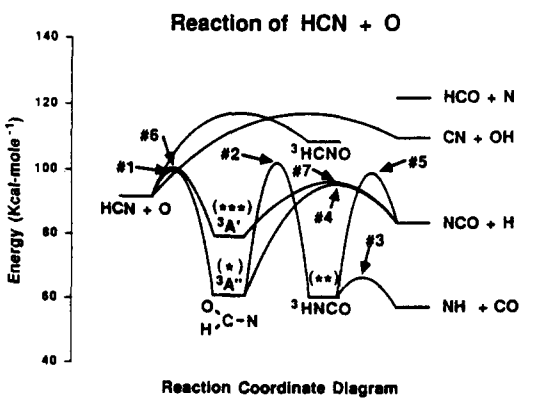

FIG. 24. Reaction coordinate diagram from BAC-MP4 calculations for the reaction O + HCN → products.

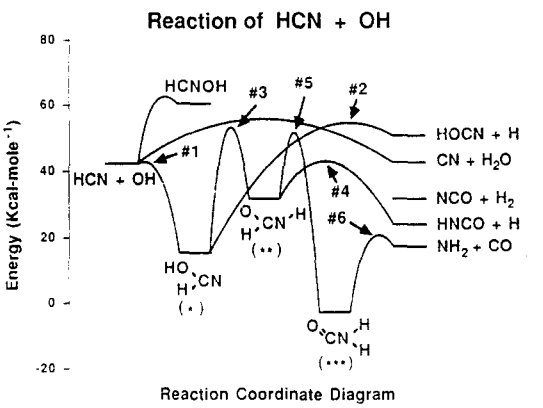

FIG. 25. Reaction coordinate diagram from BAC-MP4 calculations for the reaction OH + HCN → products.

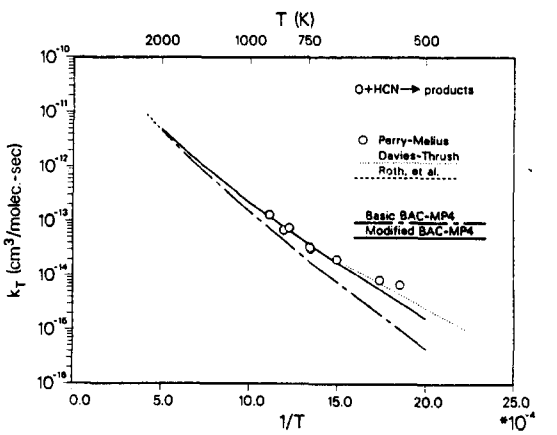

FIG. 26. Comparison with experiment of the theoretical prediction of Miller *et al.*[31] for the total rate coefficient, $k_{A176} + k_{A177}$, of the reaction HCN + O → products.

O to HCN.[31] For the specific channels, the theory accurately predicts the experimental results of Louge and Hanson[56] for k_{A176} and those of Szekely *et al.*[57] for k_{A177}. The rate coefficient expressions in the mechanism are consistent with both the theoretical and experimental results.

For the OH + HCN reaction there is very little experimental data available. In fact, the only relevant data are from the flame experiments discussed above. Figure 27 compares the theoretical prediction for the total rate coefficient, $k_T = k_{A172} + k_{A173} + k_{A174}$, with the experimental results, which are sensitive only to this sum. The agreement between theory and experiment is remarkably good. The rate expressions in the present model are based on the theoretical results, which show $k_{A172} > k_{A173} > k_{A174}$ under most combustion conditions.

For k_{A182} (CN + OH → NCO + H (A182)), which controls the rate of the process that is second order in OH, we have adopted the Haynes[49]/Morley[50] rate coefficient without modification. However, it is possible that their determination of this rate coefficient was hampered to some extent by interference from the O + HCN reaction, which would also be second order in OH under their experimental conditions.

Both the O + HCN and the OH + HCN reactions have direct hydrogen abstraction channels that should be considered,

$$O + HCN \rightleftharpoons CN + OH \qquad (A178)$$

and

$$OH + HCN \rightleftharpoons CN + H_2O. \qquad (A171)$$

Reaction (A178) is quite endothermic and slow,[31,57] it is never very important to HCN removal under normal combustion conditions. In contrast, however, reaction (A171) is relatively fast at combustion temperatures. Figure 27 shows a comparison of the theoretical prediction for k_{A171} of Miller and Melius with the experimental expression given by Szekely *et al.*[58] (used in the present mechanism), which is based on their experimental data for the reverse reaction at high temperature (2460 K < T < 2840 K) and the lower-temperature (500 K < T < 700 K) data for the forward reaction of Fritz *et al.*[59] Although the agreement between theory and experiment is not as good as one might hope, both indicate that the abstraction is the fastest of the OH + HCN channels. This result limits the conditions under which the other OH + HCN steps, reactions (A172)–(A174), can be effective in removing HCN to those where the abstraction reaction (A171) is nearly equilibrated.

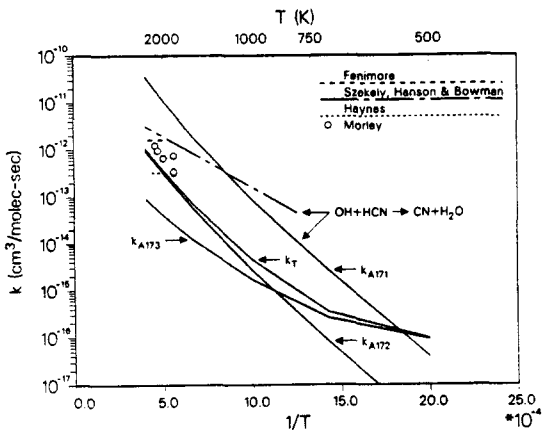

FIG. 27. Comparison with experiment of the theoretical prediction of Miller and Melius[53] for the total rate coefficient. $k_T = k_{A172} + k_{A173} + k_{A174}$, of the reaction OH + HCN → products. Also shown are predictions and experiments for reaction (A171), OH + HCN → CN + H_2O.

The present kinetics model incorporates the experimental observations of Miller *et al.* and those of Haynes, Morley, and Fenimore about HCN removal. What conditions favor the different mechanisms? Experience in modeling a variety of flame, stirred reactor, and flow reactor conditions indicates that the O + HCN sequence shown in Fig. 21 almost always plays the major role. The OH + HCN reactions normally come into play only under conditions that are both rich and nearly equilibrated. If HCN conversion takes place in a highly nonequilibrium reaction zone, even under very rich conditions, the O + HCN sequence still is likely to be dominant.

5.2. *The NO → HCN → N_2 Mechanism*

As noted by many investigators,[60–63] in rich combustion systems there is the possibility of reaction of NO with hydrocarbon free radicals, leading to the formation of hydrogen cyanide and, eventually, of molecular nitrogen. Moreover, Myerson[60,62] and Wendt and coworkers[61] have suggested that processes in which CH_i + NO reactions are significant can be utilized as effective NO_x control strategies. One such practical control technique is reburning,[64,65] which is based on the early work of Myerson and Wendt *et al.*

The principal objective of this section is to identify the mechanism by which the NO → HCN → N_2 conversion is accomplished under combustion conditions. To this end we consider first the low-pressure premixed flame experiments of Thorne *et al.*[12] In these experiments, the flames are nominally the rich, ϕ = 1.5, H_2/O_2/Ar flame of Miller *et al.*,[10] to which small quantities of acetylene, hydrogen cyanide, and nitric oxide were added in various combinations. Acetylene was used as the hydrocarbon because of the ease with which it yields low molecular weight hydrocarbon free radicals through the O + C_2H_2 reaction.[12]

Figure 28 shows a comparison of the model predictions with the experimental data of Thorne *et al.* for the nitrogen-containing species in the flame to which

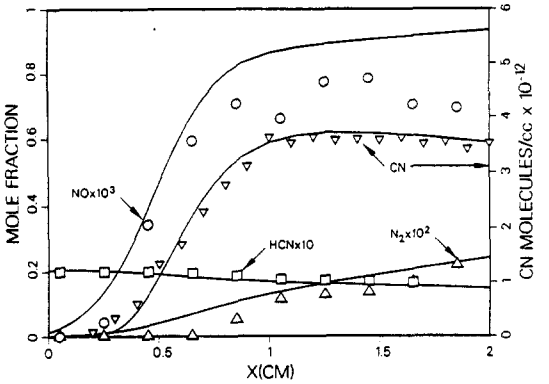

FIG. 28. Comparison of model predictions with the experiments of Thorne *et al.*[12] for a rich (ϕ = 1.5) H_2/O_2/Ar flame at 25 torr to which 2% C_2H_2 and 2% HCN were added.

2% acetylene and 2% hydrogen cyanide were added. The agreement between model and experiment is very good. An analysis of the computation shows that the HCN → NO → N_2 conversion mechanism in this flame is the same as that for the case where there is no acetylene addition, i.e. there is no direct interaction between the hydrocarbon and nitrogen chemistry in this flame.[12] The most important feature of the flame is the CN profile, whose measurement requires a single calibration factor to yield number density from the LIF (laser-induced fluorescence) signal. In fact, a single calibration factor makes quantitative the CN measurements in all the flames considered by Thorne *et al.*[12] This calibration factor can be obtained by noting that CN becomes nearly equilibrated with HCN by reactions of the type,

$$\mathrm{HCN} + Y \rightleftharpoons \mathrm{CN} + \mathrm{H}Y,$$

where Y = H, OH, or O, at distances above the burner greater than about 1.6 cm. This can be seen from Fig. 29, where the function $f_i(x)$,

$$f_i(x) = \frac{X_{CN} X_{HY}}{X_{HCN} X_Y} / K_i, \qquad (5.1)$$

is plotted for the reactions of interest. In this equation, the subscript i denotes the i^{th} reaction ((A171), (A178), or (−A179)) and K_i denotes its equilibrium constant. The proximity of f_i to unity measures the degree to which each reaction is equilibrated. Since the hydrocarbon and nitrogen chemistry are decoupled in this flame, and since the CN is equilibrated with the HCN sufficiently high above the burner surface, the CN concentration at these heights is governed simply by thermochemistry, by the rate coefficient for the O + HCN reaction (i.e. $k_{A176} + k_{A177}$), and by the rate coefficients of several reactions in the H_2/O_2 chemistry. Since the values of these parameters are known to good accuracy, the computed CN number density at 2 cm above the burner was used to calibrate all the CN LIF measurements of Thorne *et al.* With this calibration factor the agreement between model and experiment for CN number density in Fig. 28 is almost perfect.

The more interesting experiments performed by Thorne *et al.* are the ones in which acetylene and nitric oxide were added to the basic H_2/O_2/Ar flame. A comparison of the model predictions with these flame data for the nitrogen-containing species are shown in Figs 30 and 31. The CN LIF data in these experiments

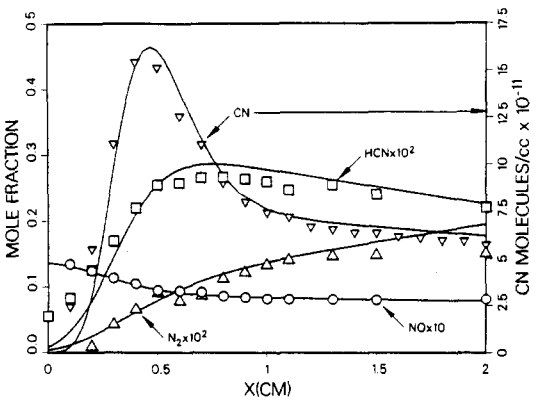

FIG. 30. Comparison of model predictions with the experiments of Thorne *et al.*[12] for a rich (ϕ = 1.5) H_2/O_2/Ar flame at 25 torr to which 1.97% C_2H_2 and 1.35% NO were added.

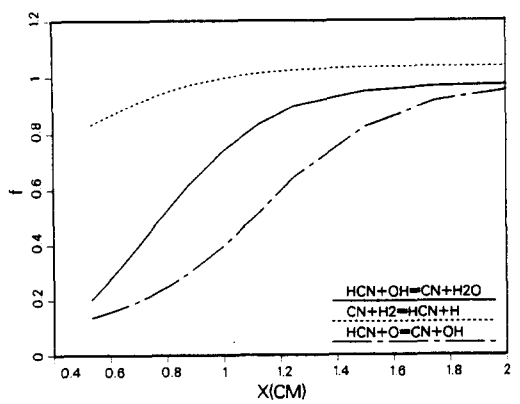

FIG. 29. Degree of equilibration of the reactions HCN + $Y \rightleftharpoons$ CN + HY, where Y is H, OH, or O. The function $f_i(x)$ is defined in Eq. (5.1).

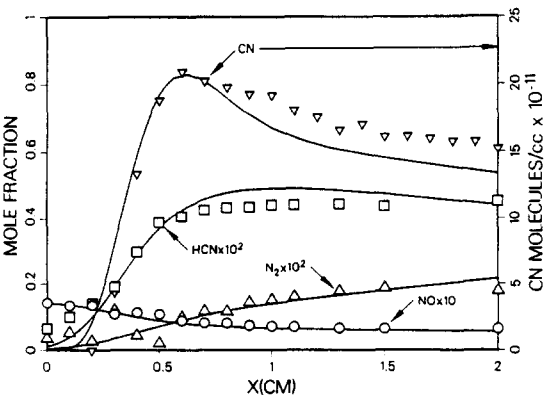

FIG. 31. Comparison of model predictions with the experiments of Thorne *et al.*[12] for a rich (ϕ = 1.5) H_2/O_2/Ar flame at 25 torr to which 2.9% C_2H_2 and 1.4% NO were added.

were converted to number densities using the calibration factor determined above. Again the agreement between model prediction and experiment is excellent. Both show the initial conversion of the NO to HCN and CN and the subsequent formation of N_2 on a slower time scale.

Sensitivity profiles for NO, CN and HCN in the flame of Fig. 30 are shown in Figs 32–34; sensitivity profiles for the other flame are similar. The most surprising feature of these flames is the sharp peak in the CN number density at about 4 mm above the burner. This peak is reproduced by the model only if the NO conversion results in CN as a precursor to HCN a substantial fraction of the time (more than half). The sensitivity analysis shows that the CN is produced and destroyed in this region of the flame by the sequence

$$C + NO \rightleftharpoons CN + O \qquad (A156)$$

$$CN + H_2 \rightleftharpoons HCN + H. \qquad (A179)$$

The main reaction paths involved in converting NO to N_2 through HCN and CN are shown in Fig. 35. The improvement in the agreement between the model calculations and the experimental data, particularly in the CN profile of Fig. 31, over that reported by Thorne *et al.* is due to the increased importance in the present model of the $C_2H_2 \rightarrow$ HCCO path, followed by the sequence.

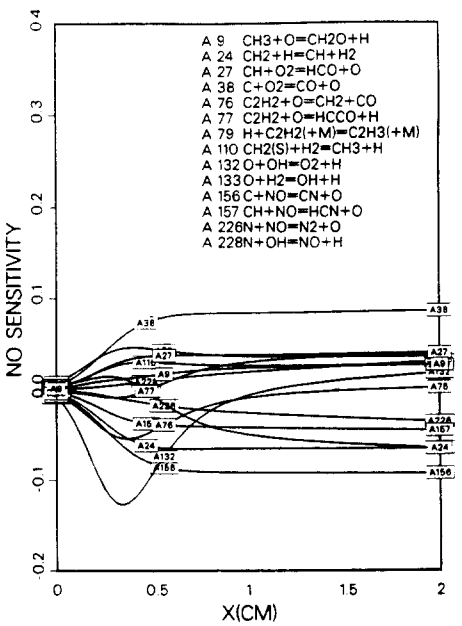

FIG. 32. Sensitivity plot for NO for the flame of Fig. 30.

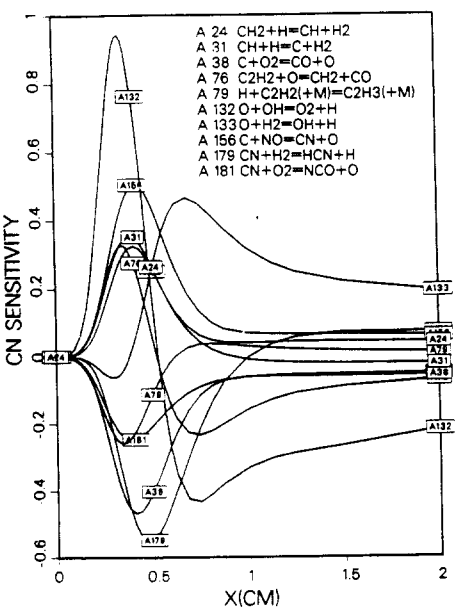

FIG. 33. Sensitivity plot for CN for the flame of Fig. 30.

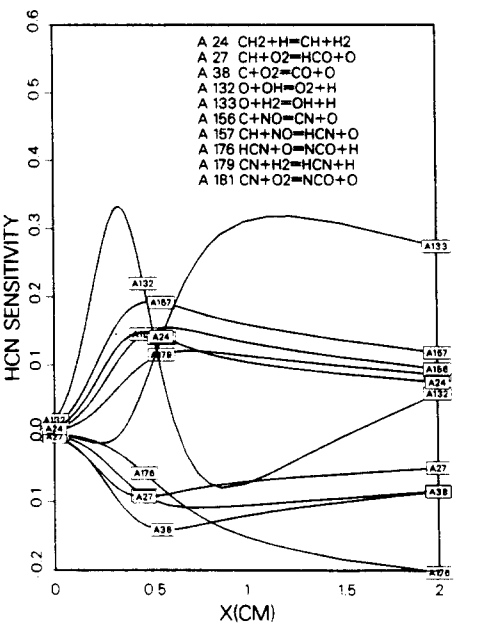

FIG. 34. Sensitivity plot of selected reactions for HCN for the flame of Fig. 30.

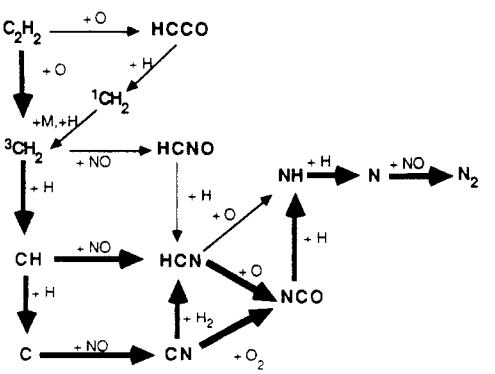

FIG. 35. Reaction path diagram illustrating the NO → HCN → N_2 conversion mechanism in the NO-added flames of Thorne *et al.*[12] The bold lines indicate the most important reaction paths.

$$H + HCCO \rightleftharpoons {}^1CH_2 + CO \quad (A101)$$

$$^1CH_2 + H_2 \rightleftharpoons CH_3 + H. \quad (A110)$$

Reaction (A110) is very fast[66] and inhibits the formation of CH and C (and thus CN) early in the flame. In addition to the sequence involving carbon atoms, HCN is produced directly by the reaction,

$$CH + NO \rightleftharpoons HCN + O. \quad (A157)$$

Hydrogen cyanide is partially converted to N_2 in the flame by the reaction sequence discussed above,

$$O + HCN \rightleftharpoons NCO + H \quad (A176)$$

$$NCO + H \rightleftharpoons NH + CO \quad (A192)$$

$$NH + H \rightleftharpoons N + H_2 \quad (A211)$$

$$N + NO \rightleftharpoons N_2 + O. \quad (A232)$$

In the calculations the CN peak of Fig. 30 occurs as a result of the reaction between carbon atoms and nitric oxide. However, there is another possibility—the reaction between CH and NO could produce CN + OH directly. Reaction (A157), CH + NO → HCN + O, cannot occur adiabatically on the ground-state singlet surface since it does not conserve electron spin, but the CN + OH product channel can. Figure 36 shows estimated potential energy parameters involved in the two reactions on the singlet surface. Unfortunately, the high points along the reaction coordinates of the two reactions are too close together to draw a definitive conclusion about the CN + OH channel. The situation is complicated even further by the possibility of reaction (A157), the HCN + O channel, also occurring on a triplet surface. For the present we must acknowledge both possibilities for the early CN formation in Fig. 30,

$$C + NO \rightleftharpoons CN + O \quad (A156)$$

and

$$CH + NO \rightleftharpoons CN + OH,$$

although the model includes only reaction (A156).

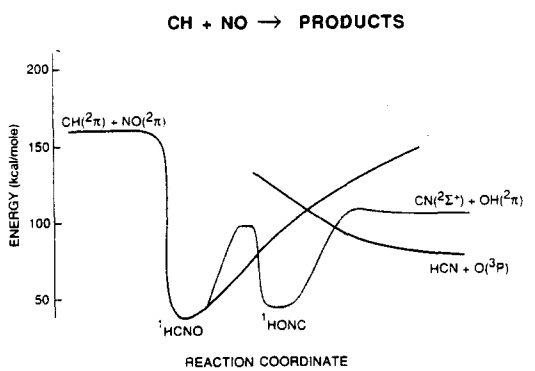

FIG. 36. Hypothetical reaction coordinate diagram for the reaction CH + NO → products. The intersection between the singlet and triplet surfaces is based on a similar intersection for N_2O (isoelectronic). The barrier for the 1,3 hydrogen shift is estimated to be the same as that for CH_3NO determined by BAC-MP4 calculations.

The temperatures and pressure in the flame experiments of Thorne *et al.* are lower than are encountered in typical reburning situations, and it is possible that reaction channels other than those discussed above play a role in NO removal by reburning. Roby and Bowman[174] have shown that in atmospheric-pressure, fuel-rich $H_2/O_2/Ar$ flames to which small amounts of nitric oxide were added, significant removal of the NO ($\simeq 40\%$) occurs by the reaction sequence,

$$H + NO + M \rightleftharpoons HNO + M \quad (-A228)$$

$$HNO + H \rightleftharpoons NH + OH \quad (-A208)$$

$$NH + H \rightleftharpoons N + H_2 \quad (A211)$$

$$N + NO \rightleftharpoons N_2 + O. \quad (A232)$$

Seery and Zabielski[175] have reported significant NO removal in a low-pressure, fuel-rich $H_2/O_2/Ar$ flame to which nitric oxide was added, although Cattolica[176] reported no NO removal in a fuel-rich $H_2/O_2/Ar$ flame at an identical pressure but much lower temperatures. Roby and Bowman observed additional NO removal when small amounts of acetylene were added to the atmospheric-pressure, fuel-rich $H_2/O_2/NO/Ar$ flame. This additional NO removal was attributed to the CH_i + NO reaction sequence discussed above. However, in this flame, the principal NO-removal process still was the NO → HNO → N_2 sequence. Sarv and Cernansky[177] have suggested that the NO → HNO → N_2 sequence also may be important in NO removal in atmospheric-pressure, fuel-rich hydrocarbon–air flames. To examine the role of HNO reactions in NO removal in hydrocarbon flames, we have performed a calculation for a fuel-rich (ϕ = 1.37) atmospheric-pressure methane–air flame to which 1000 ppmv of NO was added. The calculated temperature and the NO and HCN concentration profiles are shown in Fig. 37, and the NO sensitivity profile is shown in Fig. 38. A significant amount of the input NC is removed in this flame and a significant amount of HCN is formed. Sensitivity analysis shows that the NO removal occurs primarily by the NO → HCN → N_2 mechanism, with only a small contribution from the NO → HNO → N_2 mechanism. Hence, the present model suggests that in hydrocarbon flames and in reburning with hydrocarbon fuels, the primary NO-removal process is NO → HCN → N_2. Further progress in modeling NO removal in flames requires more accurate kinetic

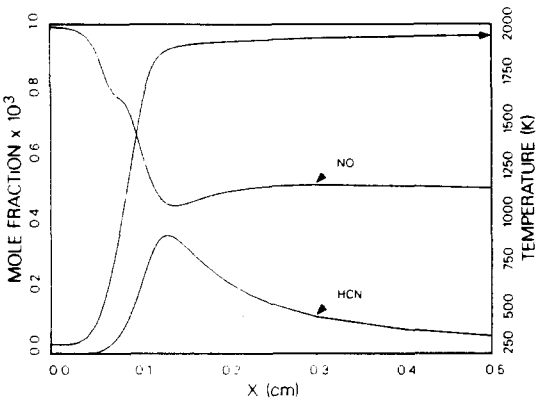

FIG. 37. Calculated temperature, NO and HCN profiles for an atmospheric-pressure, 13% methane in air flame (ϕ = 1.37) to which 1000 ppmv NO was added.

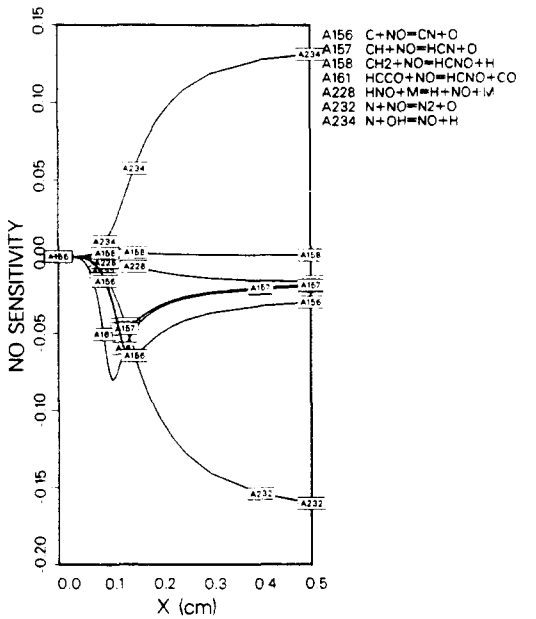

FIG. 38. Sensitivity plot for NO for the flame of Fig. 37.

data on reactions between carbon-containing radicals and NO, notably (A156)–(A158) and (A161), and on reaction (−A228), H + NO + M ⇌ HNO + M, at combustion temperatures.

5.3. *The Oxidation of NH_3*

In this section, we discuss the mechanism of ammonia conversion to NO, as well as some additional features of fuel-nitrogen chemistry in combustion. In discussing ammonia oxidation, we restrict ourselves to considering NH_3/O_2 flames. Miller *et al.*,[15] as well as others[67–70,84] have discussed NH_3 oxidation in flames previously. Since the mechanism proposed here, Appendix B, is essentially the same as that of Ref. 15, the discussion will be brief.

Figure 39 outlines schematically the principal reactions by which ammonia is oxidized to nitric oxide and by which nitric oxide is converted to molecular nitrogen in NH_3/O_2 flames. In addition to the reaction steps shown in the diagram, there also are reactions forming N_2 that do not involve NO:[15,69,71,72]

$$NH_2 + NH \rightleftharpoons N_2H_2 + H \qquad \text{(B61)}$$

$$N_2H_2 + M \rightleftharpoons NNH + H + M \qquad \text{(B64)}$$

$$N_2H_2 + H \rightleftharpoons NNH + H_2 \qquad \text{(B65)}$$

and

$$NNH \rightleftharpoons N_2 + H \qquad \text{(B43/A221)*}$$

or

$$NNH + NO \rightleftharpoons N_2 + HNO. \qquad \text{(B44/A222)}$$

This reaction sequence, involving N_2H_i species, occurs even in moderately lean ammonia flames. However, its importance appears to be limited to flames for which elemental nitrogen is a *major* component of the fuel. Consequently, in most practical situations, where the fuel contains low levels of nitrogen, $NH_i + NH_j$ (i, j = 0, 1, 2) reactions are negligible.

The important features of the ammonia oxidation mechanism, Fig. 39, can be summarized as follows. Ammonia is converted to NH_2 by hydrogen abstraction. For most conditions, the primary abstraction reaction is

$$NH_3 + OH \rightleftharpoons NH_2 + H_2O. \qquad \text{(B40/A218)}$$

However, for lean conditions, reaction with oxygen atoms and for rich conditions, reaction with hydrogen

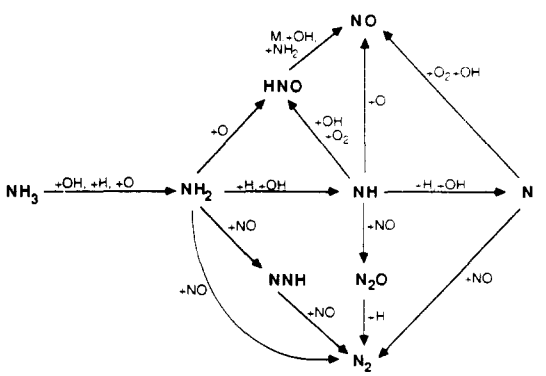

FIG. 39. Reaction path diagram for the oxidation of ammonia in flames.

* In this section, when a reaction in the Appendix B mechanism is also included in the Appendix A mechanism, both B and A numbers are given.

atoms also make significant contributions to NH_2 formation,

$$NH_3 + O \rightleftharpoons NH_2 + OH \quad \text{(B42/A220)}$$

$$NH_3 + H \rightleftharpoons NH_2 + H_2. \quad \text{(B41/A219)}$$

Successively smaller amine free radicals are formed by reaction with hydrogen atoms and to a lesser extent by reaction with OH,

$$NH_i + H(OH) \rightleftharpoons NH_{i-1} + H_2(H_2O), \quad i = 1, 2.$$

Each NH_i free radical can undergo subsequent reaction by one of two mechanisms:

(a) oxidation leading to NO formation;
(b) reaction with NO leading to the formation of molecular nitrogen.

The chemical identity of the NH_i free radical primarily responsible for determining the NO/N_2 product distribution depends on the equivalence ratio. For very lean flames, the critical amine free radical is NH_2, but as the equivalence ratio increases the greater abundance of hydrogen atoms results in a shift in the critical NH_i species from NH_2 to NH to N. Under most conditions, all three NH_i species play some role, although even in moderately rich flames the N-atom is dominant.

Amidogen (NH_2) is oxidized to NO through nitroxyl (HNO) by the reaction sequence,

$$O + NH_2 \rightleftharpoons HNO + H \quad \text{(B34/A212)}$$

$$HNO + M \rightleftharpoons NO + H + M \quad \text{(B50/A228)}$$

$$HNO + OH \rightleftharpoons NO + H_2O \quad \text{(B51/A229)}$$

$$HNO + NH_2 \rightleftharpoons NO + NH_3. \quad \text{(B53/A230)}$$

The formation of N_2 from NO by reaction with NH_2 occurs either directly,

$$NH_2 + NO \rightleftharpoons N_2 + H_2O, \quad \text{(B39)}$$

or through the NNH intermediate,

$$NH_2 + NO \rightleftharpoons NNH + OH \quad \text{(B38/A216)}$$

$$NNH \rightleftharpoons N_2 + H \quad \text{(B43/A221)}$$

$$NNH + NO \rightleftharpoons N_2 + HNO. \quad \text{(B44/A222)}$$

Imidogen (NH) can be oxidized to NO both directly,

$$NH + O_2 \rightleftharpoons NO + OH \quad \text{(B22/A201)}$$

$$NH + O \rightleftharpoons NO + H, \quad \text{(B33)}$$

and through nitroxyl,

$$NH + O_2 \rightleftharpoons HNO + O \quad \text{(B21/A200)}$$

$$NH + OH \rightleftharpoons HNO + H. \quad \text{(B29/A208)}$$

The reaction of NH with NO produces N_2O, which is converted to N_2 principally by reaction with hydrogen atoms,

$$NH + NO \rightleftharpoons N_2O + H \quad \text{(B23/A202)}$$

$$N_2O + H \rightleftharpoons N_2 + OH. \quad \text{(B24/A204)}$$

Reaction (B23) is the source of virtually all the N_2O that has been detected in ammonia flames.[15,67-69] The production and destruction of NO by nitrogen atoms occurs via the extended Zeldovich mechanism,

$$N + NO \rightleftharpoons N_2 + O \quad \text{(B56/A232)}$$

$$N + O_2 \rightleftharpoons NO + O \quad \text{(B57/A233)}$$

$$N + OH \rightleftharpoons NO + H. \quad \text{(B58/A234)}$$

Since the appearance of Ref. 15, several improvements in the kinetics model have been brought about by more reliable determinations of important rate parameters, and some rate-parameter estimates and conjectures have been placed on firmer ground. Most notably, the rate coefficients of the reactions of ammonia with OH,[73-75] H,[76-78] and O[73,79,80] have now been determined reliably over broad temperature ranges. Hack, Kurzke, and Wagner[81] have determined the rate coefficient of reaction (B22)

$$NH + O_2 \rightleftharpoons NO + OH \quad \text{(B22/A201)}$$

up to $T = 543$ K and have confirmed the products inferred theoretically from BAC-MP4 calculations.[82] This same group[83] has also measured the rate coefficient of reaction (B61),

$$NH_2 + NH \rightleftharpoons N_2H_2 + H, \qquad (B61)$$

at room temperature. Their k-value is consistent with the estimate made theoretically by Miller *et al.*[15,69] and values subsequently inferred at high temperature from shock tube[72] and flame[71] experiments.

To demonstrate the predictive capability of the ammonia oxidation mechanism of Appendix B, we have made comparisons of model predictions with the results of the low-pressure flame experiment reported recently by Bian, Vandooren, and Van Tiggelen.[70] Comparisons of model predictions with other ammonia flame data were reported previously in Ref. 15.

The comparisons between the model predictions and the experimental results are shown in Figs 40–44. Overall, the agreement between model and experiment is good. There is a discrepancy of approximately a factor of two between calculated and reported hydrogen atom concentrations; however, uncertainties in the measurement of hydrogen atoms by molecular beam mass spectrometry are of this order. The model calculations and the experiment agree

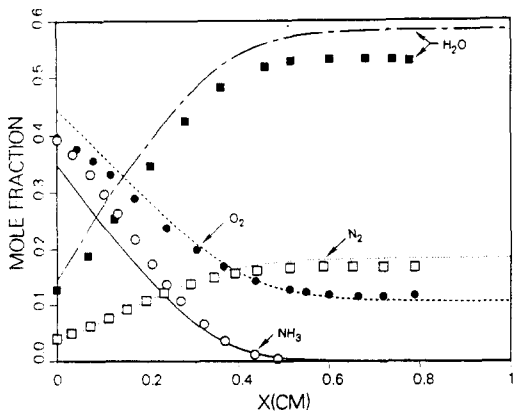

FIG. 40. Comparison of profiles of major species calculated using the mechanism of Appendix B with the data of Bian *et al.*[70] for a low-pressure (35 torr) NH_3–O_2–Ar (0.48/0.51/0.01) flame.

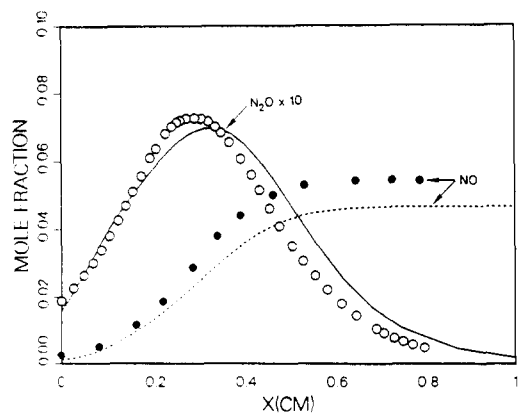

FIG. 41. Comparison of profiles of NO and N_2O calculated using the mechanism of Appendix B with the data of Bian *et al.*[70]

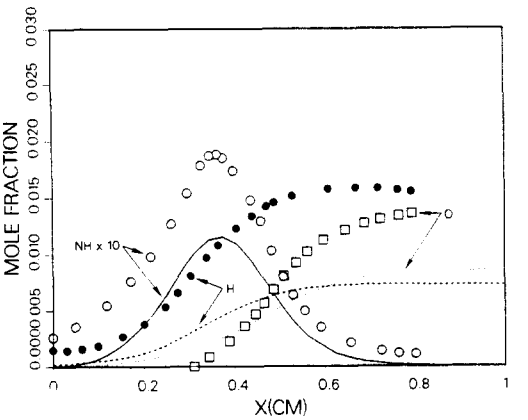

FIG. 42. Comparison of profiles of NH, H, and O calculated using the mechanism of Appendix B with the data of Bian *et al.*[70]

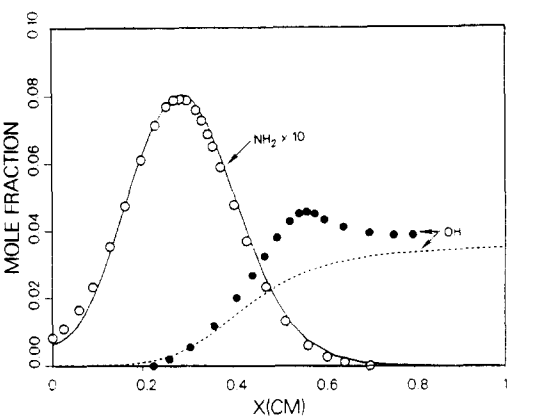

FIG. 43. Comparison of profiles of NH_2 and OH calculated using the mechanism of Appendix B with the data of Bian *et al.*[70]

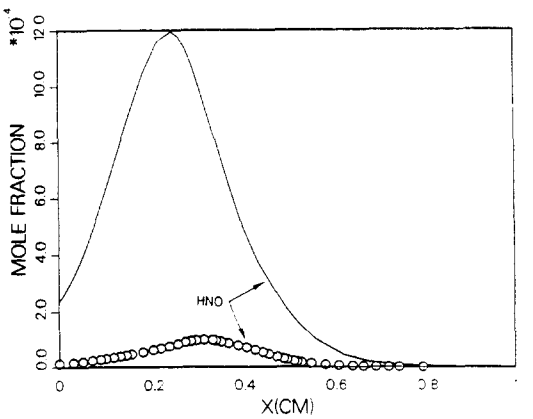

FIG. 44. Comparison of the HNO profiles calculated using the mechanism of Appendix B with the data of Bian *et al.*[70]

somewhat better for O and OH. Such differences are probably within the experimental uncertainty for molecular beam/mass spectrometric measurements of these free radicals. The agreement of model and experiment for the major stable species (NH_3, O_2, N_2, and H_2O) and for the oxides of nitrogen (NO and N_2O) is almost perfect. The amine free radical concentrations (NH_2 and NH) also are predicted very well by the model; a discrepancy of only 30% occurs for the maximum NH concentration, and the NH_2 profile is predicted almost perfectly everywhere. The most serious discrepancies occur for the HNO and the nitrogen atom. Figure 44 shows that the model predicts about an order of magnitude more HNO than is observed experimentally, and our prediction of 3×10^{-4} for the maximum nitrogen atom mole fraction is significantly higher than the experimentally determined upper limit of 1×10^{-5}. However, there appears to be no reasonable way in which the mechanism can be modified to improve the overall agreement. The intermediate species concentrations (free radicals, N_2O, and NO) are so strongly coupled that a change in the mechanism that has a large effect on one species profile normally has a large effect on several of the others.

Our main interest in this flame is the NO and N_2O profiles. Sensitivity plots for these species are presented in Figs 45 and 46. The NO in this flame is formed both through the nitroxyl route and by N-atom reactions. The main rate-controlling reactions are the formation of nitroxyl via reactions (B29) and (B34),

$$NH + OH \rightleftharpoons HNO + H$$

(B29/A208)

$$NH_2 + O \rightleftharpoons HNO + H.$$

(B34/A212)

and the N-atom reactions themselves.

$$N + O_2 \rightleftharpoons NO + O$$

(B56/A233)

$$N + OH \rightleftharpoons NO + H.$$

(B58/A234)

Early in the flame, the NO concentration also is influenced by the rate of HNO dissociation and by the chain branching step,

$$H + O_2 \rightleftharpoons OH + O.$$

(−B3/−A132)

The NO is removed primarily by reaction with nitrogen atoms,

$$N + NO \rightleftharpoons N_2 + O,$$

(B57/A232)

with only secondary contributions from the NH_2 + NO and NH + NO reactions.

The N_2O is formed by reaction (B23/A202)

$$NH + NO \rightleftharpoons N_2O + H$$

(B23/A202)

and removed by reaction (B24/A204)

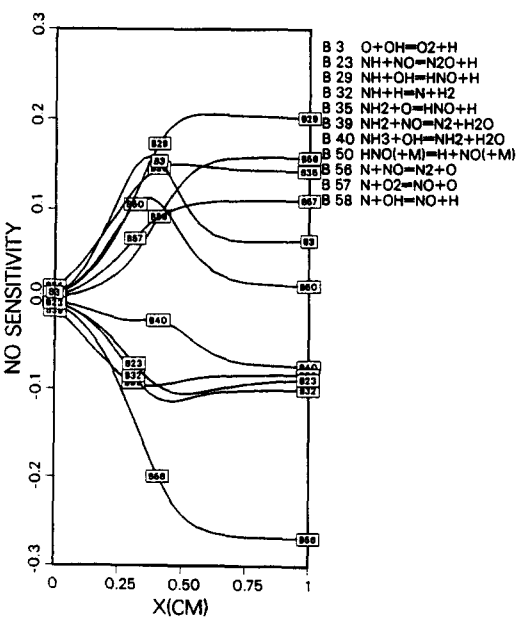

FIG. 45. Sensitivity plot for NO for the flame conditions of Bian *et al.*[70]

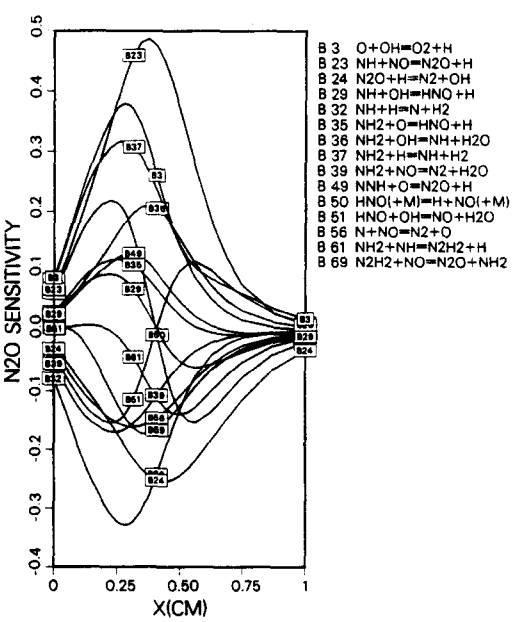

FIG. 46. Sensitivity plot for N_2O for the flame conditions of Bian *et al.*[70]

$$N_2O + H \rightleftharpoons N_2 + OH. \qquad \text{(B24/A204)}$$

In addition to these two reactions, Fig. 46 shows that the N_2O concentration is sensitive to reactions that establish the NH and NO concentrations (and to a lesser extent to reactions that determine the H-atom concentration). Since the NH_2 (from which NH is formed), NH, and NO profiles are predicted accurately, we are confident that we have correctly identified the N_2O formation and destruction mechanism in this and in other ammonia flames.

The rate coefficients used in the present model for reactions (B23/A202) and (B24/A204) are discussed in more detail in Section 8. However, it should be noted that reducing k_{B23} any further compromises the agreement between the predicted and experimental N_2O profiles, as one might expect from the sensitivity analysis. On the other hand, increasing k_{B23} at high temperature is easily compensated for by increasing k_{B28},

$$N_2O + OH \rightleftharpoons N_2 + HO_2, \qquad \text{(B28/A203)}$$

without seriously affecting anything else. The possibility of increased values of k_{B23} and k_{B28} should not be overlooked.[85]

5.4. *Fuel–Nitrogen Conversion in Well-Stirred Reactors*

Longwell and coworkers[86,87] at M.I.T. have recently performed a set of experiments in a jet-stirred reactor that provides a useful test of the present reaction mechanism in predicting fuel–nitrogen conversion under reasonably practical conditions. Burning ethylene in air with a small quantity of added ammonia (1.5% of fuel by mass), they measured both the stable hydrocarbon products (as well as CO and CO_2) and the stable nitrogenous species as a function of equivalence ratio (from $\phi = 1$ to $\phi = 1.9$) for a fixed temperature and residence time ($T = 1750$ K and $\tau = 7$ msec). They have compared their results with PSR (perfectly stirred reactor) model predictions based on the mechanism of Glarborg, Miller, and Kee.[11] The agreement is very good for both the hydrocarbons[86] and the nitrogenous species. We include here only a discussion of the nitrogen results in comparison with the PSR predictions based on the mechanism of Appendix A, which is a slight extension and improvement over the Glarborg–Miller–Kee mechanism used by the M.I.T. workers.

The M.I.T. experiments are particularly valuable in that they provide information not only about the NO produced, but also about the other principal stable fixed-nitrogen compounds, HCN and NH_3. The comparisons between the model predictions and the experimental results for these species are shown in Figs 47–49. A comparison for the total fixed nitrogen (TFN $\equiv$ NO + HCN + NH_3) is shown in Fig. 50. The agreement between the model and experiment is excellent for NO and HCN, less good (but still quite acceptable) for NH_3. The comparison for the TFN

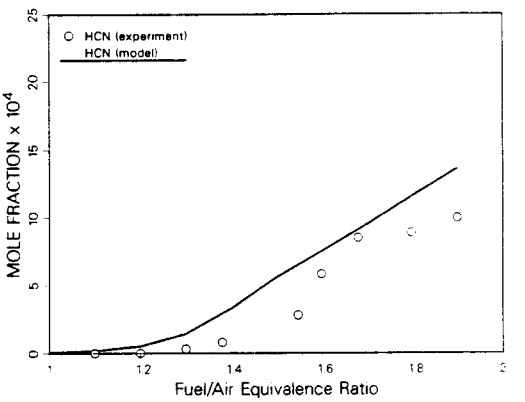

FIG. 48. Comparison of the model predictions of HCN concentrations with the well-stirred reactor data of Sun *et al.*[87]

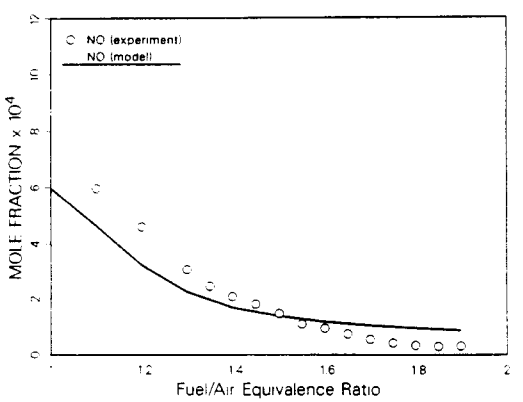

FIG. 47. Comparison of the model predictions of NO concentrations with the well-stirred reactor data of Sun *et al.*[87] Fuel nitrogen = NH_3 ($\simeq$ 2600 ppmv); $T = 1750$ K, residence time = 7 msec.

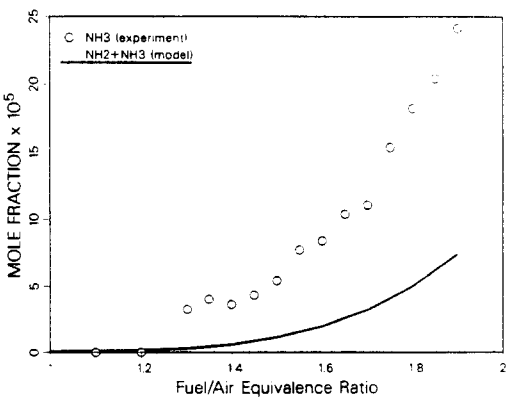

FIG. 49. Comparison of the model predictions of NH_3 concentrations with the well-stirred reactor data of Sun *et al.*[87]

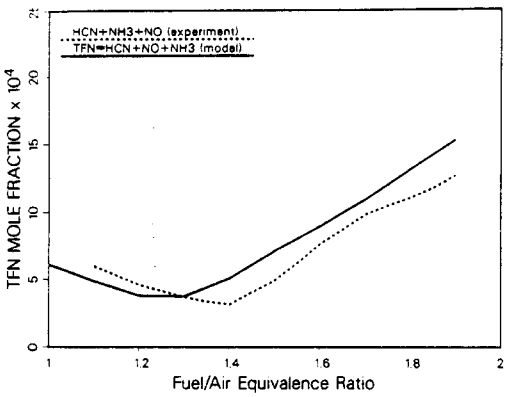

FIG. 50. Comparison of the model predictions of TFN (TFN = NO + HCN + NH_3) with the well-stirred reactor data of Sun *et al.*[87]

reflects directly the NO and HCN results since NH_3 is never a significant component of TFN. The discrepancies shown are relatively small and have three possible sources: measurement error, inadequacies in the reaction mechanism, or incompatibility of the experimental conditions with a PSR model (i.e. incomplete microscale mixing). In any event, we can find no acceptable method of modifying the mechanism to improve the agreement.

Both the calculations and the experiments in Fig. 50 show a minimum in the total fixed nitrogen at an equivalence ratio between 1.2 and 1.4. The experimental minimum is somewhat broader than the model predicts (due to the differences in the HCN), but the model nevertheless accurately predicts both the location of the minimum and the amount of TFN remaining. The existence of this minimum in the total fixed nitrogen is key to an important NO_x-control strategy, two-stage combustion. The idea behind two-stage combustion is to operate a rich first stage as close as possible to the minimum-TFN equivalence ratio. The second stage is then operated lean to complete the burning of the hydrocarbons, carbon monoxide, and hydrogen (produced in the rich first stage) and with careful temperature control to inhibit thermal NO formation. Normally, most of the residual TFN from the first stage is converted to NO in the second stage.

Figure 51 shows plots of calculated TFN versus equivalence ratio for three different conditions:

(a) the same conditions as for the M.I.T. experiments except that a fixed quantity of NH_3 (2600 ppm) was added as the fuel nitrogen source;
(b) the same conditions as in (a) except that ammonia is replaced by hydrogen cyanide;
(c) the same conditions as in (a) except that ammonia is replaced by nitric oxide.

There is remarkably little difference in the results, and the optimum (minimum TFN) equivalence ratio is the same as that found in the calculations of Glarborg *et al.*[11] for NO added to a methane/air PSR at a 2 msec residence time. The similarity of all these results suggests that the optimum equivalence ratio for minimum TFN emissions is a relatively weak function of fuel type, source of fuel nitrogen, and residence time.

Another interesting point arises from the three calculations cited above. Figure 52 shows the speciation of the TFN for the three different cases. One can infer from the plots that the differences in the TFN and its speciation among the three cases arise from the fuel-nitrogen source passing unreacted through the reactor. That is, for the case where NO is the initial fuel-nitrogen source, more NO is emitted from the reactor than in the other two cases, which have essentially the same amount of emitted NO. Similar statements apply for the hydrogen cyanide and ammonia cases. These results suggest that some of the discrepancy between the model predictions and the M.I.T. experiments shown above (particularly for the ammonia) may be due to incomplete mixing, resulting in unreacted or 'partially' reacted pockets of gas passing through the reactor—initial conversion of the fuel-nitrogen source is clearly a rate-limiting factor. However, this explanation appears inconsistent with the finding of the M.I.T. group that unreacted pockets of ethylene, the fuel, did not pass through the reactor.

As we suggested in the section on prompt NO, the mechanisms of prompt-NO formation and fuel-nitrogen conversion are remarkably similar. In Figs 53–55, sensitivity coefficients as a function of equivalence ratio are shown. Up to an equivalence ratio of approximately 1.3, the fixed nitrogen is predominantly in the form of nitric oxide, and the mechanism that determines its concentration is simple. In this regime, all the hydrogen is stripped rapidly from ammonia, leaving only nitrogen atoms. The NO (and TFN) concentration is determined almost exclusively by the N-atom reactions,

$$N + OH \rightleftharpoons NO + H \qquad (A234)$$

and

$$N + NO \rightleftharpoons N_2 + O. \qquad (A232)$$

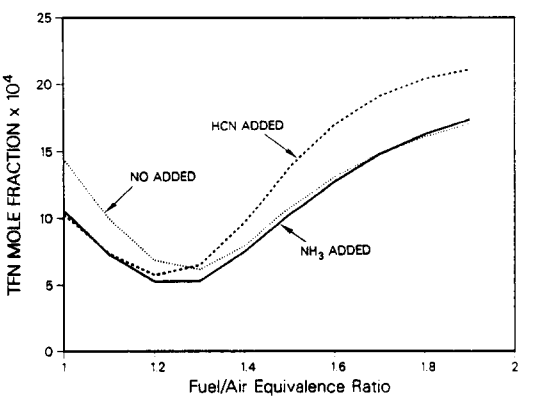

FIG. 51. Plots of TFN vs equivalence ratio for the conditions of the stirred-reactor experiments of Sun *et al.* for three different fuel nitrogen sources: NH_3, HCN, and NO.

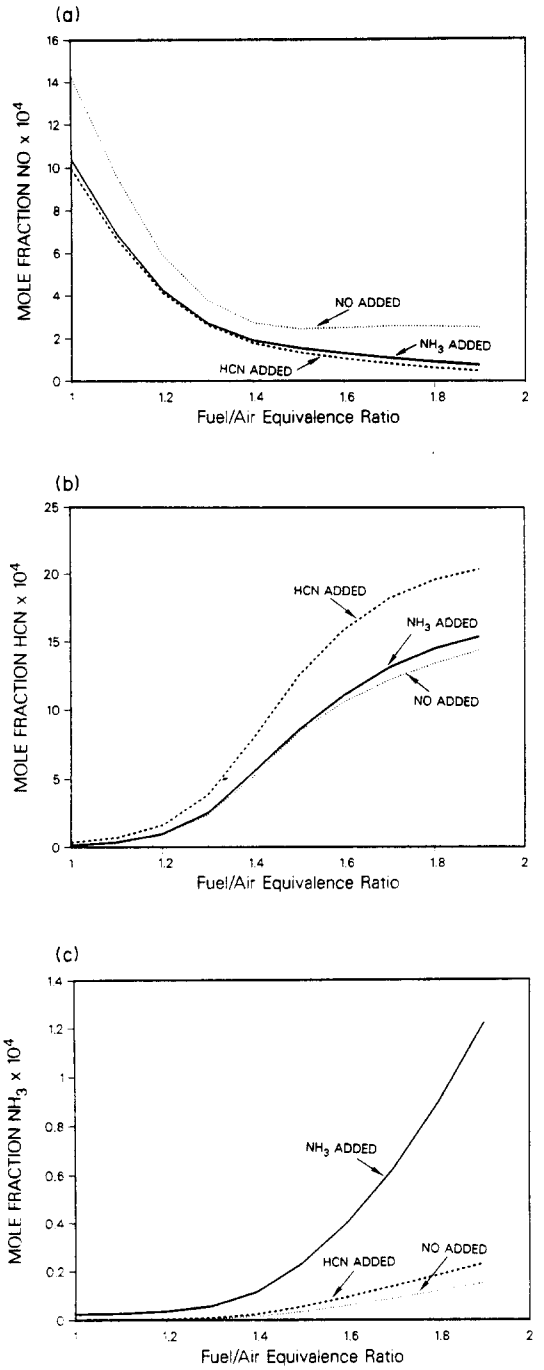

FIG. 52. Calculated (a) NO, (b) HCN, and (c) NH_3 concentrations as a function of equivalence ratio for the three different fuel–nitrogen sources. All calculations were performed for the conditions of the stirred-reactor experiments of Sun *et al.*[87]

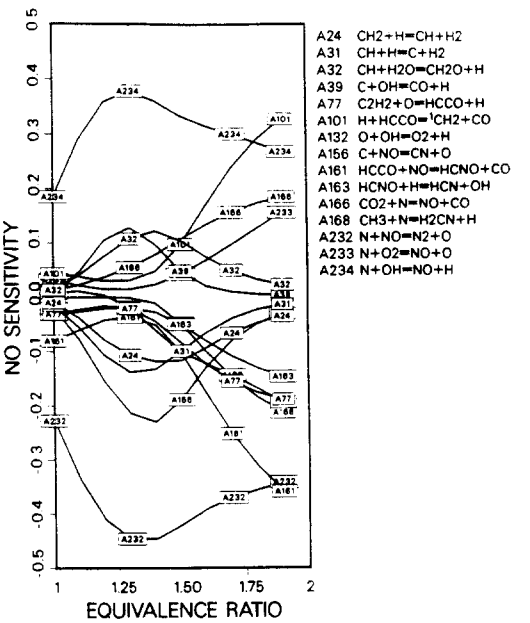

FIG. 53. Sensitivity plot for NO for the conditions of the stirred-reactor experiments of Sun *et al.*[87]

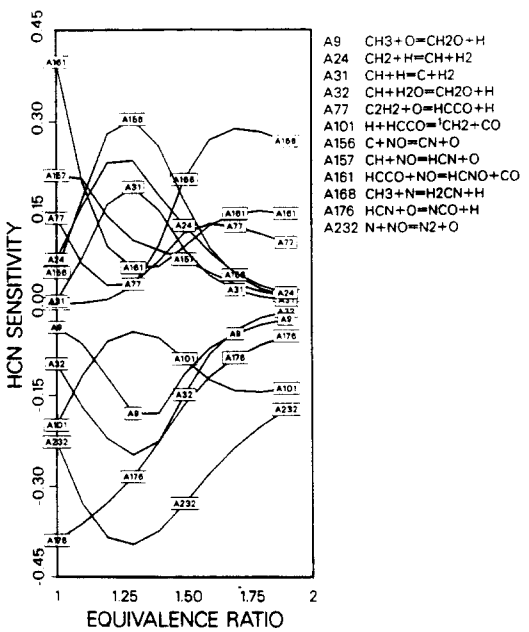

FIG. 54. Sensitivity plot of selected reactions for HCN for the conditions of the stirred-reactor experiments of Sun *et al.*[87]

The agreement between model and experiment in this regime is excellent, reflecting a precise knowledge of these rate coefficients.

Starting roughly at $\phi = 1.3$, reaction of NO with hydrocarbon free radicals (C and CH),

$$C + NO \rightleftharpoons CN + O \qquad (A156)$$

$$CH + NO \rightleftharpoons HCN + O \qquad (A157)$$

begins to compete with the N + NO reaction, leading to hydrogen cyanide formation. For this regime (and for all $\phi \geq 1.3$), the mechanism is much more complicated than for leaner conditions, as evidenced by several reactions having comparable sensitivities. The most important direct (i.e. involving nitrogen compounds directly) steps determining the TFN and its speciation for $1.3 < \phi < 1.5$ are conversion of NO to HCN via reactions (A156) and (A157),

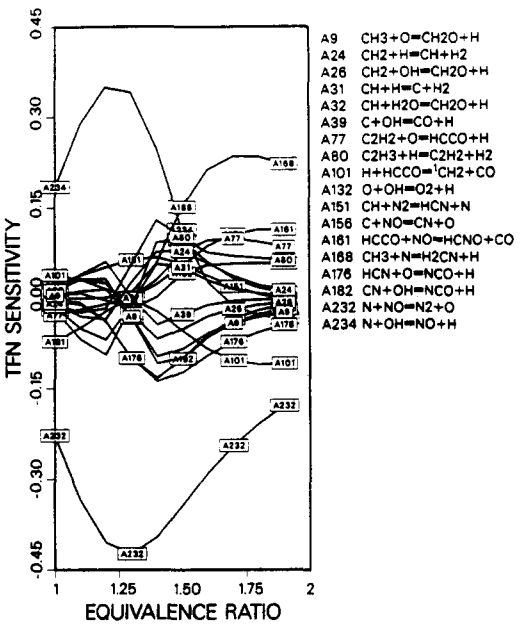

FIG. 55. Sensitivity plot for TFN for the conditions of the stirred-reactor experiments of Sun *et al.*[87]

removal of HCN via reaction (A176),

$$O + HCN \rightleftharpoons NCO + H, \quad \text{(A176)}$$

and the formation and destruction of NO by N-atom reactions (A234) and (A232).

For equivalence ratios greater than about 1.5, there is another change in mechanisms. In this regime, OH levels are so low that nitrogen atoms begin to react with CH_3 rather than OH. The principal HCN formation route is

$$CH_3 + N \rightleftharpoons H_2CN + H \quad \text{(A168)}$$

$$H_2CN + M \rightleftharpoons HCN + H + M. \quad \text{(A155)}$$

However, the conversion of HCN to N_2 is still dominated by the $HCN \xrightarrow{+O} NCO \xrightarrow{+H} NH \xrightarrow{+H} N \xrightarrow{+NO} N_2$ sequence discussed in previous sections. The rate-limiting steps in this sequence for determining the TFN and HCN concentrations are reactions (A168)—$CH_3 + N \rightleftharpoons H_2CN + H$, (A176)—$HCN + O \rightleftharpoons NCO + H$, and (A232)—$N + NO \rightleftharpoons N_2 + O$. In this regime, there is still some NO → HCN recycle occurring, but the dominant mechanism has changed. Because of the dearth of chain carriers (primarily hydrogen atoms), the reaction sequence that produces CH and C from acetylene no longer takes place readily. Instead of reacting with H, $^3CH_2$ and $^1CH_2$ preferentially react with H_2 to produce CH_3. Consequently, the main channel for producing HCN from NO becomes

$$HCCO + NO \rightleftharpoons HCNO + CO \quad \text{(A161)}$$

$$HCNO + H \rightleftharpoons HCN + OH \quad \text{(A163)}$$

with the HCCO being produced from reaction (A77),

$$C_2H_2 + O \rightleftharpoons HCCO + H. \quad \text{(A77)}$$

The possible significance of reaction (A161) in the NO → HCN recycle mechanism is a new proposal —there are no experimental determinations of its rate coefficient. We have estimated k_{A161} from the rate coefficient for the isoelectronic reaction

$$NCO + NO \rightleftharpoons N_2O + CO. \quad \text{(A197)}$$

In Figs 53 through 55, several reactions not involving nitrogen directly show significant sensitivities. The function of these reactions is to determine the availability of the active chain carriers (H, O, and OH) and the small hydrocarbon free radicals (mainly CH and C). Of course, the latter play a dominant role in the NO → HCN recycle mechanism.

6. THERMAL De-NO_x AND RAPRENO$_x$ MECHANISMS

Two strategies that have been used for controlling NO_x emissions from fuel nitrogen are combustion modification and aftertreatment of combustor exhaust products. Staged combustion[88-92] and reburning[64,65] are examples of combustion modification techniques. Selective catalytic reduction (SCR),[93] Thermal De-NO_x[94,95] and RAPRENO$_x$[96,97] are examples of aftertreatment processes. Catalytic processes are outside the scope of the present discussion of gas-phase chemistry. However, Thermal De-NO_x and RAPRENO$_x$ are essentially homogeneous, gas-phase, chemical processes whose underlying kinetics are related to the kinetics of fuel-nitrogen conversion. In this section, we concentrate on Thermal De-NO_x since it has been utilized, studied, and tested more extensively than has RAPRENO$_x$.

6.1. *Thermal De-NO_x Mechanism*

In the thermal De-NO_x process ammonia is injected into the exhaust gases of stationary combustors, initiating a sequence of reactions that convert nitric oxide to molecular nitrogen. The process has been studied extensively,[13,98-108] both because of its practical importance and because it possesses some fascinating chemical features. Among these features are the following:

(1) The process works only in a narrow temperature window centered at approximately 1250 K (roughly between 1100 K and 1400 K) in the absence of other additives.
(2) The process must be implemented under excess-oxygen conditions. Ammonia addition is effective in reducing nitric oxide only if molecular oxygen

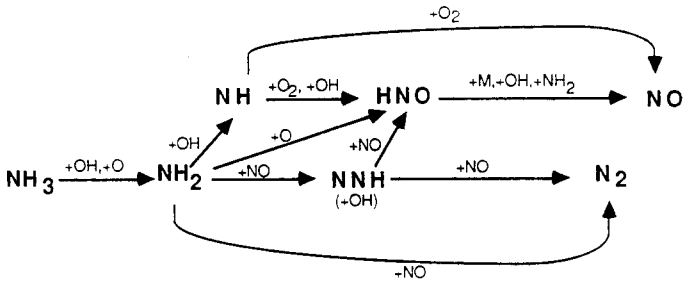

FIG. 56. Reaction path diagram for the Thermal De-NO_x process.

is present in sufficient quantities.

(3) If hydrogen or hydrogen peroxide (or perhaps other additives) is added with ammonia, the effective temperature window is shifted to lower temperatures without significantly changing its width.

(4) Increasing the NH_3 concentration to where it is comparable to the O_2 concentration inhibits the process under certain conditions.

(5) The presence of water has a slight inhibiting effect on the NO reduction in that the optimum temperature is increased slightly.

The reaction mechanism of Appendix B is able to predict all these features, quantitatively in most instances. The most important reaction paths in the Thermal De-NO_x process are shown in Fig. 56. Figure 57 shows the temperature window and the effect on the window of adding H_2 with the ammonia; the calculations are compared with experimental data of Lyon and Hardy.[99] Figure 58 shows the effect of adding NH_3 in quantities that exceed the O_2 and the effect of the absence of oxygen. Figures 59 and 60 show the effect on the NO and the NH_3, respectively, of adding water. The calculations in Figs 59 and 60 are compared with experimental data presented by Lyon.[100]

The important kinetic features underlying Thermal De-NO_x have been discussed previously.[13,99,100,103–105,107] However, several key kinetic parameters have been determined reliably only in the

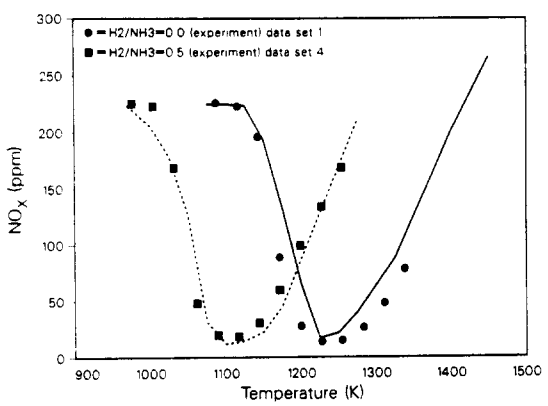

FIG. 57. Comparison of model prediction of the temperature window and the influence of H_2 on the temperature window with experiments for Thermal De-NO_x. Initial conditions for the experiments and calculations are as follows: data set 1: NO = 225 ppm, NH_3 = 450 ppm, O_2 = 1.23%, remainder He, P = 1.1 atm.; data set 4: same as data set 1 except 225 ppm H_2 displaces an equal amount of He. Reaction time t = 0.1 sec.

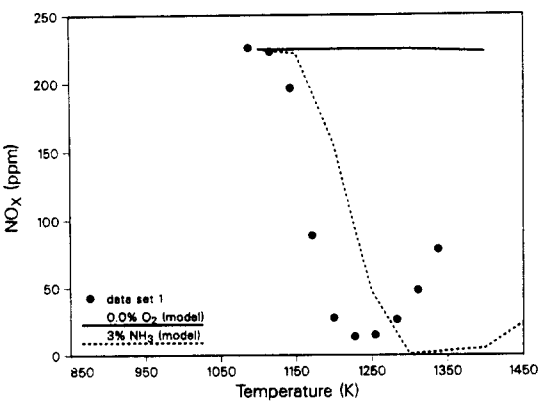

FIG. 58. The effect of the absence of oxygen and the effect of excessive NH_3 addition on NO removal in Thermal De-NO_x. The initial conditions correspond nominally to data set 1 (see Fig. 57). In the calculations the conditions of data set 1 are adjusted by changing the helium concentration. Reaction time t = 0.1 sec.

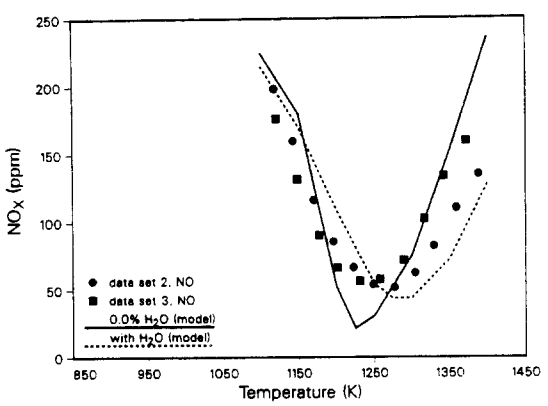

FIG. 59. The effect of water on NO removal in Thermal De-NO_x. Reaction time t = 0.1 sec. Initial conditions: data set 2: NO = 225 ppm, NH_3 = 385 ppm, O_2 = 4%, H_2O = 10%, remainder He, P = 1.2 atm.; data set 3: same as data set 2 except that He displaces the H_2O.

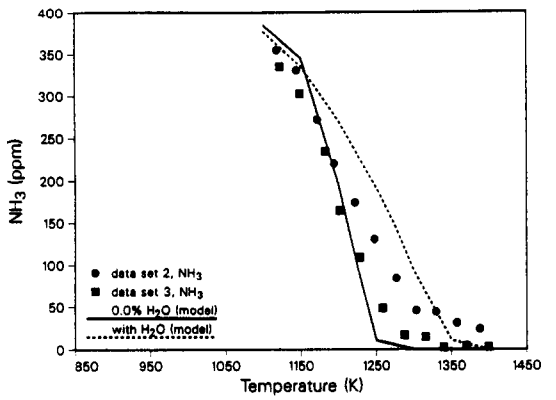

FIG. 60. The effect of water on the NH_3 concentration at a reaction time of $t = 0.1$ sec. Same conditions as Fig. 59.

past few years, and some of these are reliable only in narrow temperature ranges. Among the important parameters are the rate coefficients for reaction of ammonia with OH, O, and H, the rate coefficient and product distribution for the $NH_2 + O$ reaction,[83]

$$NH_2 + O \rightleftharpoons HNO + H \qquad \text{(B34/A212)}$$

$$NH_2 + O \rightleftharpoons NH + OH \qquad \text{(B35/A213)}$$

and the rate coefficient and products of the $NH + O_2$ reaction,[81]

$$NH + O_2 \rightleftharpoons NO + OH. \qquad \text{(B22/A201)}$$

By far the most important aspect of the Thermal De-NO_x mechanism is the identity of the products of the $NH_2 + NO$ reaction. However, a discussion of this point is deferred until later in this section.

Thermal De-NO_x works because the $NH_2 + NO$ reaction has a significant (perhaps dominant) chain-branching component, allowing the overall reaction to be self-sustaining.[13,107] The ammonia is converted to NH_2 principally by reaction with OH,

$$NH_3 + OH \rightleftharpoons NH_2 + H_2O, \qquad \text{(B40/A218)}$$

but also in the absence of water vapor by reaction with oxygen atoms,

$$NH_3 + O \rightleftharpoons NH_2 + OH. \qquad \text{(B42/A220)}$$

In order to be self-sustaining the $NH_2 + NO$ reaction must directly or indirectly regenerate OH and O to continue the $NH_3 \rightarrow NH_2$ conversion. In the model presented here, this regeneration is accomplished by the following reaction sequence.

$$NH_2 + NO \rightleftharpoons NNH + OH \qquad \text{(B38/A216)}$$

$$NNH + NO \rightleftharpoons N_2 + HNO \qquad \text{(B44/A222)}$$

$$HNO + M \rightleftharpoons H + NO + M. \qquad \text{(B50/A228)}$$

The H atom produced in reaction (B50) reacts with molecular oxygen to produce OH and O via

$$H + O_2 \rightleftharpoons OH + O. \qquad (-B3/-A132)$$

Since reaction (B42) converts NH_3 to NH_2 without losing a chain carrier, the reaction sequence (B40), (B38), (B44), (B50), (B3), (B42) results in a net gain of three chain carriers per cycle. In the presence of water the oxygen atom reacts with H_2O,

$$O + H_2O \rightleftharpoons OH + OH, \qquad (-B9/-A138)$$

and there is still a net gain of three chain carriers (OH) per cycle. As long as chain termination processes do not interrupt this pattern a majority of the time, i.e. as long as the branching sequence occurs at least a quarter of the time, the overall reaction is self-sustaining. The important chain termination reactions in the present mechanism are

$$NH_2 + NO \rightleftharpoons N_2 + H_2O, \qquad \text{(B39/A217)}$$

$$NH_2 + HNO \rightleftharpoons NH_3 + NO, \qquad \text{(B53/A231)}$$

and

$$OH + HNO \rightleftharpoons H_2O + NO. \qquad \text{(B51/A229)}$$

Reaction (B39), although it converts NO to N_2 directly, is detrimental to the NO reduction scheme because it is chain terminating.

At the low-temperature end of the effective temperature range, the NO reduction is limited principally by the rates of the chain termination reactions that compete with the branching sequence described above. As temperature increases, the growth in chain-carrier concentrations becomes so rapid that eventually, in the absence of water, reaction (B34),

$$NH_2 + O \rightleftharpoons HNO + H,$$

(B34/A212)

begins to compete favorably with reactions (B38) and (B39) for NH_2. Reaction (B34), followed by (B50), (B51), or (B53), leads to NO formation. Under conditions of interest, the primary HNO reaction is (B50), and this sequence is chain-branching. At sufficiently high temperatures (about 1400 K for the case without H_2 addition in Fig. 57), the oxidation sequence is sufficiently dominant that a net increase in the NO concentration results. In the presence of water this oxidation sequence is replaced by

$$O + H_2O \rightleftharpoons OH + OH$$

(−B9/−A138)

$$OH + NH_2 \rightleftharpoons NH + H_2O$$

(B36/A214)

and

$$NH + O_2 \rightleftharpoons NO + OH$$

(B22/A201)

or

$$NH + O_2 \rightleftharpoons HNO + O$$

(B21/A200)

followed by HNO dissociation.

To illustrate some of these points quantitatively, the calculated NO and NH_3 time histories for the 1150 K and 1350 K cases (no H_2) of Fig. 57 are plotted in Figs 61 and 62 and the corresponding NO sensitivity profiles are shown in Figs 63 and 64. For the low-temperature case, increasing the reaction time beyond $t = 0.1$ sec increases the NO reduction. However, for the high-temperature case the reaction is complete in about 0.03 sec. The high-temperature case also exhibits the interesting behavior that the NO concentration first decreases and then increases rapidly near the end of the reaction zone. This increase in the NO concentration occurs when the OH and O concentrations have risen to the point where reactions (B34) and (B36) can compete for NH_2 with the NH_2 + NO reaction.

The sensitivity plots in Figs 63 and 64 illustrate the essential features of the reaction process. For 1150 K (below the optimum temperature for NO reduction), chain branching processes enhance the reduction, whereas termination processes inhibit it. More precisely, any reaction that increases the availability of NH_2 enhances the reduction. Reaction (B38), $NH_2 + NO \rightarrow NNH + OH$, is favorable to NO reduction, and reaction (B39), $NH_2 + NO \rightarrow N_2 + H_2O$, is equally unfavorable. The situation changes somewhat at 1350 K (above the optimum temperature). In this case, chain branching is favorable at early times, but unfavorable at later times because of

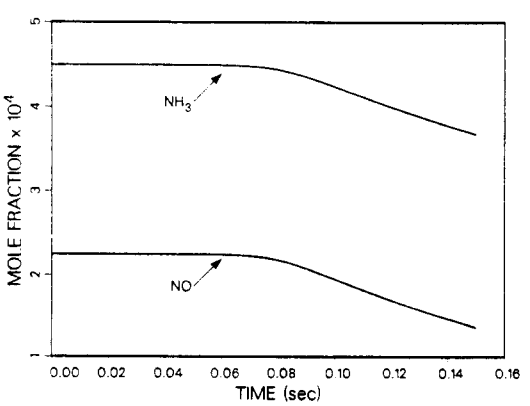

FIG. 61. NH_3 and NO time histories. Initial conditions correspond to data set 1 (see Fig. 57), $T = 1150$ K.

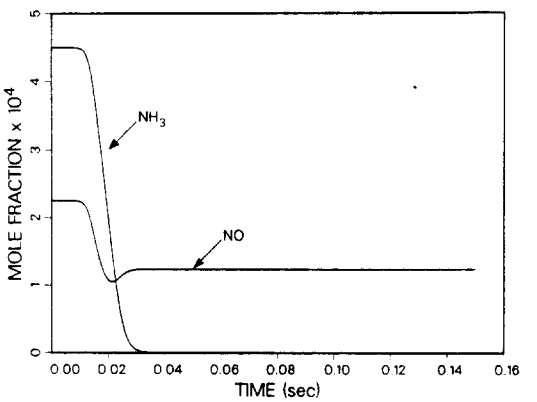

FIG. 62. NH_3 and NO time histories. Initial conditions correspond to data set 1 (see Fig. 57), $T = 1350$ K.

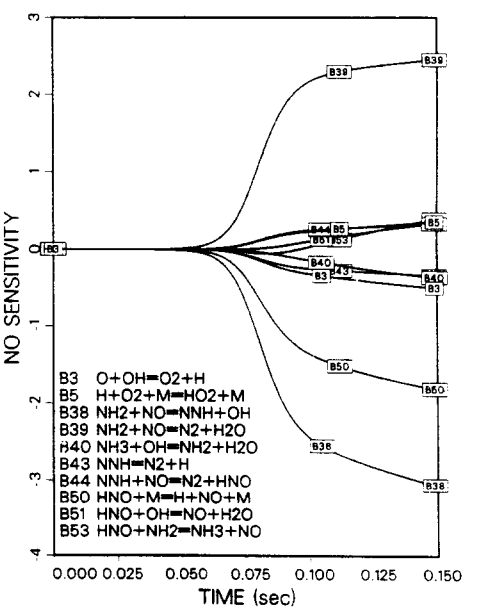

FIG. 63. Sensitivity plot for NO for the conditions of Fig. 61.

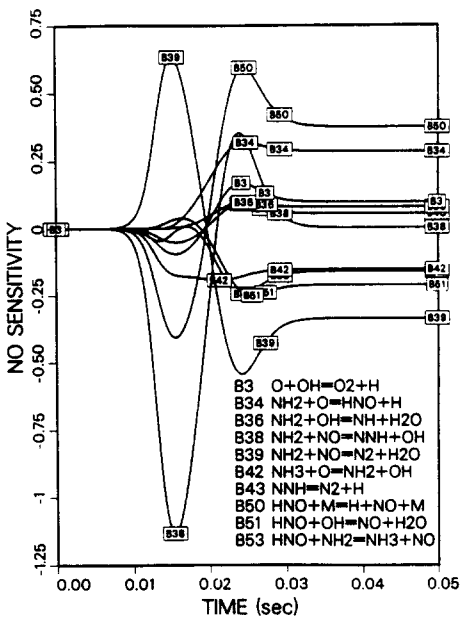

FIG. 64. Sensitivity plot for NO for the conditions of Fig. 62.

the 'switch' in mechanism discussed above. The chain branching process that allows Thermal De-NO_x to work in general actually contributes to its failure at high temperature by enhancing the rate at which NH_2 is converted to NO.[13,107] Although these results are based on a first-order sensitivity analysis, the fact remains that reducing the chain branching below a critical value quenches the process completely.

It is instructive to look at the sensitivity of the NO concentration to the NH_2 + NO reaction in a slightly different way. Instead of considering k_{B38} and k_{B39} to be independent parameters, k_T and α can be considered to be independent, where $k_T = k_{B38} + k_{B39}$ is the total rate coefficient and α is the branching fraction, $\alpha = k_{B38}/(k_{B38} + k_{B39})$. Using the chain rule, sensitivity coefficients of NO for α and A_T, the temperature-independent factor in k_T, can be obtained from the raw sensitivity data. For this purpose, define $\beta(A_T)$ and $\beta(\alpha)$ as

$$\beta(A_T) = \frac{A_T}{X_{NO}^{(max)}} \frac{\partial X_{NO}}{\partial A_T}$$

and

$$\beta(\alpha) = \frac{\alpha}{X_{NO}^{(max)}} \frac{\partial X_{NO}}{\partial \alpha}.$$

For the two cases considered above (1150 K and 1350 K), $\beta(\alpha)$ and $\beta(A_T)$ are plotted in Figs 65 and 66. For the low-temperature case, NO removal is extremely sensitive to the branching fraction and relatively insensitive to the total rate coefficient; increases in both parameters enhance the NO removal. For the high-temperature case, an increase in α enhances the NO removal process at early times and inhibits it when the O and OH concentrations have increased to sufficiently large values, as discussed above. Increasing A_T is favorable to NO removal at all times.

With an understanding of the reaction mechanism, particularly its chain-branching character, the features of the Thermal De-NO_x process can be understood. The requirement for oxygen is obvious. Reaction (B3) plays an essential role in producing the chain carriers O and OH; without reaction (B3), hydrogen atoms react only with NH_3 at too slow a rate to result in NO removal on time scales of interest. The shifting of the temperature window to lower temperatures when hydrogen is added occurs because of the increased rate of chain branching brought about by the reactions (B2) and (B4),

$$OH + H_2 \rightleftharpoons H_2O + H \quad \text{(B2/A131)}$$

$$O + H_2 \rightleftharpoons OH + H. \quad \text{(B4/A133)}$$

As noted above, chain branching is favorable at lower temperatures and unfavorable at higher temperatures. The addition of hydrogen peroxide has a similar, but

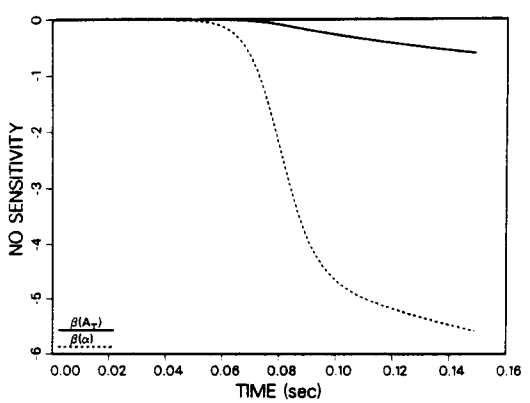

FIG. 65. Sensitivity of NO to the total rate coefficient and branching fraction of the reaction NH_2 + NO → products for the conditions of Fig. 57 (no H_2), T = 1150 K. $\beta(A_T)$ and $\beta(\alpha)$ are defined in the text.

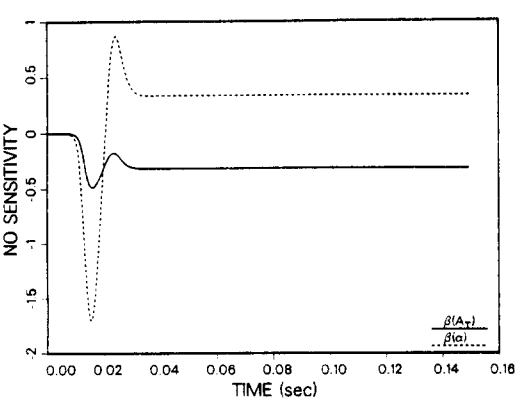

FIG. 66. Sensitivity of NO to the total rate coefficient and branching fraction of the reaction NH_2 + NO → products for the conditions of Fig. 57 (no H_2), T = 1350 K. $\beta(A_T)$ and $\beta(\alpha)$ are defined in the text.

not identical, effect—hydrogen peroxide dissociates into two hydroxyl radicals, thus increasing the chain carrier concentration. Our calculations with H_2O_2/NH_3 addition show the effective temperature window to be both broader and shifted to lower temperature when compared with calculations in which NH_3 is added alone. A discussion of the effect of hydrogen peroxide on the Thermal De-NO_x process, based on a reaction mechanism very similar to ours, is given by Cooper.[172]

The self-inhibiting effect of ammonia is shown in Fig. 58. For temperatures up to about 1275 K, 3% NH_3 addition produces less NO removal than when 385 ppm NH_3 is added (compare Fig. 57). This effect occurs as a result of reaction (B41), $H + NH_3 \rightarrow NH_2 + H_2$, beginning to compete with reaction $(-B3)$, $H + O_2 \rightarrow OH + O$, for hydrogen atoms. Consequently, the rate of chain carrier growth is reduced. At temperatures above 1275 K, NO removal is enhanced by the large quantity of added ammonia as a consequence of NH_3 inhibiting chain carrier growth, which enhances NO removal at higher temperature.

The effect of adding water is a relatively minor one, as shown in Figs 59 and 60. Nevertheless, this effect is predicted accurately by the mechanism. The principal role of water is to compete for oxygen atoms through reaction $(-B9)$, $O + H_2O \rightarrow OH + OH$. At lower temperatures this reaction competes with reaction (B42), $NH_3 + O \rightarrow NH_2 + OH$, and inhibits NO removal. At higher temperatures it competes with reaction (B34), $NH_2 + O \rightarrow HNO + H$, and inhibits NO formation. The result is a shift of the optimum temperature for the process to a higher value.

The key to the Thermal De-NO_x process is the $NH_2 + NO$ reaction. As discussed above, for Thermal De-NO_x to work this reaction must produce free radicals *at least* a quarter of the time at temperatures roughly above 900 K. The identity of these radicals is not completely clear at the present time. Subsequent to the appearance of Refs 13 and 107, several groups[109-114] have tried to determine directly the branching fraction of the reaction to free radicals. The strategy in all the experiments to date has been to try to detect the appearance of OH, either directly or indirectly, as a product at *room temperature*. No experiments have been conducted at temperatures directly applicable to Thermal De-NO_x. Two of the groups have also looked for hydrogen atoms in an attempt to distinguish between the reactions

$$NH_2 + NO \rightleftharpoons NNH + OH \qquad \text{(B38/A216)}$$

and

$$NH_2 + NO \rightleftharpoons N_2 + H + OH.$$

In these studies there is no consensus on the branching fraction to produce OH: the results vary from less than 15%[109] to greater than 65%.[114] Neither of the two groups that attempted to detect hydrogen atoms were successful. This latter result implies that the radical products, if they occur at room temperature, are NNH + OH and not $N_2 + H + OH$. The situation has been further complicated by the suggestion[115] that the OH detected in the discharge-flow experiments[114] was produced by the reaction sequence,

$$F + NH_3 \rightleftharpoons NH_2 + HF$$

$$F + NH_2 \rightleftharpoons NH + HF$$

$$NH + NO \rightleftharpoons N_2 + OH,$$

as a result of not having the NH_3 sufficiently in excess to prevent the occurrence of the $F + NH_2$ reaction. However, this suggestion does not seem to have merit. Although it is plausible that NH is produced by F-atom reactions in the discharge flow reactor experiments, it is unlikely that the NH + NO reaction produces appreciable OH. BAC-MP4 electronic structure calculations[116] (supported by the flame modeling work discussed here) strongly suggest that the only significant products from the NH + NO reaction are $N_2O + H$.

Considerable insight into the $NH_2 + NO$ reaction has been gained from *ab initio* electronic structure calculations.[116-119] Figure 67 shows a reaction coordinate diagram, constructed from BAC-MP4 calculations, for this reaction. Products are formed as a consequence of a series of rearrangements of the intermediate $NH_2 \ldots NO$ complex. These rearrangements are surprisingly facile.[116,117] The products obtained are determined principally by the fate of the complex,

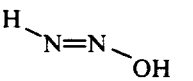

(II)

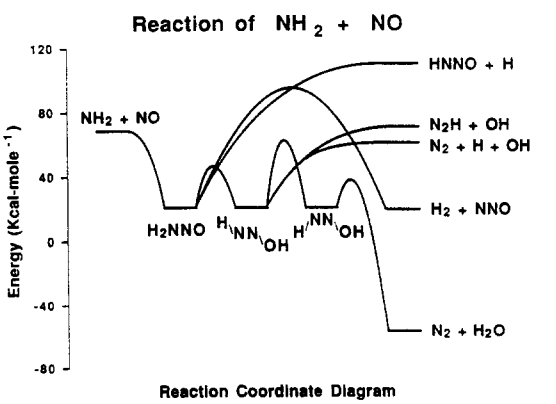

FIG. 67. Reaction coordinate diagram from BAC-MP4 calculations for the reaction $NH_2 + NO \rightarrow$ products.

formed by 1,3 hydrogen transfer from the initial addition complex,

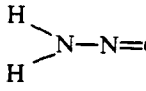

(I)

If Complex (II) undergoes *cis–trans* isomerization, N_2 and H_2O are the products, as shown in the figure. However, Complex (II) also may dissociate into NNH and OH. The BAC-MP4 calculations indicate that the $N_2 + H_2O$ channel is energetically favored but that $NH_2 + NO \rightarrow NNH + OH$ also is possible as an exothermic reaction.

An important consideration in establishing the relative importance of the various channels of the $NH_2 + NO$ reaction is the lifetime of the NNH radical. This molecule dissociates exothermically to $N_2 + H$ with a barrier to dissociation of unknown height (BAC-MP4 calculations indicate only 6 kcal/mol). Using the low energy barrier, Curtiss *et al.*[118] have estimated the lifetime of NNH with respect to tunneling to $N_2 + H$ and have obtained a value of approximately 10^{-11} sec, a very small lifetime. This result implies that the radical-producing channel of the $NH_2 + NO$ reaction could be written as

$$NH_2 + NO \rightleftharpoons N_2 + H + OH$$

equally as well as

$$NH_2 + NO \rightleftharpoons NNH + OH.$$

This result directly contradicts the experimental observations discussed above that show OH, but not H, to be a direct product of the $NH_2 + NO$ reaction. There are several factors in the calculation that could cause it to be biased toward a short lifetime. These include the small barrier to dissociation, the one-dimensionality of the dynamical calculation (including tunneling), the assumption that the potential energy along the dissociation coordinate can be described as a parabola, and simplifying assumptions about the internal dynamics of the NNH molecule. To what extent improving these aspects of the calculation will increase the lifetime is not clear.

Another factor that favors a long lifetime for NNH is the modeling of experiments associated with Thermal De-NO_x. The radical-producing reaction $NH_2 + NO \rightarrow NNH + OH$ has a self-inhibiting effect on the NO reduction process, whereas $NH_2 + NO \rightarrow N_2 + H + OH$ does not. This self-inhibition arises in the model because NNH does not always dissociate; if its lifetime is sufficiently long, it may undergo subsequent reactions that lead to chain termination. In the present model these subsequent reactions are initiated by

$$NNH + NO \rightleftharpoons N_2 + HNO. \qquad \text{(B44/A222)}$$

Early in the reaction HNO dissociates,

$$HNO + M \rightleftharpoons H + NO + M, \qquad \text{(B50/A228)}$$

but as the free radical concentrations increase, the HNO more frequently reacts with OH or NH_2,

$$HNO + OH \rightleftharpoons NO + H_2O \qquad \text{(B51/A229)}$$

$$HNO + NH_2 \rightleftharpoons NH_3 + NO, \qquad \text{(B53/A231)}$$

resulting in chain termination. Consequently, with NNH + OH as the radical products of the $NH_2 + NO$ reaction, the reaction limits itself and a larger branching fraction is required than if the products are $N_2 + H + OH$ (i.e. if NNH has a vanishingly small lifetime).

To support the conjecture that modeling Thermal De-NO_x requires a long lifetime for NNH, a series of calculations was performed with the lifetime of NNH reduced to $\tau_{NNH} = 10^{-11}$ sec, in which the branching fraction, α, of the $NH_2 + NO$ reaction to free radicals was varied to find an optimum value. The results of these calculations are compared with the experimental data of Fig. 57 (no H_2) in Fig. 68. For a 25% branching fraction ($\alpha = 0.25$), no significant NO removal is predicted to occur in 0.1 sec. For $\alpha = 0.508$ (the value used in the preferred model), NO is removed at temperatures well below 900 K, illustrating the importance of the self-limiting character of the mechanism in which NNH has a long lifetime. As α is reduced below 0.508, the optimum temperature for NO reduction increases and the effective temperature window gets narrower. Overall, the best agreement is obtained with $\alpha \approx 0.30$. Even for this case the agreement with experiment is not as good as for the preferred model, but the combination

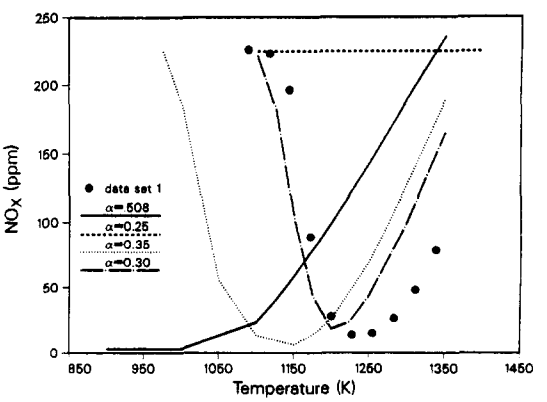

FIG. 68. The dependence of NO removal on α for the small τ_{NNH} model. $\tau_{NNH} = 10^{-11}$ sec in all calculations, reaction time $t = 0.1$ sec. The experimental points correspond to data set 1 (see Fig. 57).

of possible uncertainty in the experimental data and uncertainty in other rate parameters in the mechanism may make this level of agreement acceptable. In Figs 69 and 70 the $\alpha = 0.30$ model predictions are compared with the experimental data of Fig. 59 (4% O_2, with and without added water). For the case without water the agreement again is not as good as for the preferred model, but it may be adequate. The real discrepancy arises for the case with 10% added H_2O, or perhaps, more correctly, in the differences predicted with and without H_2O. The experimental results in Fig. 70 at $T = 1200$ K show that approximately two-thirds of the NO is removed in 0.1 sec, whereas the model predicts that virtually none is removed. The experiments clearly show that the effect of adding water between 1100 K and 1200 K is minimal, an effect predicted by the preferred (long NNH lifetime) mechanism. In contrast, the short NNH-lifetime model leads to the conclusion that water significantly inhibits the NO removal process between 1100 K and 1200 K (compare Figs 69 and 70), contrary to the experimental results.

The origin of the difference between the predictions of the short and long NNH-lifetime models is interesting. In forcing the lifetime of NNH to be vanishingly small, it was necessary to reduce the value of α from 0.508 to 0.30 in order to optimize the agreement with the Thermal De-NO_x data (no H_2O). In doing so, a greater burden for producing chain-carrier growth is placed on the reaction

$$H + O_2 \rightleftharpoons OH + O,$$

(−B3/−A132)

which at the low end of the temperature window is in competition with the chain termination step,

$$H + O_2 + M \rightleftharpoons HO_2 + M.$$

(B5/A134)

In the short NNH-lifetime model, when water is added, the increased effectiveness of H_2O in promoting $H + O_2$ recombination suppresses chain-carrier growth and inhibits NO removal in the 1100–1200 K temperature range. This effect does not occur significantly for the long NNH-lifetime model because a greater portion of the chain-carrier growth comes directly from the $NH_2 + NO$ reaction. For the short NNH-lifetime model to be consistent with the Thermal De-NO_x experiments, it is necessary for the effectiveness of water in promoting reaction (B5) to be essentially the same as that of a noble gas, a requirement that is contradicted by a relatively large body of experimental data.[1]

The previous discussion notwithstanding, model predictions for Thermal De-NO_x are insensitive to many details of the mechanism. For example, the self-limiting aspect of the long NNH-lifetime model could result directly from reactions of NNH with OH and NH_2, rather than through the HNO reaction described above. There may be other possibilities as well. In addition, one may exchange increases in α for decreases in NNH lifetime over a range of conditions without substantially modifying the model predictions. A question that arises in the long NNH-lifetime model is why NO_2 is not formed through the sequence[13,120]

$$NNH + O_2 \rightleftharpoons N_2 + HO_2$$

$$HO_2 + NO \rightleftharpoons NO_2 + OH.$$

(B59/A188)

The failure of experiments to detect NO_2 in Thermal De-NO_x places a severe restriction on the rate of the first of these steps.[13,120] Even though our knowledge of many details in the mechanism is lacking, the process can be described accurately by models such as the one discussed above.

6.2. *RAPRENO$_x$ Mechanism*

Another promising NO_x abatement scheme based on aftertreatment of combustor exhaust products is

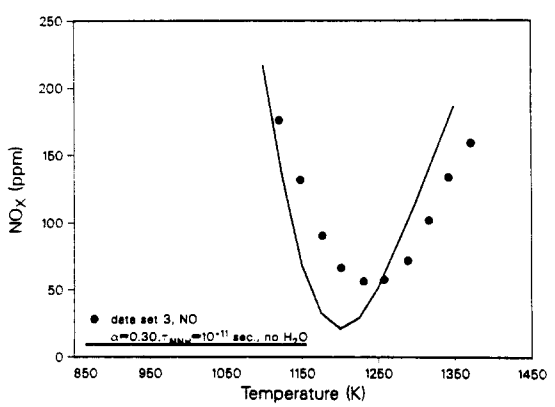

FIG. 69. Comparison of the small τ_{NNH} model ($\alpha = 0.30$) with the NO experimental data of Fig. 59 for the case with no added water.

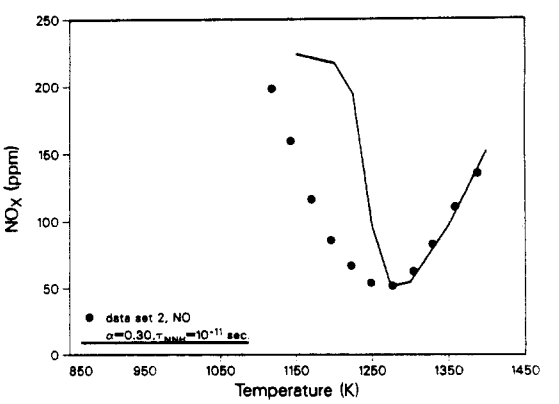

FIG. 70. Comparison of the small τ_{NNH} model ($\alpha = 0.30$) with the NO experimental data of Fig. 59 for the case with 10% added water.

RAPRENO$_x$.[96,97] In RAPRENO$_x$, cyanuric acid, a commerically available chemical, is injected into an exhaust stream containing NO. When heated, cyanuric acid sublimes and decomposes to form isocyanic acid,

$$(HOCN)_3 \longrightarrow 3HNCO.$$

At sufficiently high temperatures, the isocyanic acid will decompose either in the gas-phase or on surfaces and initiate a sequence of reactions leading to NO removal. Perry and Siebers[97] reported NO removal in simulated and real exhaust gas streams at temperatures as low as 600 K in a stainless steel flow reactor. Later experimental work by Siebers and Caton,[121] by Lyon and Cole,[161] and by Heap *et al.*[162] indicated that at temperatures below 1000 K surface decomposition of HNCO initiates the RAPRENO$_x$ process and that NO reduction does not occur at low temperatures in the absence of such surfaces. In recent experiments in a quartz flow reactor,[163-165] Siebers and Caton found that there is a temperature window for the RAPRENO$_x$ process and that the effectiveness of the process depends on the composition of the gas stream. In addition, under some conditions, relatively high concentrations of N_2O are formed as a by-product of the process. Figure 71a, taken from Ref. 165, shows the concentrations of NO, HNCO, CO, CO_2, and N_2O in a simulated exhaust gas stream measured at the exit of the quartz flow reactor as a function of reactor temperature. For the conditions of this experiment, significant NO removal begins to occur at a temperature of 1000 K, coincident with significant reductions in the concentrations of CO and HNCO and an increase in the CO_2 concentration. As the temperature increases to 1200 K, nearly all of the NO present initially in the gas stream is removed. For temperatures above 1200 K, the NO reduction decreases with increasing temperature. Coincident with the onset of NO reduction is an increase in the N_2O concentration in the gas stream. At 1150 K, the temperature giving maximum NO reduction, the N_2O concentration reaches a maximum value, corresponding approximately to one mole of N_2O formed for each mole of NO removed.

The data in Fig. 71a present an interesting challenge to the combustion modeler. There is not nearly so much known about the reaction kinetics underlying the RAPRENO$_x$ process as there is about those underlying Thermal De-NO$_x$. Perry and Siebers[97] proposed the following mechanism to describe the RAPRENO$_x$ process:

$$\left.\begin{aligned} HNCO &\rightleftharpoons NH + CO \\ NH + NO &\rightleftharpoons N_2O + H \end{aligned}\right\} \text{initiation}$$

$$H + HNCO \rightleftharpoons NH_2 + CO$$

$$NH_2 + NO \rightleftharpoons \begin{matrix} N_2 + H_2O \\ NNH + OH \end{matrix}$$

$$NNH \rightleftharpoons N_2 + H$$

$$CO + OH \rightleftharpoons CO_2 + H.$$

Hence, it appears that the gas-phase RAPRENO$_x$ mechanism comprises reactions important in the Thermal De-NO$_x$ process, reactions involving HNCO, and reactions important in the oxidation of moist CO. In order to model the data in Fig. 71a, we have combined the Thermal De-NO$_x$ mechanism of Appendix B with the moist CO oxidation reactions from Appendix A (reactions (A61)-(A64); (A131)-(A150)), the HNCO reactions shown in Table 3, and reactions (A192)-(A198) involving NCO.

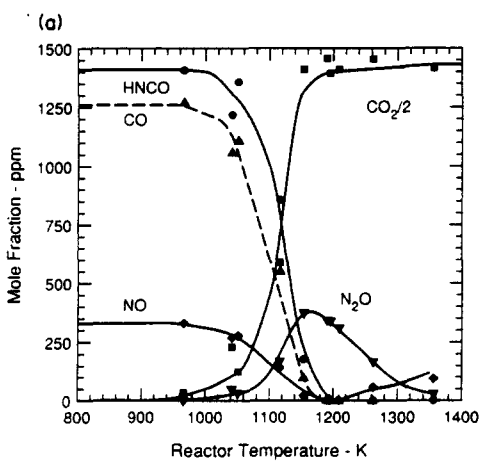

FIG. 71(a). Measured species concentrations at the exit of a quartz flow reactor as a function of reactor temperature for fixed initial mole fractions of NO (330 ppmv), CO (1260 ppmv), O_2 (12.3%), H_2O (4.5%) and cyanuric acid (470 ppmv, corresponding to 1410 ppmv HNCO at complete conversion), with the balance N_2. The residence time in the reactor is approximately 0.8 sec. The data are from Ref. 165.

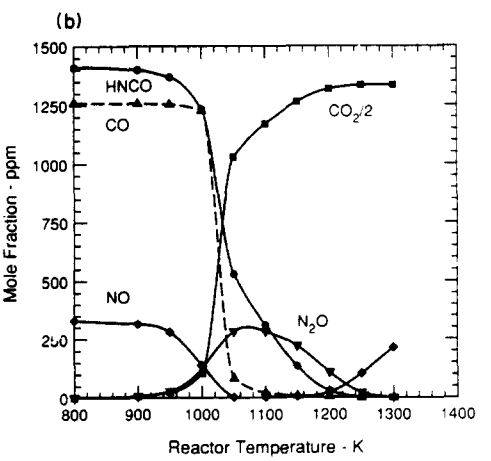

FIG. 71(b). Calculated species concentrations at the exit of an isothermal flow reactor as a function of reactor temperature for the initial conditions of Fig. 71(a). Reaction time = 0.8 sec.

TABLE 3. Reactions involving HNCO in the RAPRENO$_x$ mechanism

Reaction	A	β	E	Ref.
HNCO + M → NH + CO + M	1.14×10^{16}	0.0	86800	166
H + HNCO → NH_2 + CO	2.0×10^{13}	0.0	3000	(Appendix A)
NH + HNCO → NH_2 + NCO	3.0×10^{13}	0.0	23700	166
NH_2 + HNCO → NH_3 + NCO	5.0×10^{12}	0.0	6200	166
OH + HNCO → NCO + H_2O	2.65×10^{12}	0.0	5540	167
O + HNCO → NH + CO_2	3.25×10^{12}	0.0	10300	167

Rate coefficients are in the form $k_f = AT^{\beta}_{exp}(-E/RT)$. Units are moles, cubic centimeters, seconds, kelvins and calories/mole.

Recent studies have provided reasonably accurate overall rate parameters for the most important HNCO reactions, although the relative importance of the product channels for some of the reactions are uncertain. A discussion of the available kinetic data for important HNCO reactions will be deferred until later in this section.

The results of our model calculations are compared with the experimental data of Siebers and Caton in Fig. 71. The model predicts all of the trends of the experiment, with the model reaction initiating at a temperature approximately 100 K lower than observed. Both the level of NO reduction and amount of N_2O formed are predicted accurately by the model. At temperatures above 1250 K, the model predicts somewhat less NO reduction than is observed. Figure 72 shows contribution factors for NO at 1000 K, where the model predicts significant NO removal and N_2O formation. Figure 72 shows that while the reaction sequence,

$$NH_2 + NO \rightleftharpoons \begin{matrix} NNH + OH & \text{(B38/A216)} \\ N_2 + H_2O & \text{(B39/A217)} \end{matrix}$$

$$NNH + NO \rightleftharpoons HNO + N_2 \quad \text{(B44/A222)}$$

contributes to NO removal, the primary NO removal step is

$$NCO + NO \rightleftharpoons N_2O + CO. \quad \text{(A197)}$$

This somewhat surprising result provides an explanation for the high levels of N_2O observed in the experiment, and the contribution factor plot for N_2O (Fig. 73) supports this conclusion. The sensitivity plot for NO (Fig. 74) shows that, in addition to the moist CO oxidation reactions,

$$CO + OH \rightleftharpoons CO_2 + H \quad \text{(A62)}$$

$$H + O_2 \rightleftharpoons OH + O \quad (-\text{A132})$$

$$H + O_2 + M \rightleftharpoons HO_2 + M \quad \text{(A134)}$$

which are the principal H/O radical generation and termination steps in the RAPRENO$_x$ mechanism, the NO removal is most sensitive to the rates of two HNCO reactions,

$$H + HNCO \rightleftharpoons NH_2 + CO \quad \text{(A199)}$$

$$OH + HNCO \rightleftharpoons NCO + H_2O$$

which produce the precursor species involved in the primary NO removal reactions. There have been several recent studies of the kinetics of these two

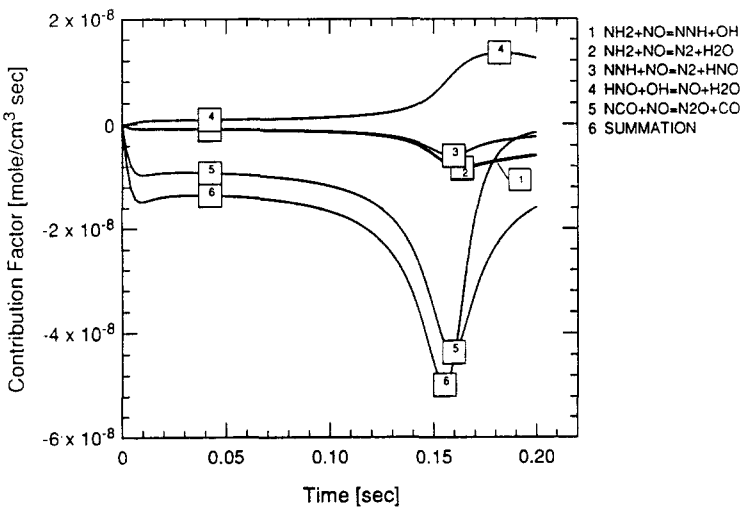

FIG. 72. Contribution factor plot for NO from the present RAPRENO$_x$ reaction mechanism for the initial mole fraction of NO, CO, O_2, H_2O, and HNCO of Fig. 71 at 1050 K.

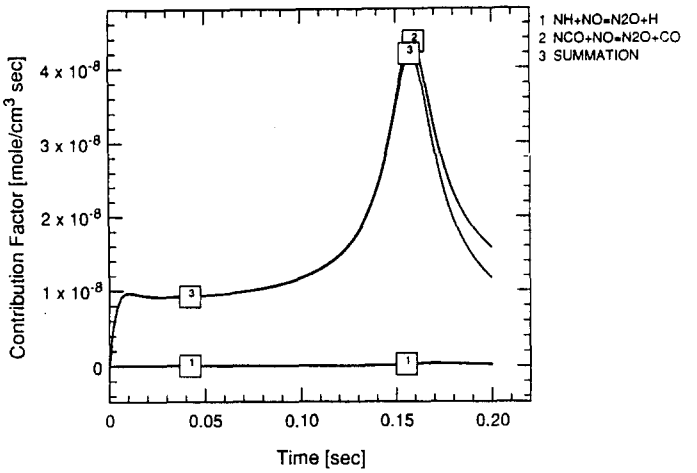

FIG. 73. Contribution factor plot for N_2O from the present RAPRENO$_x$ reaction mechanism for the conditions of Fig. 72.

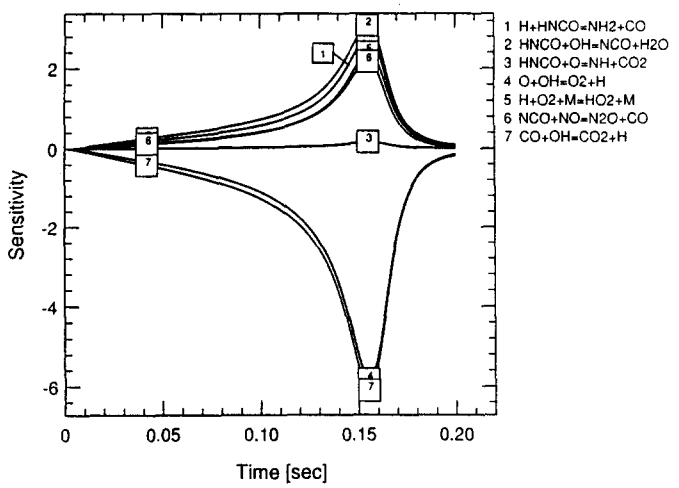

FIG. 74. Sensitivity plot for NO from the present RAPRENO$_x$ reaction mechanism for the conditions of Fig. 72.

reactions,[166,167] and the rate parameters for the overall reactions are reasonably well known. However, at the present time, no information is available on the relative importance of the various product channels of these reactions. The most likely product channels for the H + HNCO reaction are,

$$\mathrm{H + HNCO} \rightleftharpoons \begin{matrix}\mathrm{NH_2 + CO}\ (\Delta H = -8.2\ \mathrm{kcal/mol}) \\ \mathrm{H_2 + NCO}\ (\Delta H = 10.9\ \mathrm{kcal/mol}).\end{matrix}$$

In our calculations, we assumed that the NH_2 channel is the primary product channel, in accordance with Ref. 166. Tully *et al.*[167] have investigated the kinetics of the OH + HNCO reaction and suggest the following product channels,

$$\mathrm{OH + HNCO} \rightleftharpoons \begin{matrix}\mathrm{NCO + H_2O}\ (\Delta H = -4\ \mathrm{kcal/mol}) \\ \mathrm{NH_2 + CO_2}\ (\Delta H = -33\ \mathrm{kcal/mol}).\end{matrix}$$

We assumed that the abstraction channel is the major product channel at elevated temperatures, although some contribution from the NH_2-producing channel cannot be ruled out at this time. The sensitivity plot, Fig. 74, indicates that the reaction of O-atoms with HNCO plays only a minor role in the RAPRENO$_x$ mechanism.

In addition to the NO-removal channels involving NCO and NH_2, there also is an NO-formation sequence involving NH_2,

$$\mathrm{NH_2 + O} \rightleftharpoons \begin{matrix}\mathrm{HNO + H} & \text{(B34/A212)} \\ \mathrm{NH + OH} & \text{(B35/A213)}\end{matrix}$$

$$NH_2 + OH \rightleftharpoons NH + H_2O \quad (B36/A214)$$

followed by

$$NH + O_2 \rightleftharpoons \begin{matrix} HNO + O & (B21/A200) \\ NO + OH & (B22/A201) \end{matrix}$$

$$HNO + OH \rightleftharpoons NO + H_2O. \quad (B51/A229)$$

The NO produced by this reaction sequence may be reduced by reactions (A197), (B38/A216), and (B39/A217) or, at higher temperatures, it may be emitted in the exhaust stream. This NO production from HNCO is, in part, responsible for the observation that the initial HNCO/NO ratio must be larger than unity for complete removal of the NO initially in the exhaust stream.

The results from the contribution factor and sensitivity plots are summarized in Fig. 75, which shows the primary nitrogen species pathways in the RAPRENO$_x$ reaction. Further refinement of the RAPRENO$_x$ reaction mechanism will require determination of the branching ratios of the product channels of the reactions of HNCO with H and OH.

7. NITROGEN DIOXIDE MECHANISM

Experimental studies have shown that a significant fraction of the nitrogen oxide emissions from some combustion sources, such as gas turbines and gas appliances, can be NO_2[122-124] and *in situ* measurements of NO_x concentrations in premixed[125-127] and non-premixed flames[128-131] indicate that there are relatively large NO_2/NO ratios near the flame zone. While some of the NO_2 has been attributed to probe reactions,[131-134] detailed kinetics calculations[135-137] suggest that NO_2 formation and destruction in flames can occur by the following reactions sequence,

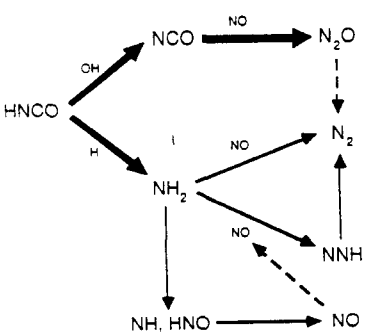

FIG. 75. Reaction path diagram illustrating the major steps for nitrogen species in the present RAPRENO$_x$ mechanism. The bold lines indicate the most important reaction paths.

$$NO + HO_2 \rightleftharpoons NO_2 + OH \quad (A188)$$

$$NO_2 + H \rightleftharpoons NO + OH \quad (A189)$$

$$NO_2 + O \rightleftharpoons NO + O_2. \quad (A190)$$

In the low-temperature regions of flames, significant HO_2 concentrations are found that can react with NO formed in the high-temperature regions and transported by diffusion to the low-temperature region. The NO_2 removal reactions are rapid, and in the presence of high radical concentrations, NO_2 will be converted rapidly back to NO.

These features are illustrated in Fig. 76, which shows concentration profiles of NO, NO_2, HO_2, and H and the temperature profile calculated using the reaction mechanism of Appendix A for an atmospheric pressure, fuel-rich (ϕ = 1.05) methane–air flame. The NO_2 sensitivity profiles (Fig. 77) show the most important reaction channels for NO_2 in this flame. The principal NO_2 formation reaction is

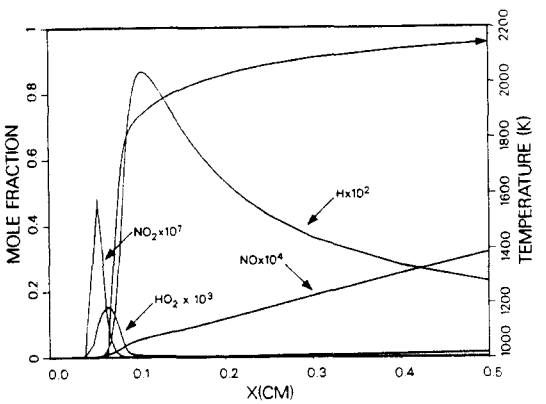

FIG. 76. Calculated profiles of NO, NO_2, HO_2, H-atom and temperature for an atmospheric-pressure, 10% methane in air flame (ϕ = 1.05).

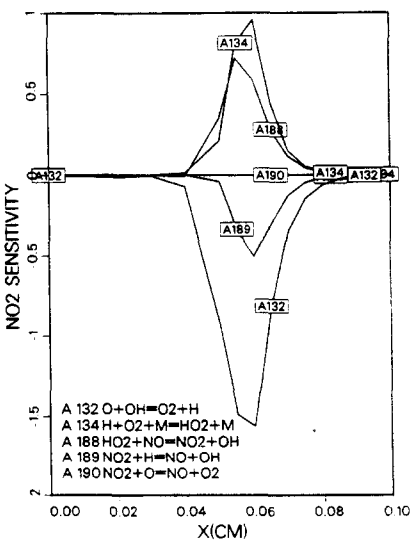

FIG. 77. Sensitivity plot for NO_2 for the flame of Fig. 76.

(A188). Since the rate of this reaction depends on the HO_2 concentration, NO_2 formation also is sensitive to reactions forming and removing HO_2. Of particular importance is

$$H + O_2 + M \rightleftharpoons HO_2 + M, \quad (A134)$$

which is the principal HO_2 formation reaction in the low-temperature region of the flame. The H-atoms needed for this reaction are transported from the high-temperature regions by molecular diffusion. Because of the role that H-atoms play in HO_2 formation, NO_2 formation also is sensitive to reaction (A132). The principal NO_2 removal step in this flame is reaction (A189). Of much less importance for NO_2 removal in this flame is reaction (A190).

From the above discussion, it is clear that the accuracy of predictions of NO_2 concentrations in flames is dependent both on the accuracy of the kinetics parameters of reactions (A188) and (A189) and on the accuracy of the species diffusional transport calculations, especially for NO and H-atoms. The kinetics parameters for the principal NO_2 formation reaction, (A188), are well known in the temperature range of 230–1760 K, with an estimated uncertainty of $\pm 30\%$ from the expression tabulated in Appendix A.[2] There are no high-temperature data for either of the two important NO_2 removal channels. However, both of these reactions have a very small temperature dependence. Hence, extrapolation of the low-temperature data to flame conditions can be done with confidence. Estimated uncertainties in the rate coefficients for both reactions are $\pm 30\%$ in the temperature range 298–650 K.[2] Perhaps the largest kinetic uncertainty is introduced through uncertainties in the third body efficiencies for reaction (A134), particularly for collision partners such as CH_4 and H_2O. As noted above, diffusional transport plays a major role in the NO_2 formation and removal process in flames. Uncertainties in multicomponent diffusion coefficients for species such as NO, NO_2, HO_2, and H-atom will result in uncertainties in calculated NO_2 profiles in flames that may exceed those introduced by kinetic uncertainties. While additional high-temperature rate data on reactions (A188, A189) are desirable, the reaction mechanism and rate parameters for NO_2 formation and removal are adequate for combustion calculations.

At flame temperatures NO_2 can exist only as a transient species. If NO_2 is to persist in the combustion products, then there must be quenching of the NO_2 formed in the flame. This quenching might occur in turbulent flames by rapid mixing of hot and cold fluid elements, which serves to quench the NO_2-removing reactions by reduction in radical concentrations.[136,138–140]

8. NITROUS OXIDE MECHANISM

Relatively high concentrations of N_2O have been measured in flue gas samples extracted from coal and oil-fired furnaces, while the measured N_2O levels in the stack gases of gas-fired combustors are low.[141–146] Recently, it has been suggested that a sampling artifact is responsible for the high N_2O levels reported in coal and oil flames and that the N_2O levels in these flames are similar to those measured in gas flames.[178] As noted earlier, a significant amount of N_2O is formed as a by-product of the RAPRENO$_x$ process and N_2O is an important nitrogen oxide under fuel-lean conditions. Hence, the mechanism for N_2O formation and removal is of interest.

Studies in laminar premixed flames[147] indicate that N_2O is a very short-lived species in hot combustion gases and that the principal N_2O formation reactions involve NO and various nitrogen-containing radicals.

$$NH + NO \rightleftharpoons N_2O + H \quad (A202)$$

$$NCO + NO \rightleftharpoons N_2O + CO. \quad (A197)$$

The N_2O formed in these reactions rapidly reacts to form N_2, principally by

$$N_2O + H \rightleftharpoons N_2 + OH. \quad (A204)$$

These conclusions are illustrated in Figs 46 and 78–80, which show results of N_2O sensitivity and rate-of-production analyses for three different flames and a well-stirred reactor. Figure 46 shows the principal N_2O formation and removal channels in a low-pressure, lean ($\phi = 0.71$) $NH_3 - O_2$ flame.[70] As discussed in Section 5.3, the principal N_2O formation reaction is (A202), and the primary N_2O removal channel is (A204). Figure 78 shows the principal N_2O formation and removal channels in an atmospheric-pressure, rich ($\phi = 1.37$) methane–air flame with 1300 ppm of added NO. In this flame, the NH + NO → N_2O + H channel is somewhat more important than NCO + NO → N_2O + CO for

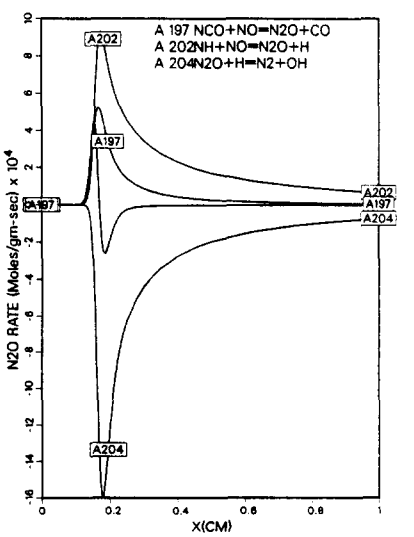

FIG. 78. Contribution factor plot for N_2O in an atmospheric-pressure, 13% methane in air flame to which 1300 ppm NO was added ($\phi = 1.37$).

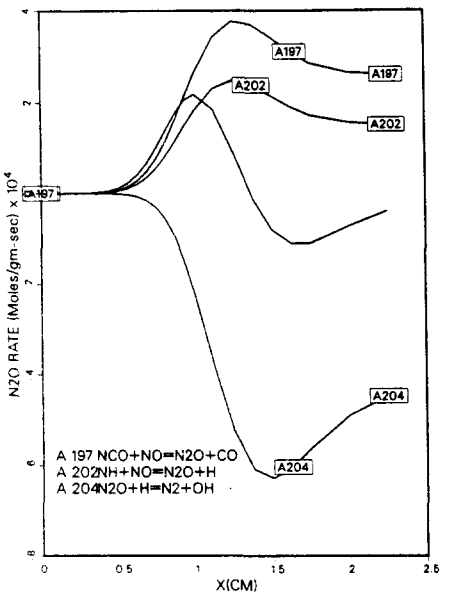

FIG. 79. Contribution factor plot for N_2O in a low-pressure (25 torr) rich (ϕ = 1.5) H_2–O_2–Ar flame to which 2% HCN was added.

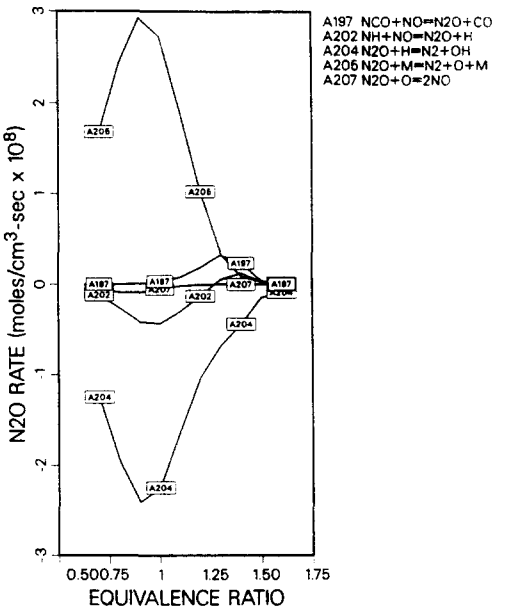

FIG. 80. Contribution factor plot for N_2O in a well-stirred reactor for the experimental conditions of Bartok *et al.*[36]

N_2O formation. As for the ammonia flame, the only significant N_2O removal channel is $N_2O + H \rightarrow N_2 + OH$. From this figure it can be seen that the N_2O formed by reactions (A202) and (A197) is rapidly and quantitatively removed by reaction (A204). Figure 79 shows results for a low-pressure (25 torr) rich (ϕ = 1.5) H_2–O_2–Ar flame with 2% added HCN.[10] Here, the principal N_2O formation channel is NCO + NO → N_2O + CO, although NH + NO → N_2O + H makes a significant contribution to N_2O formation. As before, the principal N_2O removal channel is $N_2O + H \rightarrow N_2 + OH$. Figure 80 shows the principal N_2O formation and removal channels in a well-stirred reactor for methane and air.[36] For lean and moderately rich fuel–air mixtures ($\phi < 1.2$), the principal N_2O formation reaction is

$$O + N_2 + M \rightleftharpoons N_2O + M. \qquad (-A205)$$

For richer mixtures, reactions (A197) and (A202) become the principal N_2O-formation steps. For lean mixtures, the most important N_2O-removal reaction is (A204), forming N_2, with a small contribution from reactions (−A202) and (A207), forming NO. For stoichiometric and rich mixtures the principal N_2O-removal reaction is (A204). Because of the high radical concentrations and long residence times, any N_2O formed is almost completely removed and very little N_2O is predicted in the reactor (less than 1 ppmv).

Available rate data for N_2O-formation reactions (A202) and (A197) are summarized in Figs 81 and 82, respectively. There is excellent agreement among the low-temperature studies for the rate of the overall reaction NH + NO → products. However, there is considerable disagreement among the high-

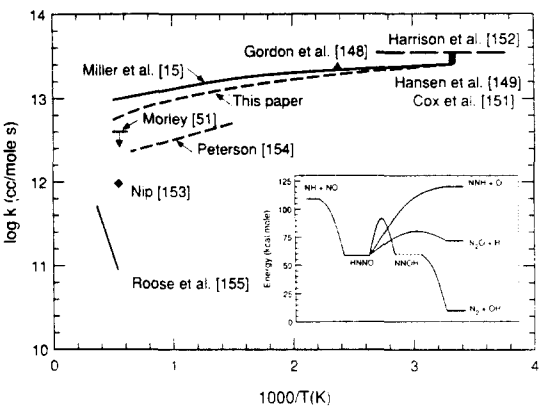

FIG. 81. Compilation of rate coefficients for NH + NO → products, and an energy diagram for various intermediates and products from Ref. 116.

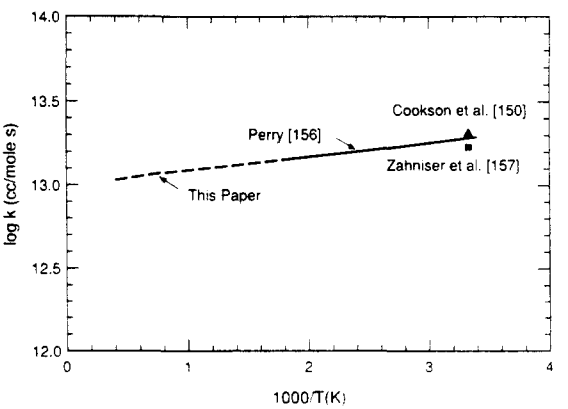

FIG. 82. Compilation of rate coefficients for NCO + NO → products.

temperature studies, all of which involved an indirect determination of the reaction rate. In none of the studies published to date has a direct measurement been made of the products of this reaction. The results of a BAC-MP4 calculation,[116] shown as an inset in Fig. 81, indicate that the NH + NO reaction proceeds through a stable HNNO intermediate to three possible sets of products. The energy barriers associated with the subsequent reactions of HNNO indicate that the primary product channel at temperatures of interest in combustion is

$$NH + NO \rightleftharpoons HNNO \longrightarrow N_2O + H, \qquad (A202)$$

even though the channel yielding N_2 + OH is 60 kcal/mol more exothermic. These calculations also show that there is no barrier to forming the HNNO intermediate, indicating that reaction (A202) could have a small negative temperature dependence. The rate coefficient expression used in the present calculations,

$$k_{A202} = 2.46 \times 10^{15} T^{-0.8} \text{ cm}^3/\text{mol-sec},$$

is based on an extrapolation of the low-temperature data[148-152] so as to pass near the upper limit for k_{A202} at 1790 K set by Morley.[51] The present value of k_{A202} at flame temperatures lies somewhat higher than several indirect determinations.[153-155] However, any significant reduction in k_{A202} will compromise the agreement between calculated and measured N_2O profiles in the low-pressure NH_3 - O_2 flame (Fig. 41). An increase in k_{A202} at high temperatures is possible without altering the results of Fig. 41 if the rate coefficient of the N_2O removal step,

$$N_2O + OH \rightleftharpoons N_2 + HO_2, \qquad (A203/B28)$$

were somewhat larger than used in the present calculations.

Data on the rate coefficient of the overall reaction NCO + NO → products are available only at temperatures below 1000 K. In Fig. 82, it is seen that there is excellent agreement among the three recent studies of this reaction. The reaction appears to exhibit a small negative temperature dependence suggesting that the reaction proceeds with no energy barrier through a stable intermediate,

$$NCO + NO \longrightarrow OCNNO \longrightarrow \text{products}.$$

There are only limited data on the products of this reaction, and BAC-MP4 calculations have not yet been extended to systems involving five heavy atoms. Perry[156] argues on thermochemical and structural grounds that the most likely channel is the exothermic reaction,

$$NCO + NO \rightleftharpoons N_2O + CO \quad (\Delta H = -65 \text{ kcal/mol}).$$

However, Perry notes that other exothermic channels, such as

$$NCO + NO \rightleftharpoons N_2 + CO_2 \quad (\Delta H = -153 \text{ kcal/mol})$$

and

$$NCO + NO \rightleftharpoons N_2 + CO + O \quad (\Delta H = -26 \text{ kcal/mol})$$

cannot be excluded. Zahniser *et al.*[157] have established a lower limit for the branching fraction of the reaction at 300 K,

$$k_{A197}/k_{\text{overall}} \geq 0.4,$$

suggesting that the N_2O channel is the dominant channel at low temperatures, in agreement with Perry. In the present study, we have used a rate coefficient expression for reaction (A197) that is an extrapolation of the low-temperature rate expression, suggested by Perry, for the overall reaction NCO + NO → products, assuming a branching fraction of unity; i.e.

$$k_{A197} = 1.0 \times 10^{13} \exp(390 \text{ cal}/RT) \text{ cm}^3/\text{mol-sec}.$$

There have been numerous studies of the important N_2O removal channel,

$$N_2O + H \longrightarrow \text{products},$$

in the temperature range 390–3000 K. However, only two studies[158,159] have measured the reaction rate directly and, to date, there have been no direct determinations of the reaction products. Rate data from the two direct studies are presented in Fig. 83, together with the recommendation from the Leeds compilation.[1] There is generally good agreement among these results in the range of overlapping tem-

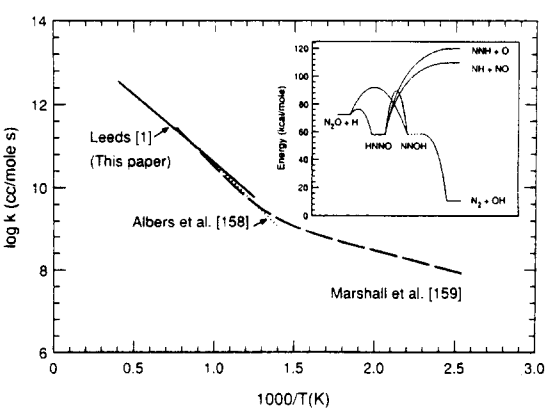

FIG. 83. Compilation of rate coefficients for N_2O + H → products, and an energy diagram for various intermediates and products from Ref. 159.

peratures. The reaction exhibits distinct curvature on an Arrhenius diagram below 750 K, which has been attributed to tunneling.[159] Results from BAC-MP4 calculations for the reaction[159] are shown as an inset on Fig. 83. These calculations indicate that the dominant channel at combustion temperatures is

$$N_2O + H \longrightarrow \ldots \longrightarrow N_2 + OH.$$

At 2000 K, the rate of the NO-producing channel

$$N_2O + H \longrightarrow \ldots \longrightarrow NH + NO$$

is estimated to be less than 7% of the overall reaction rate. In the present model calculations, we have used the rate expression in the Leeds compilation, which is in close agreement with the direct measurements at temperatures above 800 K. In the temperature range 800–2000 K, the estimated uncertainty of the rate coefficient expression is ±50%.

9. CONCLUDING REMARKS

In this paper we have tried to synthesize an extensive amount of information into a consistent and coherent description of the mechanism by which nitrogen compounds react under conditions typically found in combustion systems. While the reaction mechanism has been tested against experimental data over a relatively broad range of temperatures, pressures, stoichiometries, and fuel types, caution should be exercised in applying the mechanism outside of the range of conditions considered in this paper.

In the process of surveying rate data on elementary reactions in the mechanism and comparing model predictions with experimental data, we identified several areas where additional kinetic information is needed. Notable among these are the reactions between carbon-containing radicals and N_2 and NO, particularly

$$CH + N_2 \rightleftharpoons HCN + N$$

and

$$CH + NO \rightleftharpoons HCN + O$$

$$C + NO \rightleftharpoons CN + O$$

$$CH_2 + NO \rightleftharpoons HCNO + H$$

$$HCCO + NO \rightleftharpoons HCNO + CO.$$

The branching fraction of the $NH_2 + NO \rightarrow$ products reaction. particularly at high temperature, and the lifetime of NNH are still uncertain and need to be determined accurately for a truly fundamental understanding of NO aftertreatment schemes. The extent to which reactions such as $NH + NO \rightarrow$ products and $NCO + NO \rightarrow$ products produce N_2O is not yet firmly established. Lastly, the role played by $^1CH_2$ in producing low-molecular-weight hydrocarbon free radicals needs further clarification. Very little information is available on reactions of $^1CH_2$ at any temperature, particularly at temperatures of interest in combustion.

It is unlikely that the mechanism presented here is the final word on the subject. However, future modifications are more likely to be quantitative rather than qualitative, and diagrams such as Fig. 11 are likely to remain relatively unaltered. We hope that the present article (and the reaction mechansim) will be a useful point of departure for future discussions of nitrogen chemistry in combustion.

Acknowledgements—We would like to thank Fran Rupley for preparing the figures for this paper. In addition, we acknowledge John Kramlich, Dick Lyon, Dennis Siebers, and Mark Zahniser for providing copies of some of their papers prior to publication. JAM is grateful to Bob Kee (Sandia), Peter Glarborg (Technical University of Denmark), and Carl Melius (Sandia) for their past and continuing influence on his thinking about modeling of nitrogen chemistry in combustion. We are also grateful to Peter Glarborg for doing the initial calculations that resulted in Figs 5 and 6. CTB would like to thank Dan Seery, Brian Haynes, and Ron Hanson for many stimulating discussions of the kinetics of nitrogen species in flames.

REFERENCES

1. Baulch, D. L., Drysdale, D. D., Horne, D. G. and Lloyd, A. C. *Evaluated Kinetic Data for High Temperature Reactions*, Vol. 1 and Vol. 2, CRC Press, Cleveland (1973).
2. Hanson, R. K. and Salimian, S. Survey of rate constants in the N/H/O system, *Combustion Chemistry*, W.C. Gardiner, Jr (Ed.), Springer, New York (1984).
3. Kee, R. J., Miller, J. A. and Jefferson, T. H. CHEMKIN: A general-purpose, problem-independent, transportable, Fortran chemical kinetics code package, *Sandia Rep. SAND80-8003* (1980).
4. Kee, R. J., Rupley, F. M. and Miller, J. A. The chemkin thermodynamic data base, *Sandia Rep. SAND87-8215* (1987).
5. Kee, R. J., Dixon-Lewis, G., Warnatz, J., Coltrin, M. E. and Miller, J. A. A Fortran computer package for the evaluation of gas-phase, multicomponent transport properties, *Sandia Rep. SAND87-8246* (1986).
6. Kee, R. J., Grcar, J. F., Smooke, M. D. and Miller, J. A. A Fortran program for modeling steady laminar one-dimensional premixed flames, *Sandia Rep. SAND85-8240* (1985).
7. Glarborg, P., Kee, R. J., Grcar, J. F. and Miller, J. A. PSR: A Fortran program for modeling well-stirred reactors, *Sandia Rep. SAND 86-8209* (1986).
8. Lutz, A. E., Kee, R. J. and Miller, J. A. SENKIN: A Fortran program for predicting homogeneous gas phase chemical kinetics with sensitivity analysis, *Sandia Rep. SAND87-8248* (1988).
9. Grcar, J. F., Kee, R. J., Smooke, M. D. and Miller, J. A. *21st Symp. (Int.) Combust.*, pp. 1773–1782, The Combustion Institute, Pittsburgh (1987).

10. MILLER, J. A., BRANCH, M. C., MCLEAN, W. J., CHANDLER, D. W., SMOOKE, M. D. and KEE, R. J. *20th Symp. (Int.) Combust.*, pp. 673–684, The Combustion Institute, Pittsburgh (1985).
11. GLARBORG, P., MILLER, J. A. and KEE, R. J. *Combust. Flame* **65**, 177 (1986).
12. THORNE, L. R., BRANCH, M. C., CHANDLER, D. W., KEE, R. J. and MILLER, J. A. *21st Symp. (Int.) Combust.*, pp. 965–977, The Combustion Institute, Pittsburgh (1986).
13. MILLER, J. A., BRANCH, M. C. and KEE, R. J. *Combust. Flame* **43**, 81 (1981).
14. MILLER, J. A., MITCHELL, R. E., SMOOKE, M. D. and KEE, R. J. *19th Symp. (Int.) Combust.*, pp. 181–196, The Combustion Institute, Pittsburgh (1982).
15. MILLER, J. A., SMOOKE, M. D., GREEN, R. M. and KEE, R. J., *Combust. Sci. Technol.* **34**, 149 (1983).
16. WAGNER, A. F. and WARDLAW, D. M. *J. Phys. Chem.* **92**, 2462 (1988).
17. STEWART, P. H., SMITH, G. P. and GOLDEN, D. M. The pressure and temperature dependence of methane decomposition, *Int. J. Chem. Kinet.*, in press.
18. MONAT, J. P., HANSON, R. K. and KRUGER, C. H. *17th Symp. (Int.) Combust.*, pp. 543–552, The Combustion Institute, Pittsburgh (1979).
19. ZELDOVICH, YA. B., SADOVNIKOV, P. YA. and FRANK-KAMENETSKII, D. A. Oxidation of nitrogen in combustion, translated by M. Shelef, Academy of Sciences of the USSR, Moscow (1947). (See also ZELDOVICH, Ya. B., BARENBLATT, G. I., LIBROVICH, V. B. and MAKHVILADZE, G. M. *The Mathematical Theory of Combustion and Explosions*, pp. 30–36, Consultants Bureau, New York (1985).)
20. FENIMORE, C. P. *13th Symp. (Int.) Combust.*, pp. 373–379, The Combustion Institute, Pittsburgh (1971).
21. IVERACH, D., KIROV, N. K. and HAYNES, B. S., *Combust. Sci. Technol.* **8**, 139 (1973).
22. BACHMEIER, F., EBERIUS, K. H. and JUST, TH. *Combust. Sci. Technol.* **7**, 77 (1973).
23. HAYHURST, A. N. and MCLEAN, H. G., *Nature* **251**, 303 (1974).
24. HAYHURST, A. N. and VINCE, I. M. *Prog. Energy Combust. Sci.* **6**, 35 (1980).
25. IVERACH, D., BASDEN, K. S. and KIROV, N. Y. *14th Symp. (Int.) Combust.*, pp. 767–775, The Combustion Institute, Pittsburgh (1973).
26. BLAUWENS, J., SMETS, B. and PEETERS, J. *16th Symp. (Int.) Combust.*, pp. 1055–1064, The Combustion Institute, Pittsburgh (1977).
27. MIYAUCHI, T., MORI, Y. and IMAMURA, A. *16th Symp. (Int.) Combust.*, pp. 1073–1082, The Combustion Institute, Pittsburgh (1977).
28. MATSUI, Y. and NOMAGUCHI, T. *Combust. Flame* **32**, 205 (1978).
29. MATSUI, Y. and YUUKI, A. *Jap. J. Appl. Phys.* **24**, 598 (1985).
30. PERRY, R. A. and MELIUS, C. F. *20th Symp. (Int.) Combust.*, pp. 639–646, The Combustion Institute, Pittsburgh (1984).
31. MILLER, J. A., PARRISH, C. and BROWN, N. J. *J. Phys. Chem.* **90**, 3339 (1986).
32. BENSON, S.W. *16th Symp. (Int.) Combust.*, p. 1062, The Combustion Institute, Pittsburgh (1977).
33. SANDERS, W. A., LIN, C. Y. and LIN, M. C. *Combust. Sci. Technol.* **51**, 103 (1987).
34. BAIR, R. A. Annual Report, Theoretical Chemistry Group (Chemistry Division), Argonne National Laboratory, September (1985).
35. BERMAN, M. R. and LIN, M. C. *J. Phys. Chem.* **87**, 3933 (1983).
36. BARTOK, W., ENGLEMAN, V. S., GOLDSTEIN, R. and DEL VALLE, E. G. *AIChE Symp.*, Ser. 126 **68**, 30 (1972).
37. WHYTE, A. R. and PHILLIPS, L. F. *Chem. Phys. Lett.* **98**, 590 (1983).
38. SLACK, M. W. *J. Chem. Phys.* **64**, 228 (1976).
39. NATARAJAN, K. and ROTH, P. *21st Symp. (Int.) Combust.*, pp. 729–737, The Combustion Institute, Pittsburgh (1986).
40. GLARBORG, P. Kinetisk modellering of dannelse og nedbrydning af NO_x ved forbraending af simple kulbrinter, Doctoral thesis, Technical University of Denmark (1987) (in Danish).
41. MALTE, P. C. and PRATT, D. T. *Combust. Sci. Technol.* **9**, 221 (1974).
42. MALTE, P. C. and PRATT, D. T. *15th Symp. (Int.) Combust.*, pp. 1061–1070, The Combustion Institute, Pittsburgh (1975).
43. ZABARNICK, S., FLEMING, J. W. and LIN, M. C. *21st Symp. (Int.) Combust.*, pp. 713–719, The Combustion Institute, Pittsburgh (1986).
44. FENIMORE, C. P. *Combust. Flame* **19**, 289 (1972).
45. AXWORTHY, A. E. and DAYAN, V. H. Chemical reactions in the conversion of fuel nitrogen to NO_x: Fuel pyrolysis studies, *2nd EPA Stationary Source Combust. Symp.*, September (1977).
46. FENIMORE, C. P. *Combust. Flame* **26**, 249 (1976).
47. DE SOETE, G. G. *15th Symp. (Int.) Combust.*, pp. 1093–1102, The Combustion Institute, Pittsburgh (1975).
48. HOUSER, T. J., HULL, M., ALWAY, R. M. and BIFTU, T. *Int. J. Chem. Kinet.* **12**, 579 (1980).
49. HAYNES, B. S. *Combust. Flame* **28**, 113 (1977).
50. MORLEY, C. *Combust. Flame* **27**, 189 (1976).
51. MORLEY, C. *18th Symp. (Int.) Combust.*, pp. 23–32, The Combustion Institute, Pittsburgh (1981).
52. FENIMORE, C. P. *17th Symp. (Int.) Combust.*, pp. 661–670, The Combustion Institute, Pittsburgh (1979).
53. MILLER, J. A. and MELIUS, C. F. *21st Symp. (Int.) Combust.*, pp. 919–927, The Combustion Institute, Pittsburgh (1986).
54. DAVIES, P. B. and THRUSH, B. A. *Trans. Faraday Soc.* **64**, 1836 (1968).
55. ROTH, P., LOHR, R. and HERMANNS, H. D. *Ber. Bunsenges. Phys. Chem.* **84**, 835 (1980).
56. LOUGE, M. Y. and HANSON, R. K. *20th Symp. (Int.) Combust.*, pp. 665–672, The Combustion Institute, Pittsburgh (1984).
57. SZEKELY, A., HANSON, R. K. and BOWMAN, C. T. *20th Symp. (Int.) Combust.*, pp. 647–654, The Combustion Institute, Pittsburgh (1984).
58. SZEKELY, A., HANSON, R. K. and BOWMAN, C. T. *Int. J. Chem. Kinet.* **16**, 1609 (1984).
59. FRITZ, B., LORENTZ, K., STEINERT, W. and ZELLNER, R. *Oxidation Commun.* **6**, 363 (1984).
60. MYERSON, A. L., TAYLOR, F. R. and FAUNCE, B. G. *6th Symp. (Int.) Combust.*, pp. 154–163, Reinhold, NY (1957).
61. WENDT, J. O. L., STERNLING, C. V. and MATOVICH, M. A. *14th Symp. (Int.) Combust.*, pp. 897–904, The Combustion Institute, Pittsburgh (1973).
62. MYERSON, A. L. *15th Symp. (Int.) Combust.*, pp. 1085–1092, The Combustion Institute, Pittsburgh (1975).
63. SONG, Y. H., BLAIR, D. W., SIMINSKI, V. J. and BARTOK, W. *18th Symp. (Int.) Combust.*, pp. 53–63, The Combustion Institute, Pittsburgh (1981).
64. CHEN, S. L., MCCARTHY, J. M., CLARK, W. D., HEAP, M. P., SEEKER, W. R. and PERSHING, D. W. *21st Symp. (Int.) Combust.*, pp. 1159–1169, The Combustion Institute, Pittsburgh (1986).
65. MIYAME, S., IKEBE, H. and MAKINO, K. Evaluation of in-furnace NO_x reduction, *Proc. 1985 Joint Symp. Stationary Combustion NO_x Control* (1986).
66. LANGFORD, A. O., PETEK, H. and MOORE, C. B. *J.*

Chem. Phys. **78,** 6650 (1983).
67. FENIMORE, C. P. and JONES, G. W. *J. Phys. Chem.* **65,** 298 (1961).
68. MACLEAN, D. I. and WAGNER, H. GG. *11th Symp. (Int.) Combust.*, pp. 871–878, The Combustion Institute, Pittsburgh (1967).
69. MILLER, J. A., SMOOKE, M. D., GREEN, R. M. and KEE, R. J. Kinetic modelling of the oxidation of ammonia in flames, *Western States Section/Combust. Inst. Meet.*, Pap. 82–93, (1982).
70. BIAN, J., VANDOOREN, J. and VAN TIGGELEN, P. J. *21st Symp. (Int.) Combust.*, pp. 953–963, The Combustion Institute, Pittsburgh (1986).
71. DEAN, A. M., CHOU, M. S. and STERN, D. Nitrogen chemistry in flames: Observations and detailed modeling, *185th Nat. ACS Meet.* (1983).
72. SALIMIAN, S., HANSON, R. K. and KRUGER, C. H. *Combust. Flame* **56,** 83 (1984).
73. SALIMIAN, S., HANSON, R. K. and KRUGER, C. H. *Int. J. Chem. Kinet.* **16,** 725 (1984).
74. ZABIELSKI, M. F. and SEERY, D. J. *Int. J. Chem. Kinet.* **17,** 1191 (1985).
75. JEFFRIES, J. B. and SMITH, G. P. *J. Phys. Chem.* **90,** 487 (1986).
76. MICHAEL, J. V., SUTHERLAND, J. W. and KLEMM, R.B. *J. Phys. Chem.* **90,** 497 (1986).
77. HACK, W., ROUVEIROLLES, P. and WAGNER, H. GG. *J. Phys. Chem.* **90,** 2505 (1986).
78. MARSHALL, P. and FONTIJN, A. *J. Chem. Phys.* **85,** 2637 (1986).
79. COHEN, N. *Int. J. Chem. Kinet.* **19,** 319 (1987).
80. PERRY, R. A. *Chem. Phys. Lett.* **106,** 223 (1984).
81. HACK, W., KURZKE, H. and WAGNER, H. GG. *J. Chem. Soc. Faraday Trans. 2* **81,** 949 (1985).
82. BINKLEY, J. S. and MELIUS, C. F. Oxidation of NH and NH_2 radicals, *Western States Combust. Inst. Meet.*, Pap. 82–96, (1982).
83. DRANSFELD, P., HACK, W., KURZKE, H., TEMPS, F. and WAGNER, H. GG. *20th Symp. (Int.) Combust.*, pp. 655–663, The Combustion Institute, Pittsburgh (1984).
84. GREEN, R. M. and MILLER, J. A. *J. Quant. Spectrosc. Radiat. Trans.* **26,** 313 (1981).
85. SCHOFIELD, K. *21st Symp. (Int.) Combust.*, p. 963, The Combustion Institute, Pittsburgh (1986).
86. VAUGHN, C. B., SUN, W. H., HOWARD, J. B. and LONGWELL, J. P. Measurements and modeling of light hydrocarbons in rich C_2H_4 combustion in a jet-stirred reactor, *Combust. Flame*, submitted for publication.
87. SUN, W. H., LONGWELL, J. P. and SAROFIM, A. F. Rich mixture reactions of nitrogen species in a stirred reactor with ethylene fuel, paper presented at the Symposium on the Formation and Control of NO_x Emissions from Combustion Sources, ACS Award Symposium on the Chemistry of Contemporary Technological Problems (honoring William Bartok), *193rd ACS Nat. Meet.* (1987). Also SUN, W. H., WIKSTROM, C. V., VAUGHN, C. B., LONGWELL, J. P. and SAROFIM, A. F. Reactions of nitrogen species during ammonia doped ethylene combustion in a stirred reactor, *Combust. Flame*, submitted for publication.
88. SAROFIM, A. F. and FLAGAN, R. C. *Prog. Energy Combust. Sci.* **2,** 1 (1976).
89. BARHNART, D. H. and DIEHL, E. K. *J. Air Pollut. Control Ass.* **10,** 397 (1960).
90. SIEGMUND, C. W. and TURNER, D. W. *J. Engng Pwr* **96,** 1 (1974).
91. YAMAGISHI, K., NOZAWA, M., YOSHIE, T., TOKUMOTO, T. and KAKEGAWA, Y. *15th Symp. (Int.) Combust.*, pp. 1157–1166, The Combustion Institute, Pittsburgh (1975).
92. LEFEBVRE, A. H. *15th Symp. (Int.) on Combust.*, pp. 1169–1180, The Combustion Institute, Pittsburgh (1975).
93. ROSENBERG, H. S., CURRAN, L. M., SLACK, A. V., ANDO, J. and OXLEY, J. H. *Prog. Energy Combust. Sci.* **6,** 287 (1980).
94. LYON, R. K. Method for the reduction of the concentration of NO in combustion effluents using ammonia, *U.S. Pat. 3,900,544* (1975).
95. LYON, R. K. *Envir. Sci. Technol.* **21,** 231 (1987).
96. PERRY, R. A. NO reduction using sublimation of cyanuric acid, *U.S. Pat. 4,731,231* (1988).
97. PERRY, R. A. and SIEBERS, D. L. *Nature* **324,** 657 (1986).
98. LYON, R. K. and BENN, D. J. *17th Symp. (Int.) Combust.* pp. 601–610, The Combustion Institute, Pittsburgh (1979).
99. LYON, R. K. and HARDY, J. E. *Ind. Engng. Chem. Fund.* **25,** 19 (1986).
100. LYON, R. K. Kinetics and mechanism of thermal $DeNO_x$: A review, *194th Ann. ACS Meet., Div. Fuel Chem.* **32,** 433 (1987).
101. LYON, R. K. *Int. J. Chem. Kinet.* **8,** 315 (1976).
102. MUZIO, L. J., ARAND, J. K. and TEIXEIRA, D. P. *16th Symp. (Int.) Combust.*, pp. 199–208, The Combustion Institute, Pittsburgh (1977).
103. SALIMIAN, S. and HANSON, R. K. *Combust. Sci. Technol.* **23,** 225 (1980).
104. SILVER, J. A. *Combust. Flame* **53,** 17 (1983).
105. KIMBALL-LINNE, M. A. and HANSON, R. K. *Combust. Flame* **64,** 337 (1986).
106. DEAN, A. M., HARDY, J. E. and LYON, R. K. *19th Symp. (Int.) Combust.*, pp. 97–105, The Combustion Institute, Pittsburgh (1983).
107. MILLER, J. A., BRANCH, M. C. and KEE, R. J. A chemical kinetic model for the selective reduction of nitric oxide by ammonia, *Sandia Rep. SAND80-8635* (1980).
108. LUCAS, D. and BROWN, N. J. *Combust. Flame* **47,** 219 (1982).
109. DOLSON, D. A. *J. Phys. Chem.* **90,** 6714 (1986).
110. STEIF, L. J., BROBST, W. D., NAVA, D. F., BORKOWSKI, R. P. and MICHAEL, J. V. *J. Chem. Soc. Faraday Trans. 2* **78,** 1391 (1982).
111. SILVER, J. A. and KOLB, E. C. *J. Phys. Chem.* **80,** 3240 (1982).
112. SILVER, J. A. and KOLB, C. E. *J. Phys. Chem.* **91,** 3713 (1987).
113. HALL, J. L., ZEITZ, D., STEPHANS, J. W., KASPAR, J. V. V., GLASS, G. P., CURL, R. F. and TITTEL, F. K. *J. Phys. Chem.* **90,** 2051 (1986).
114. ANDRESEN, P., JACOBS, A., KLEINERMANNS, C. and WOLFRUM, J. *19th Symp. (Int.) Combust.*, pp. 11–22, The Combustion Institute, Pittsburgh (1982).
115. PHILLIPS, L. F. *Chem. Phys. Lett.* **135,** 269 (1987).
116. MELIUS, C. F. and BINKLEY, J. S. *20th Symp. (Int.) Combust.*, pp. 578–583, The Combustion Institute, Pittsburgh (1984).
117. ABOU-RACHID, H., POUCHAN, C. and CHAILLET, M. *Chem. Phys.* **90,** 243 (1984).
118. CURTISS, L. A., DRAPCHO, D. L. and POPLE, J. A. *Chem. Phys. Lett.* **103,** 437 (1984).
119. HARRISON, J. A., MACLAGAN, R. G. A. R. and WHITE, A. R. *J. Phys. Chem.* **91,** 6683 (1987).
120. MILLER, J. A. *19th Symp. (Int.) Combust.*, pp. 20–21, The Combustion Institute, Pittsburgh (1982).
121. SIEBERS, D. L. and CATON, J. A. Reduction of nitrogen oxides by The RAPRENO$_x$ process, *Sandia Rep. SAND88-8731B* (1988). Also *Central States Section/Combust. Inst. Meet.*, Pap 53 (1988).
122. JOHNSON, G. M. and SMITH, M. Y. *Combust. Sci. Technol.* **19,** 67 (1978).
123. COUTANT, R. W., MERRYMAN, E. L. and LEVY, A. *Envir. Int.* **8,** 185 (1982).
124. TRAYNOR, G. W., GIRMAN, J. R., APTE, M. G., DILLWORD, J. F. and WHITE, P. D. *J. Air Pollut. Conf.*

Ass. **35,** 231 (1985).
125. MERRYMAN, E. L. and LEVY, A. *15th Symp. (Int.) Combust.*, pp. 1073–1083, The Combustion Institute, Pittsburgh (1975).
126. FENIMORE, C. P. *Combust. Flame* **25,** 85 (1975).
127. HARGREAVES, K. J. A., HARVEY, R., ROPER, F. G. and SMITH, D. B. *18th Symp. (Int.) Combust.*, pp. 133–142, The Combustion Institute, Pittsburgh (1981).
128. CERANSKY, N. P. and SAWYER, R. F. *15th Symp. (Int.) Combust.*, pp. 1039–1048, The Combustion Institute, Pittsburgh (1975).
129. SCHEFER, R. W. and SAWYER, R. F. *16th Symp. (Int.) Combust.*, pp. 119–134, The Combustion Institute, Pittsburgh (1977).
130. OVEN, M. J., GOULDIN, F. C. and MCLEAN, W. J. *17th Symp. (Int.) Combust.*, pp. 363–374, The Combustion Institute (1979).
131. DRAKE, M. C., CORREA, S. M., PITZ, R. W., SHYY, W. and FENIMORE, C. P. *Combust. Flame* **69,** 347 (1987).
132. DUTERQUE, J., AVEZARD, N. and BORGHI, R. *Combust. Sci. Technol.* **25,** 85 (1981).
133. ALLEN, J. D. *Combust. Flame* **24,** 133 (1975).
134. JOHNSON, G. M., SMITH, M. Y. and MULCAHY, M. R. F. *17th Symp. (Int.) Combust.*, pp. 647–660, The Combustion Institute, Pittsburgh (1979).
135. SANO, T. *Combust. Sci. Technol.* **29,** 261 (1982).
136. SANO, T. *Combust. Sci. Technol.* **38,** 129 (1984).
137. SANO, T. *Combust. Sci. Technol.* **43,** 259 (1985).
138. MCLEAN, W. J. *17th Symp. (Int.) Combust.*, pp. 659–660, The Combustion Institute, Pittsburgh (1979).
139. HORI, M. *21st Symp. (Int.) Combust.*, pp. 1181–1188, The Combustion Institute, Pittsburgh (1986).
140. LEUNG, S. W., STRAND, M., SAWYER, R. F. and KOSHLAND, C. P. The formation and destruction of nitrogen dioxide, *Proc. Joint Conf. Western States Jap. Sect. Combust. Inst.*, 11–13 (1987).
141. PIEROTTI, D. and RASMUSSEN, R. A. *Geophys. Res. Lett.* **3,** 265 (1976).
142. WEISS, R. F. and CRAIG, H. *Geophys. Res. Lett.* **3,** 751 (1976).
143. HAO, W. M., WOFSY, S. C., MCELROY, M. B., BEER, J. M. and TOQAN, M. A. *J. Geophys. Res.* **92,** 3098 (1987).
144. KRAMLICH, J. C., NIHART, R. K., CHEN, S. L., PERSHING, D. W. and HEAP, M. P., *Combust. Flame* **48,** 101 (1982).
145. KRAMLICH, J. C., COLE, J. A., MCCARTHY, J. M., LANIER, W. S. and MCSORLEY, J. A. *Combust. Flame*, in press.
146. HAO, W. M., WOFSY, S. C., MCELROY, M. B., FARMAYAN, W. F., TOQAN, M. A., BEER, J. M., ZAHNISER, M. S., SILVER, J. A. and KOLB, C. E. *Combust. Sci. Technol.* **55,** 23 (1987).
147. ROBY, R. J. and BOWMAN, C. T. *Combust. Flame* **70,** 119 (1987).
148. GORDON, S., MULAC, W. and NANGIA, P. *J. Phys. Chem.* **75,** 2087 (1971).
149. HANSEN, I., HÖINGHAUS, K., ZETZSCH, C. and STUHL, F. *Chem. Phys. Lett.* **42,** 370 (1976).
150. COOKSON, J. L., HANCOCK, G. and MCKENDRICK, K. G. *Ber. Bunsenges. Phys. Chem.* **89,** 335 (1985).
151. COX, J. W., NELSON, H. H. and MCDONALD, J. R. *Chem. Phys.* **96,** 175 (1985).
152. HARRISON, J. A., WHYTE, A. R. and PHILLIPS, L. F. *Chem. Phys. Lett.* **129,** 346 (1986).
153. NIP, W. S., Ph.D. Thesis, University of Toronto (1974).
154. PETERSON, R. C., Ph.D. Thesis, Purdue University (1981).
155. ROOSE, T. R., HANSON, R. K. and KRUGER, C. H. *18th Symp. (Int.) Combust.*, pp. 853–862, The Combustion Institute, Pittsburgh (1981).
156. PERRY, R. A. *J. Chem. Phys.* **82,** 5485 (1985).
157. ZAHNISER, M. S., MCCURDY, K. and KOLB, C. E. *Chem. Phys. Lett.*, to be published.
158. ALBERS, E. A., HOYERMANN, K., SCHACKE, H., SCHMATJKO, K. J. and WAGNER, G. GG. *15th Symp. (Int.) Combust.*, pp. 765–773, The Combustion Institute, Pittsburgh (1975).
159. MARSHALL, P., FONTIJN, A. and MELIUS, C. F. *J. Chem. Phys.* **86,** 5540 (1987).
160. LESCLAUX, R. *Rev. Chem. Intermed.* **5,** 347 (1984).
161. LYON, R. K. and COLE, J. A. A reexamination of the RAPRENO$_x$ process, *Combust. Flame*, submitted for publication.
162. HEAP, M. P., CHEN, S. L., MCCARTHY, J. M., KRAMLICH, J. C. and PERSHING, D. W. An advanced selective reduction process for NO$_x$ control, *Nature*, submitted for publication.
163. SIEBERS, D. L. and CATON, J. A. Removal of nitric oxide from exhaust gas with cyanuric acid, *Western States Sect./Combust. Inst. Meet.*, Pap. 88–66 (1988).
164. CATON, J. A. and SIEBERS, D. L. Reduction of nitrogen oxides in engine exhaust gases by the addition of cyanuric acid, *Sandia Rep. SAND88-8693* (1988). Also *ASME J. Eng. Gas Turbines Pwr*, submitted for publication.
165. CATON, J. A. and SIEBERS, D. L. Comparison of nitric oxide removal by cyanuric acid and by ammonia, *Western States Sect./Combust. Inst. Meet.*, Pap. 88–67 (1988).
166. MERTENS, J. D., CHANG, A. Y., HANSON, R. K. and BOWMAN, C. T. Decomposition kinetics of HNCO at high temperatures, *Western States Sect./Combust. Inst. Meet.*, Pap. 88–64 (1988).
167. TULLY, F. P., PERRY, R. A., THORNE, L. R. and ALLENDORF, M. A. Free-radical oxidation of isocyanic acid, presented at the *22nd Symp. (Int.) Combust.*, (1988).
168. ROTH, P. and IBREIGHITH, M. *Combust. Flame* **55,** 279 (1984).
169. WARNATZ, J. Rate coefficients in the C/H/O System, *Combustion Chemistry*, W. C. Gardiner, Jr (Ed.), Springer, New York, (1984).
170. TSANG, W. and HAMPSON, R. F. *J. Phys. Chem. Ref. Data* **15,** 1087 (1986).
171. DEAN, A. J., DAVIDSON, D. F., HANSON, R. K. and BOWMAN, C. T. Development and application of CH laser absorption diagnostic for shock tube kinetic studies, *Western States Sect./Combust. Inst. Meet.*, Pap. 88–91 (1988).
172. COOPER, D. A. *J. Inst. Energy* **61,** 78 (1988).
173. DEAN, A. J., DAVIDSON, D. F. and HANSON, R. K. C-atom ARAS diagnostic for shock tube studies of $C + N_2 \rightarrow CN + N$, *Proc. 17th Int. Symp. Shock Waves Shock Tubes* (1989).
174. ROBY, R. J. and BOWMAN, C. T. Effects of hydrocarbons on nitric oxide removal in rich, premixed hydrogen–oxygen flames, *Joint Meet. Western States Canadian Sect. Combust. Inst.*, Pap. 86–8 (1986).
175. SEERY, D. J. and ZABIELSKI, M. F. *18th Symp. (Int.) Combust.*, pp. 397–404, The Combustion Institute, Pittsburgh (1981).
176. CATTOLICA, R. J. *22nd Symp. (Int.) Combust.*, pp. 1165–1173, The Combustion Institute, Pittsburgh (1989).
177. SARV, H. and CERNANSKY, N. P. *Combust. Flame* **76,** 265 (1989).
178. MUZIO, L. J. and KRAMLICH, J. C. *Geophys. Res. Lett.* **15,** 1369 (1988).
179. DUTERQUE, J., AVEZARD, N. and BORGHI, R. *Combust. Sci. Technol.* **25,** 85 (1981).

APPENDIX A.

Reaction Mechanism Rate Coefficients In Form $k_f = AT^{\beta}\exp(-E/RT)$.
Units are moles, cubic centimeters, seconds, Kelvins and calories/mole.

	REACTION	A	β	E
1.	$2CH_3(+M) \rightleftarrows C_2H_6(+M)$			
	High pressure limit:	9.03e+16	−1.2	654.
	Low pressure limit:	3.18e+41	−7.0	2762.
	Troe parameters:[1] a= 6.04e-01, T^*= 6927.0, T^{**} = 132.			
	Enhanced third-body efficiencies:			
	H_2= 2.0, CO= 2.0, CO_2= 3.0, H_2O= 5.0			
2.	$CH_3 + H(+M) \rightleftarrows CH_4(+M)$			
	High pressure limit:	6.00e+16	−1.0	0.
	Low pressure limit:	8.00e+26	−3.0	0.
	SRI parameters:[2] 4.50e-01 797.0 979. 1.			
	Enhanced third-body efficiencies:			
	H_2= 2.0, CO= 2.0, CO_2= 3.0, H_2O= 5.0			
3.	$CH_4 + O_2 \rightleftarrows CH_3 + HO_2$	7.90e+13	0.000	56000.
4.	$CH_4 + H \rightleftarrows CH_3 + H_2$	2.20e+04	3.000	8750.
5.	$CH_4 + OH \rightleftarrows CH_3 + H_2O$	1.60e+06	2.100	2460.
5a.	$CH_4 + O \rightleftarrows CH_3 + OH$	1.02e+09	1.500	8604.
6.	$CH_4 + HO_2 \rightleftarrows CH_3 + H_2O_2$	1.80e+11	0.000	18700.
7.	$CH_3 + HO_2 \rightleftarrows CH_3O + OH$	2.00e+13	0.000	0.
8.	$CH_3 + O_2 \rightleftarrows CH_3O + O$	2.05e+19	−1.570	29229.
9.	$CH_3 + O \rightleftarrows CH_2O + H$	8.00e+13	0.000	0.
10.	$CH_2OH + H \rightleftarrows CH_3 + OH$	1.00e+14	0.000	0.
11.	$CH_3O + H \rightleftarrows CH_3 + OH$	1.00e+14	0.000	0.
12.	$CH_3 + OH \rightleftarrows CH_2 + H_2O$	7.50e+06	2.000	5000.
13.	$CH_3 + H \rightleftarrows CH_2 + H_2$	9.00e+13	0.000	15100.
14.	$CH_3O + M \rightleftarrows CH_2O + H + M$	1.00e+14	0.000	25000.
15.	$CH_2OH + M \rightleftarrows CH_2O + H + M$	1.00e+14	0.000	25000.
16.	$CH_3O + H \rightleftarrows CH_2O + H_2$	2.00e+13	0.000	0.
17.	$CH_2OH + H \rightleftarrows CH_2O + H_2$	2.00e+13	0.000	0.
18.	$CH_3O + OH \rightleftarrows CH_2O + H_2O$	1.00e+13	0.000	0.
19.	$CH_2OH + OH \rightleftarrows CH_2O + H_2O$	1.00e+13	0.000	0.
20.	$CH_3O + O \rightleftarrows CH_2O + OH$	1.00e+13	0.000	0.
21.	$CH_2OH + O \rightleftarrows CH_2O + OH$	1.00e+13	0.000	0.
22.	$CH_3O + O_2 \rightleftarrows CH_2O + HO_2$	6.30e+10	0.000	2600.
23.	$CH_2OH + O_2 \rightleftarrows CH_2O + HO_2$	1.48e+13	0.000	1500.
24.	$CH_2 + H \rightleftarrows CH + H_2$	1.00e+18	−1.560	0.
25.	$CH_2 + OH \rightleftarrows CH + H_2O$	1.13e+07	2.000	3000.
26.	$CH_2 + OH \rightleftarrows CH_2O + H$	2.50e+13	0.000	0.
27.	$CH + O_2 \rightleftarrows HCO + O$	3.30e+13	0.000	0.
28.	$CH + O \rightleftarrows CO + H$	5.70e+13	0.000	0.
29.	$CH + OH \rightleftarrows HCO + H$	3.00e+13	0.000	0.
30.	$CH + CO_2 \rightleftarrows HCO + CO$	3.40e+12	0.000	690.
31.	$CH + H \rightleftarrows C + H_2$	1.50e+14	0.000	0.
32.	$CH + H_2O \rightleftarrows CH_2O + H$	1.17e+15	−0.750	0.
33.	$CH + CH_2O \rightleftarrows CH_2CO + H$	9.46e+13	0.000	−515.
34.	$CH + C_2H_2 \rightleftarrows C_3H_2 + H$	1.00e+14	0.000	0.
35.	$CH + CH_2 \rightleftarrows C_2H_2 + H$	4.00e+13	0.000	0.
36.	$CH + CH_3 \rightleftarrows C_2H_3 + H$	3.00e+13	0.000	0.
37.	$CH + CH_4 \rightleftarrows C_2H_4 + H$	6.00e+13	0.000	0.
38.	$C + O_2 \rightleftarrows CO + O$	2.00e+13	0.000	0.
39.	$C + OH \rightleftarrows CO + H$	5.00e+13	0.000	0.
40.	$C + CH_3 \rightleftarrows C_2H_2 + H$	5.00e+13	0.000	0.

[1] Fall off reaction in the Troe form: $F_{cent}(T) = (1-a)\exp(-T/T^*) + a\exp(-T^{**}/T)$.
[2] Fall off reaction in the SRI form.

APPENDIX A. (continued)
Reaction Mechanism Rate Coefficients In Form $k_f = AT^{\beta} \exp(-E/RT)$.
Units are moles, cubic centimeters, seconds, Kelvins and calories/mole.

	REACTION	A	β	E
41.	$C + CH_2 \rightleftarrows C_2H + H$	5.00e+13	0.000	0.
42.	$CH_2 + CO_2 \rightleftarrows CH_2O + CO$	1.10e+11	0.000	1000.
43.	$CH_2 + O \rightleftarrows CO + 2H$	5.00e+13	0.000	0.
44.	$CH_2 + O \rightleftarrows CO + H_2$	3.00e+13	0.000	0.
45.	$CH_2 + O_2 \rightleftarrows CO_2 + 2H$	1.60e+12	0.000	1000.
46.	$CH_2 + O_2 \rightleftarrows CH_2O + O$	5.00e+13	0.000	9000.
47.	$CH_2 + O_2 \rightleftarrows CO_2 + H_2$	6.90e+11	0.000	500.
48.	$CH_2 + O_2 \rightleftarrows CO + H_2O$	1.90e+10	0.000	−1000.
49.	$CH_2 + O_2 \rightleftarrows CO + OH + H$	8.60e+10	0.000	−500.
50.	$CH_2 + O_2 \rightleftarrows HCO + OH$	4.30e+10	0.000	−500.
51.	$CH_2O + OH \rightleftarrows HCO + H_2O$	3.43e+09	1.180	−447.
52.	$CH_2O + H \rightleftarrows HCO + H_2$	2.19e+08	1.770	3000.
53.	$CH_2O + M \rightleftarrows HCO + H + M$	3.31e+16	0.000	81000.
54.	$CH_2O + O \rightleftarrows HCO + OH$	1.80e+13	0.000	3080.
55.	$HCO + OH \rightleftarrows H_2O + CO$	1.00e+14	0.000	0.
56.	$HCO + M \rightleftarrows H + CO + M$	2.50e+14	0.000	16802.
	Enhanced third-body efficiencies:			
	CO= 1.9, H_2= 1.9, CH_4= 2.8, CO_2= 3.0, H_2O= 5.0			
57.	$HCO + H \rightleftarrows CO + H_2$	1.19e+13	0.250	0.
58.	$HCO + O \rightleftarrows CO + OH$	3.00e+13	0.000	0.
59.	$HCO + O \rightleftarrows CO_2 + H$	3.00e+13	0.000	0.
60.	$HCO + O_2 \rightleftarrows HO_2 + CO$	3.30e+13	−0.400	0.
61.	$CO + O + M \rightleftarrows CO_2 + M$	6.17e+14	0.000	3000.
62.	$CO + OH \rightleftarrows CO_2 + H$	1.51e+07	1.300	−758.
63.	$CO + O_2 \rightleftarrows CO_2 + O$	1.60e+13	0.000	41000.
64.	$HO_2 + CO \rightleftarrows CO_2 + OH$	5.80e+13	0.000	22934.
65.	$C_2H_6 + CH_3 \rightleftarrows C_2H_5 + CH_4$	5.50e-01	4.000	8300.
66.	$C_2H_6 + H \rightleftarrows C_2H_5 + H_2$	5.40e+02	3.500	5210.
67.	$C_2H_6 + O \rightleftarrows C_2H_5 + OH$	3.00e+07	2.000	5115.
68.	$C_2H_6 + OH \rightleftarrows C_2H_5 + H_2O$	8.70e+09	1.050	1810.
69.	$C_2H_4 + H \rightleftarrows C_2H_3 + H_2$	1.10e+14	0.000	8500.
70.	$C_2H_4 + O \rightleftarrows CH_3 + HCO$	1.60e+09	1.200	746.
71.	$C_2H_4 + OH \rightleftarrows C_2H_3 + H_2O$	2.02e+13	0.000	5955.
72.	$CH_2 + CH_3 \rightleftarrows C_2H_4 + H$	3.00e+13	0.000	0.
73.	$H + C_2H_4(+M) \rightleftarrows C_2H_5(+M)$[3]			
	High pressure limit:	2.21e+13	0.0	2066.
	Low pressure limit:	6.37e+27	−2.8	−54.
	Enhanced third-body efficiencies:			
	H_2= 2.0, CO= 2.0, CO_2= 3.0, H_2O= 5.0			
74.	$C_2H_5 + H \rightleftarrows 2CH_3$	1.00e+14	0.000	0.
75.	$C_2H_5 + O_2 \rightleftarrows C_2H_4 + HO_2$	8.43e+11	0.000	3875.
76.	$C_2H_2 + O \rightleftarrows CH_2 + CO$	1.02e+07	2.000	1900.
77.	$C_2H_2 + O \rightleftarrows HCCO + H$	1.02e+07	2.000	1900.
78.	$H_2 + C_2H \rightleftarrows C_2H_2 + H$	4.09e+05	2.390	864.
79.	$H + C_2H_2(+M) \rightleftarrows C_2H_3(+M)$[3]			
	High pressure limit:	5.54e+12	0.0	2410.
	Low pressure limit:	2.67e+27	−3.5	2410.
	Enhanced third-body efficiencies:			
	H_2= 2.0, CO= 2.0, CO_2= 3.0, H_2O= 5.0			
80.	$C_2H_3 + H \rightleftarrows C_2H_2 + H_2$	4.00e+13	0.000	0.

[3] Fall off reaction in the Lindemann form.

APPENDIX A. (continued)
Reaction Mechanism Rate Coefficients In Form $k_f = AT^{\beta}\exp(-E/RT)$.
Units are moles, cubic centimeters, seconds, Kelvins and calories/mole.

	REACTION	A	β	E
81.	$C_2H_3 + O \rightleftarrows CH_2CO + H$	3.00e+13	0.000	0.
82.	$C_2H_3 + O_2 \rightleftarrows CH_2O + HCO$	4.00e+12	0.000	−250.
83.	$C_2H_3 + OH \rightleftarrows C_2H_2 + H_2O$	5.00e+12	0.000	0.
84.	$C_2H_3 + CH_2 \rightleftarrows C_2H_2 + CH_3$	3.00e+13	0.000	0.
85.	$C_2H_3 + C_2H \rightleftarrows 2C_2H_2$	3.00e+13	0.000	0.
86.	$C_2H_3 + CH \rightleftarrows CH_2 + C_2H_2$	5.00e+13	0.000	0.
87.	$OH + C_2H_2 \rightleftarrows C_2H + H_2O$	3.37e+07	2.000	14000.
88.	$OH + C_2H_2 \rightleftarrows HCCOH + H$	5.04e+05	2.300	13500.
89.	$OH + C_2H_2 \rightleftarrows CH_2CO + H$	2.18e-04	4.500	−1000.
90.	$OH + C_2H_2 \rightleftarrows CH_3 + CO$	4.83e-04	4.000	−2000.
91.	$HCCOH + H \rightleftarrows CH_2CO + H$	1.00e+13	0.000	0.
92.	$C_2H_2 + O \rightleftarrows C_2H + OH$	3.16e+15	−0.600	15000.
93.	$CH_2CO + O \rightleftarrows CO_2 + CH_2$	1.75e+12	0.000	1350.
94.	$CH_2CO + H \rightleftarrows CH_3 + CO$	1.13e+13	0.000	3428.
95.	$CH_2CO + H \rightleftarrows HCCO + H_2$	5.00e+13	0.000	8000.
96.	$CH_2CO + O \rightleftarrows HCCO + OH$	1.00e+13	0.000	8000.
97.	$CH_2CO + OH \rightleftarrows HCCO + H_2O$	7.50e+12	0.000	2000.
98.	$CH_2CO(+M) \rightleftarrows CH_2 + CO(+M)$[3]			
	High pressure limit:	3.00e+14	0.0	70980.
	Low pressure limit:	3.60e+15	0.0	59270.
99.	$C_2H + O_2 \rightleftarrows 2CO + H$	5.00e+13	0.000	1500.
100.	$C_2H + C_2H_2 \rightleftarrows C_4H_2 + H$	3.00e+13	0.000	0.
101.	$H + HCCO \rightleftarrows {}^1CH_2 + CO$	1.00e+14	0.000	0.
102.	$O + HCCO \rightleftarrows H + 2CO$	1.00e+14	0.000	0.
103.	$HCCO + O_2 \rightleftarrows 2CO + OH$	1.60e+12	0.000	854.
104.	$CH + HCCO \rightleftarrows C_2H_2 + CO$	5.00e+13	0.000	0.
105.	$2HCCO \rightleftarrows C_2H_2 + 2CO$	1.00e+13	0.000	0.
106.	${}^1CH_2 + M \rightleftarrows CH_2 + M$	1.00e+13	0.000	0.
	Enhanced third-body efficiencies: $H = 0.0$			
107.	${}^1CH_2 + CH_4 \rightleftarrows 2CH_3$	4.00e+13	0.000	0.
108.	${}^1CH_2 + C_2H_6 \rightleftarrows CH_3 + C_2H_5$	1.20e+14	0.000	0.
109.	${}^1CH_2 + O_2 \rightleftarrows CO + OH + H$	3.00e+13	0.000	0.
110.	${}^1CH_2 + H_2 \rightleftarrows CH_3 + H$	7.00e+13	0.000	0.
111.	${}^1CH_2 + H \rightleftarrows CH_2 + H$	2.00e+14	0.000	0.
112.	$C_2H + O \rightleftarrows CH + CO$	5.00e+13	0.000	0.
113.	$C_2H + OH \rightleftarrows HCCO + H$	2.00e+13	0.000	0.
114.	$2CH_2 \rightleftarrows C_2H_2 + H_2$	4.00e+13	0.000	0.
115.	$CH_2 + HCCO \rightleftarrows C_2H_3 + CO$	3.00e+13	0.000	0.
116.	$CH_2 + C_2H_2 \rightleftarrows C_3H_3 + H$	1.20e+13	0.000	6600.
117.	$C_4H_2 + OH \rightleftarrows C_3H_2 + HCO$	6.66e+12	0.000	−410.
118.	$C_3H_2 + O_2 \rightleftarrows HCO + HCCO$	1.00e+13	0.000	0.
119.	$C_3H_3 + O_2 \rightleftarrows CH_2CO + HCO$	3.00e+10	0.000	2868.
120.	$C_3H_3 + O \rightleftarrows CH_2O + C_2H$	2.00e+13	0.000	0.

APPENDIX A. (continued)
Reaction Mechanism Rate Coefficients In Form $k_f = AT^{\beta}\exp(-E/RT)$.
Units are moles, cubic centimeters, seconds, Kelvins and calories/mole.

	REACTION	A	β	E
121.	$C_3H_3 + OH \rightleftarrows C_3H_2 + H_2O$	2.00e+13	0.000	0.
122.	$2C_2H_2 \rightleftarrows C_4H_3 + H$	2.00e+12	0.000	45900.
123.	$C_4H_3 + M \rightleftarrows C_4H_2 + H + M$	1.00e+16	0.000	59700.
124.	$^1CH_2 + C_2H_2 \rightleftarrows C_3H_3 + H$	3.00e+13	0.000	0.
125.	$C_4H_2 + O \rightleftarrows C_3H_2 + CO$	1.20e+12	0.000	0.
126.	$C_2H_2 + O_2 \rightleftarrows HCCO + OH$	2.00e+08	1.500	30100.
127.	$C_2H_2 + M \rightleftarrows C_2H + H + M$	4.20e+16	0.000	107000.
128.	$C_2H_4 + M \rightleftarrows C_2H_2 + H_2 + M$	1.50e+15	0.000	55800.
129.	$C_2H_4 + M \rightleftarrows C_2H_3 + H + M$	1.40e+16	0.000	82360.
130.	$H_2 + O_2 \rightleftarrows 2OH$	1.70e+13	0.000	47780.
131.	$OH + H_2 \rightleftarrows H_2O + H$	1.17e+09	1.300	3626.
132.	$O + OH \rightleftarrows O_2 + H$	4.00e+14	−0.500	0.
133.	$O + H_2 \rightleftarrows OH + H$	5.06e+04	2.670	6290.
134.	$H + O_2 + M \rightleftarrows HO_2 + M$	3.61e+17	−0.720	0.
	Enhanced third-body efficiencies:			
	H_2O= 18.6, CO_2= 4.2, H_2= 2.9, CO= 2.1, N_2= 1.3			
135.	$OH + HO_2 \rightleftarrows H_2O + O_2$	7.50e+12	0.000	0.
136.	$H + HO_2 \rightleftarrows 2OH$	1.40e+14	0.000	1073.
137.	$O + HO_2 \rightleftarrows O_2 + OH$	1.40e+13	0.000	1073.
138.	$2OH \rightleftarrows O + H_2O$	6.00e+08	1.300	0.
139.	$2H + M \rightleftarrows H_2 + M$	1.00e+18	−1.000	0.
	Enhanced third-body efficiencies:			
	H_2= 0.0, H_2O= 0.0, CO_2= 0.0			
140.	$2H + H_2 \rightleftarrows 2H_2$	9.20e+16	−0.600	0.
141.	$2H + H_2O \rightleftarrows H_2 + H_2O$	6.00e+19	−1.250	0.
142.	$2H + CO_2 \rightleftarrows H_2 + CO_2$	5.49e+20	−2.000	0.
143.	$H + OH + M \rightleftarrows H_2O + M$	1.60e+22	−2.000	0.
	Enhanced third-body efficiencies:			
	H_2O= 5.0			
144.	$H + O + M \rightleftarrows OH + M$	6.20e+16	−0.600	0.
	Enhanced third-body efficiencies:			
	H_2O= 5.0			
145.	$2O + M \rightleftarrows O_2 + M$	1.89e+13	0.000	−1788.
146.	$H + HO_2 \rightleftarrows H_2 + O_2$	1.25e+13	0.000	0.
147.	$2HO_2 \rightleftarrows H_2O_2 + O_2$	2.00e+12	0.000	0.
148.	$H_2O_2 + M \rightleftarrows 2OH + M$	1.30e+17	0.000	45500.
149.	$H_2O_2 + H \rightleftarrows HO_2 + H_2$	1.60e+12	0.000	3800.
150.	$H_2O_2 + OH \rightleftarrows H_2O + HO_2$	1.00e+13	0.000	1800.
151.	$CH + N_2 \rightleftarrows HCN + N$	3.00e+11	0.000	13600.
152.	$CN + N \rightleftarrows C + N_2$	1.04e+15	−0.500	0.
153.	$CH_2 + N_2 \rightleftarrows HCN + NH$	1.00e+13	0.000	74000.
154.	$H_2CN + N \rightleftarrows N_2 + CH_2$	2.00e+13	0.000	0.
155.	$H_2CN + M \rightleftarrows HCN + H + M$	3.00e+14	0.000	22000.
156.	$C + NO \rightleftarrows CN + O$	6.60e+13	0.000	0.
157.	$CH + NO \rightleftarrows HCN + O$	1.10e+14	0.000	0.
158.	$CH_2 + NO \rightleftarrows HCNO + H$	1.39e+12	0.000	−1100.
159.	$CH_3 + NO \rightleftarrows HCN + H_2O$	1.00e+11	0.000	15000.
160.	$CH_3 + NO \rightleftarrows H_2CN + OH$	1.00e+11	0.000	15000.

APPENDIX A. (continued)
Reaction Mechanism Rate Coefficients In Form $k_f = AT^{\beta}\exp(-E/RT)$.
Units are moles, cubic centimeters, seconds, Kelvins and calories/mole.

	REACTION	A	β	E
161.	$HCCO + NO \rightleftarrows HCNO + CO$	2.00e+13	0.000	0.
162.	$^1CH_2 + NO \rightleftarrows HCN + OH$	2.00e+13	0.000	0.
163.	$HCNO + H \rightleftarrows HCN + OH$	1.00e+14	0.000	12000.
164.	$CH_2 + N \rightleftarrows HCN + H$	5.00e+13	0.000	0.
165.	$CH + N \rightleftarrows CN + H$	1.30e+13	0.000	0.
166.	$CO_2 + N \rightleftarrows NO + CO$	1.90e+11	0.000	3400.
167.	$HCCO + N \rightleftarrows HCN + CO$	5.00e+13	0.000	0.
168.	$CH_3 + N \rightleftarrows H_2CN + H$	3.00e+13	0.000	0.
169.	$C_2H_3 + N \rightleftarrows HCN + CH_2$	2.00e+13	0.000	0.
170.	$C_3H_3 + N \rightleftarrows HCN + C_2H_2$	1.00e+13	0.000	0.
171.	$HCN + OH \rightleftarrows CN + H_2O$	1.45e+13	0.000	10929.
172.	$OH + HCN \rightleftarrows HOCN + H$	5.85e+04	2.400	12500.
173.	$OH + HCN \rightleftarrows HNCO + H$	1.98e-03	4.000	1000.
174.	$OH + HCN \rightleftarrows NH_2 + CO$	7.83e-04	4.000	4000.
175.	$HOCN + H \rightleftarrows HNCO + H$	1.00e+13	0.000	0.
176.	$HCN + O \rightleftarrows NCO + H$	1.38e+04	2.640	4980.
177.	$HCN + O \rightleftarrows NH + CO$	3.45e+03	2.640	4980.
178.	$HCN + O \rightleftarrows CN + OH$	2.70e+09	1.580	26600.
179.	$CN + H_2 \rightleftarrows HCN + H$	2.95e+05	2.450	2237.
180.	$CN + O \rightleftarrows CO + N$	1.80e+13	0.000	0.
181.	$CN + O_2 \rightleftarrows NCO + O$	5.60e+12	0.000	0.
182.	$CN + OH \rightleftarrows NCO + H$	6.00e+13	0.000	0.
183.	$CN + HCN \rightleftarrows C_2N_2 + H$	2.00e+13	0.000	0.
184.	$CN + NO_2 \rightleftarrows NCO + NO$	3.00e+13	0.000	0.
185.	$CN + N_2O \rightleftarrows NCO + N_2$	1.00e+13	0.000	0.
186.	$C_2N_2 + O \rightleftarrows NCO + CN$	4.57e+12	0.000	8880.
187.	$C_2N_2 + OH \rightleftarrows HOCN + CN$	1.86e+11	0.000	2900.
188.	$HO_2 + NO \rightleftarrows NO_2 + OH$	2.11e+12	0.000	−479.
189.	$NO_2 + H \rightleftarrows NO + OH$	3.50e+14	0.000	1500.
190.	$NO_2 + O \rightleftarrows NO + O_2$	1.00e+13	0.000	600.
191.	$NO_2 + M \rightleftarrows NO + O + M$	1.10e+16	0.000	66000.
192.	$NCO + H \rightleftarrows NH + CO$	5.00e+13	0.000	0.
193.	$NCO + O \rightleftarrows NO + CO$	2.00e+13	0.000	0.
194.	$NCO + N \rightleftarrows N_2 + CO$	2.00e+13	0.000	0.
195.	$NCO + OH \rightleftarrows NO + CO + H$	1.00e+13	0.000	0.
196.	$NCO + M \rightleftarrows N + CO + M$	3.10e+16	−0.500	48000.
197.	$NCO + NO \rightleftarrows N_2O + CO$	1.00e+13	0.000	−390.
198.	$NCO + H_2 \rightleftarrows HNCO + H$	8.58e+12	0.000	9000.
199.	$HNCO + H \rightleftarrows NH_2 + CO$	2.00e+13	0.000	3000.
200.	$NH + O_2 \rightleftarrows HNO + O$	1.00e+13	0.000	12000.

APPENDIX A. (continued)

Reaction Mechanism Rate Coefficients In Form $k_f = AT^{\beta}\exp(-E/RT)$.
Units are moles, cubic centimeters, seconds, Kelvins and calories/mole.

	REACTION	A	β	E
201.	$NH + O_2 \rightleftarrows NO + OH$	7.60e+10	0.000	1530.
202.	$NH + NO \rightleftarrows N_2O + H$	2.40e+15	−0.800	0.
203.	$N_2O + OH \rightleftarrows N_2 + HO_2$	2.00e+12	0.000	10000.
204.	$N_2O + H \rightleftarrows N_2 + OH$	7.60e+13	0.000	15200.
205.	$N_2O + M \rightleftarrows N_2 + O + M$	1.60e+14	0.000	51600.
206.	$N_2O + O \rightleftarrows N_2 + O_2$	1.00e+14	0.000	28200.
207.	$N_2O + O \rightleftarrows 2NO$	1.00e+14	0.000	28200.
208.	$NH + OH \rightleftarrows HNO + H$	2.00e+13	0.000	0.
209.	$NH + OH \rightleftarrows N + H_2O$	5.00e+11	0.500	2000.
210.	$NH + N \rightleftarrows N_2 + H$	3.00e+13	0.000	0.
211.	$NH + H \rightleftarrows N + H_2$	1.00e+14	0.000	0.
212.	$NH_2 + O \rightleftarrows HNO + H$	6.63e+14	−0.500	0.
213.	$NH_2 + O \rightleftarrows NH + OH$	6.75e+12	0.000	0.
214.	$NH_2 + OH \rightleftarrows NH + H_2O$	4.00e+06	2.000	1000.
215.	$NH_2 + H \rightleftarrows NH + H_2$	6.92e+13	0.000	3650.
216.	$NH_2 + NO \rightleftarrows NNH + OH$	6.40e+15	−1.250	0.
217.	$NH_2 + NO \rightleftarrows N_2 + H_2O$	6.20e+15	−1.250	0.
218.	$NH_3 + OH \rightleftarrows NH_2 + H_2O$	2.04e+06	2.040	566.
219.	$NH_3 + H \rightleftarrows NH_2 + H_2$	6.36e+05	2.390	10171.
220.	$NH_3 + O \rightleftarrows NH_2 + OH$	2.10e+13	0.000	9000.
221.	$NNH \rightleftarrows N_2 + H$	1.00e+04	0.000	0.
222.	$NNH + NO \rightleftarrows N_2 + HNO$	5.00e+13	0.000	0.
223.	$NNH + H \rightleftarrows N_2 + H_2$	1.00e+14	0.000	0.
224.	$NNH + OH \rightleftarrows N_2 + H_2O$	5.00e+13	0.000	0.
225.	$NNH + NH_2 \rightleftarrows N_2 + NH_3$	5.00e+13	0.000	0.
226.	$NNH + NH \rightleftarrows N_2 + NH_2$	5.00e+13	0.000	0.
227.	$NNH + O \rightleftarrows N_2O + H$	1.00e+14	0.000	0.
228.	$HNO + M \rightleftarrows H + NO + M$	1.50e+16	0.000	48680.
	Enhanced third-body efficiencies: H_2O= 10.0, O_2= 2.0, N_2= 2.0, H_2= 2.0			
229.	$HNO + OH \rightleftarrows NO + H_2O$	3.60e+13	0.000	0.
230.	$HNO + H \rightleftarrows H_2 + NO$	5.00e+12	0.000	0.
231.	$HNO + NH_2 \rightleftarrows NH_3 + NO$	2.00e+13	0.000	1000.
232.	$N + NO \rightleftarrows N_2 + O$	3.27e+12	0.300	0.
233.	$N + O_2 \rightleftarrows NO + O$	6.40e+09	1.000	6280.
234.	$N + OH \rightleftarrows NO + H$	3.80e+13	0.000	0.

APPENDIX B.

Reaction Mechanism Rate Coefficients In Form $k_f = AT^{\beta}\exp(-E/RT)$.
Units are moles, cubic centimeters, seconds, Kelvins and calories/mole.

	REACTION	A	β	E
1.	$H_2 + O_2 \rightleftarrows 2OH$	1.70e+13	0.000	47780.
2.	$OH + H_2 \rightleftarrows H_2O + H$	1.17e+09	1.300	3626.
3.	$O + OH \rightleftarrows O_2 + H$	4.00e+14	−0.500	0.
4.	$O + H_2 \rightleftarrows OH + H$	5.06e+04	2.670	6290.
5.	$H + O_2 + M \rightleftarrows HO_2 + M$	3.61e+17	−0.720	0.
	Enhanced third-body efficiencies: H_2O= 18.6, H_2= 2.9, N_2= 1.3			
6.	$OH + HO_2 \rightleftarrows H_2O + O_2$	7.50e+12	0.000	0.
7.	$H + HO_2 \rightleftarrows 2OH$	1.40e+14	0.000	1073.
8.	$O + HO_2 \rightleftarrows O_2 + OH$	1.40e+13	0.000	1073.
9.	$2OH \rightleftarrows O + H_2O$	6.00e+08	1.300	0.
10.	$2H + M \rightleftarrows H_2 + M$	1.00e+18	−1.000	0.
11.	$2H + H_2 \rightleftarrows 2H_2$	9.20e+16	−0.600	0.
12.	$2H + H_2O \rightleftarrows H_2 + H_2O$	6.00e+19	−1.250	0.
13.	$H + OH + M \rightleftarrows H_2O + M$	1.60e+22	−2.000	0.
	Enhanced third-body efficiencies: H_2O= 5.0			
14.	$H + O + M \rightleftarrows OH + M$	6.20e+16	−0.600	0.
	Enhanced third-body efficiencies: H_2O= 5.0			
15.	$2O + M \rightleftarrows O_2 + M$	1.89e+13	0.000	−1788.
16.	$H + HO_2 \rightleftarrows H_2 + O_2$	1.25e+13	0.000	0.
17.	$2HO_2 \rightleftarrows H_2O_2 + O_2$	2.00e+12	0.000	0.
18.	$H_2O_2 + M \rightleftarrows 2OH + M$	1.30e+17	0.000	45500.
19.	$H_2O_2 + H \rightleftarrows HO_2 + H_2$	1.60e+12	0.000	3800.
20.	$H_2O_2 + OH \rightleftarrows H_2O + HO_2$	1.00e+13	0.000	1800.
21.	$NH + O_2 \rightleftarrows HNO + O$	1.00e+13	0.000	12000.
22.	$NH + O_2 \rightleftarrows NO + OH$	7.60e+10	0.000	1530.
23.	$NH + NO \rightleftarrows N_2O + H$	2.40e+15	−0.800	0.
24.	$N_2O + H \rightleftarrows N_2 + OH$	7.60e+13	0.000	15200.
25.	$N_2O + M \rightleftarrows N_2 + O + M$	1.62e+14	0.000	51600.
26.	$N_2O + O \rightleftarrows N_2 + O_2$	1.00e+14	0.000	28200.
27.	$N_2O + O \rightleftarrows 2NO$	1.00e+14	0.000	28200.
28.	$N_2O + OH \rightleftarrows N_2 + HO_2$	2.00e+12	0.000	10000.
29.	$NH + OH \rightleftarrows HNO + H$	2.00e+13	0.000	0.
30.	$NH + OH \rightleftarrows N + H_2O$	5.00e+11	0.500	2000.
31.	$NH + N \rightleftarrows N_2 + H$	3.00e+13	0.000	0.
32.	$NH + H \rightleftarrows N + H_2$	1.00e+14	0.000	0.
33.	$NH + O \rightleftarrows NO + H$	2.00e+13	0.000	0.
34.	$NH_2 + O \rightleftarrows HNO + H$	6.63e+14	−0.500	0.
35.	$NH_2 + O \rightleftarrows NH + OH$	6.75e+12	0.000	0.
36.	$NH_2 + OH \rightleftarrows NH + H_2O$	4.00e+06	2.000	1000.
37.	$NH_2 + H \rightleftarrows NH + H_2$	6.92e+13	0.000	3650.
38.	$NH_2 + NO \rightleftarrows NNH + OH$	6.40e+15	−1.250	0.
39.	$NH_2 + NO \rightleftarrows N_2 + H_2O$	6.20e+15	−1.250	0.
40.	$NH_3 + OH \rightleftarrows NH_2 + H_2O$	2.04e+06	2.040	566.

APPENDIX B. (continued)
Reaction Mechanism Rate Coefficients In Form $k_f = AT^{\beta}\exp(-E/RT)$.
Units are moles, cubic centimeters, seconds, Kelvins and calories/mole.

	REACTION	A	β	E
41.	$NH_3 + H \rightleftarrows NH_2 + H_2$	6.36e+05	2.390	10171.
42.	$NH_3 + O \rightleftarrows NH_2 + OH$	2.10e+13	0.000	9000.
43.	$NNH \rightleftarrows N_2 + H$	1.00e+04	0.000	0.
44.	$NNH + NO \rightleftarrows N_2 + HNO$	5.00e+13	0.000	0.
45.	$NNH + H \rightleftarrows N_2 + H_2$	1.00e+14	0.000	0.
46.	$NNH + OH \rightleftarrows N_2 + H_2O$	5.00e+13	0.000	0.
47.	$NNH + NH_2 \rightleftarrows N_2 + NH_3$	5.00e+13	0.000	0.
48.	$NNH + NH \rightleftarrows N_2 + NH_2$	5.00e+13	0.000	0.
49.	$NNH + O \rightleftarrows N_2O + H$	1.00e+14	0.000	0.
50.	$HNO + M \rightleftarrows H + NO + M$	1.50e+16	0.000	48680.
	Enhanced third-body efficiencies: H_2O= 10.0, O_2= 2.0, N_2= 2.0, H_2= 2.0			
51.	$HNO + OH \rightleftarrows NO + H_2O$	3.60e+13	0.000	0.
52.	$HNO + H \rightleftarrows H_2 + NO$	5.00e+12	0.000	0.
53.	$HNO + NH_2 \rightleftarrows NH_3 + NO$	2.00e+13	0.000	1000.
54.	$2HNO \rightleftarrows N_2O + H_2O$	3.95e+12	0.000	5000.
55.	$HNO + NO \rightleftarrows N_2O + OH$	2.00e+12	0.000	26000.
56.	$N + NO \rightleftarrows N_2 + O$	3.27e+12	0.300	0.
57.	$N + O_2 \rightleftarrows NO + O$	6.40e+09	1.000	6280.
58.	$N + OH \rightleftarrows NO + H$	3.80e+13	0.000	0.
59.	$HO_2 + NO \rightleftarrows NO_2 + OH$	2.11e+12	0.000	−479.
60.	$NO_2 + H \rightleftarrows NO + OH$	3.50e+14	0.000	1500.
61.	$NH_2 + NH \rightleftarrows N_2H_2 + H$	5.00e+13	0.000	0.
62.	$2NH \rightleftarrows N_2 + 2H$	2.54e+13	0.000	0.
63.	$NH_2 + N \rightleftarrows N_2 + 2H$	7.20e+13	0.000	0.
64.	$N_2H_2 + M \rightleftarrows NNH + H + M$	5.00e+16	0.000	50000.
	Enhanced third-body efficiencies: H_2O= 15.0, O_2= 2.0, N_2= 2.0, H_2= 2.0			
65.	$N_2H_2 + H \rightleftarrows NNH + H_2$	5.00e+13	0.000	1000.
66.	$N_2H_2 + O \rightleftarrows NH_2 + NO$	1.00e+13	0.000	0.
67.	$N_2H_2 + O \rightleftarrows NNH + OH$	2.00e+13	0.000	1000.
68.	$N_2H_2 + OH \rightleftarrows NNH + H_2O$	1.00e+13	0.000	1000.
69.	$N_2H_2 + NO \rightleftarrows N_2O + NH_2$	3.00e+12	0.000	0.
70.	$N_2H_2 + NH \rightleftarrows NNH + NH_2$	1.00e+13	0.000	1000.
71.	$N_2H_2 + NH_2 \rightleftarrows NH_3 + NNH$	1.00e+13	0.000	1000.
72.	$2NH_2 \rightleftarrows N_2H_2 + H_2$	5.00e+11	0.000	0.
73.	$NH_2 + O_2 \rightleftarrows HNO + OH$	4.50e+12	0.000	25000.